AD-A115 203   LITTON SYSTEMS INC WOODLAND HILLS CA GUIDANCE AND CO—ETC F/G 17/7
               NUCLEAR MOMENT ALIGNMENT, RELAXATION AND DETECTION MECHANISMS.(U)
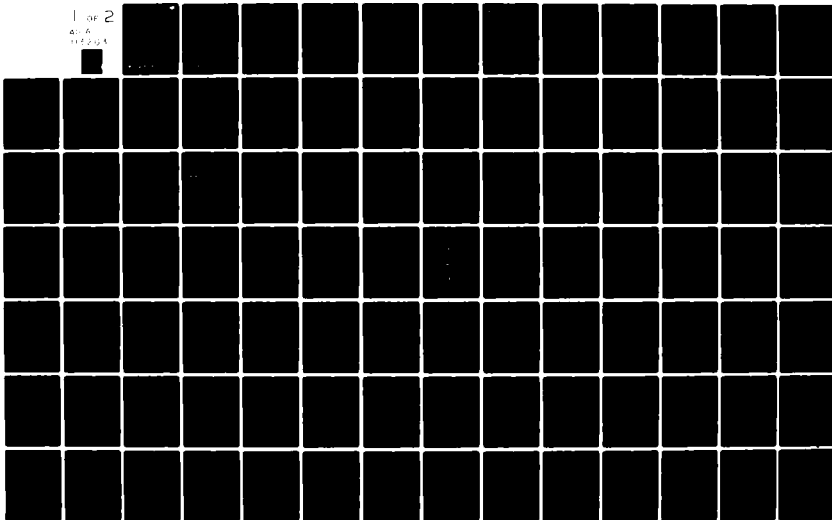   FEB 82 A T NICOL   F49620-77-C-0047
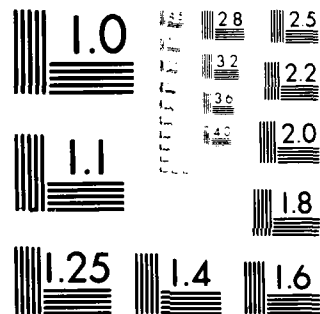UNCLASSIFIED   404720   AFOSR-TR-82-0418   . NL

1 OF 2
AD A
A115203

1.0

1.1

1.25

2.8
3.2
3.6
4.0

2.5
2.2
2.0
1.8
1.4
1.6

MICROCOPY RESOLUTION TEST CHART
NATIONAL BUREAU OF STANDARDS 1963 A

ment No. 404720
uary 1982

NUCLEAR MOMENT ALIGNMENT, RELAXATION

AND DETECTION MECHANISMS

February 1981 - January 1982

FINAL TECHNICAL REPORT

Contract No. F49620-77-C-0047

Prepared for
AIR FORCE OFFICE OF SCIENTIFIC RESEARCH

DTIC
ELECTE
JUN 0 7 1982

E

GUIDANCE & CONTROL SYSTEMS
Litton 5500 Canoga Avenue, Woodland Hills, California 91365

82 06 04 007

NUCLEAR MOMENT ALIGNMENT, RELAXATION

AND DETECTION MECHANISMS

February 1981 - January 1982

FINAL TECHNICAL REPORT

Prepared for

AIR FORCE OFFICE OF SCIENTIFIC RESEARCH

Under

Contract No. F49620-77-C-0047

Approved By:

Emery L. Moore
Manager, NMR Gyro Project

GUIDANCE & CONTROL SYSTEMS
Litton 5500 Canoga Avenue, Woodland Hills, California 91365

REPORT DOCUMENTATION PAGE	READ INSTRUCTIONS BEFORE COMPLETING FORM

1. REPORT NUMBER	2. GOVT ACCESSION NO.	3. RECIPIENT'S CATALOG NUMBER
AFOSR-TR- 82-0418	AD-A115 223	

4. TITLE (and Subtitle)	5. TYPE OF REPORT & PERIOD COVERED
NUCLEAR MOMENT ALIGNMENT, RELAXATION AND DETECTION MECHANISMS	Final (February 1977 January 1982)
	6. PERFORMING ORG. REPORT NUMBER 404720

7. AUTHOR(s)	8. CONTRACT OR GRANT NUMBER(s)
A.T. NICOL	F49620-77-C-0047

9. PERFORMING ORGANIZATION NAME AND ADDRESS	10. PROGRAM ELEMENT, PROJECT, TASK AREA & WORK UNIT NUMBERS
Litton Guidance & Control Systems 5500 Canoga Ave. Woodland Hills, CA 91365	61102F 2301/A4

11. CONTROLLING OFFICE NAME AND ADDRESS	12. REPORT DATE
Director of Physics Code FQ 8671 Air Force Office of Scientific Research Attn: NP Building 410, Bolling AFB, D.C. 20332	February 1982
	13. NUMBER OF PAGES 112

14. MONITORING AGENCY NAME & ADDRESS(If different from Controlling Office)	15. SECURITY CLASS. (of this report)
	UNCLASSIFIED
	15a. DECLASSIFICATION/DOWNGRADING SCHEDULE

16. DISTRIBUTION STATEMENT (of this Report)

Approved for public release;
distribution unlimited.

17. DISTRIBUTION STATEMENT (of the abstract entered in Block 20, if different from Report)

18. SUPPLEMENTARY NOTES

19. KEY WORDS (Continue on reverse side if necessary and identify by block number)

Nuclear Magnetic Resonance	Nuclear Moment Relaxation	Frequency Shift
Gyroscope	Quadrupole Relaxation	
Optical Pumping	Nuclear Moment Precession	
Nuclear Moment Alignment	Spin Exchange	

20. ABSTRACT (Continue on reverse side if necessary and identify by block number)

The reported physics research is part of an overall program to develop a nuclear magnetic resonance gyro that makes use of an optically pumped alkali metal vapor both to align the magnetic moments of the noble gas nuclei and to detect the weak magnetic fields that are generated by these precessing nuclear moments. —> cont next page

20. ABSTRACT (cont)

Experiments designed to hold constant the rubidium vapor density in an NMR sample cell and thus restrict the spin exchange interaction while varying the cell wall temperature are reported. These experiments lead to longer relaxation times and larger signal amplitudes for the noble gas isotopes at elevated wall temperatures than is observed in the case where alkali metal vapor density is not restricted.

^{129}Xe magnetic resonance frequency shift experiments are reported in which the transverse relaxation times are found to depend strongly on choice of polarizer, pump light intensity, and alkali vapor density. The results are explained in terms of internally generated field gradients due to spacially non-uniform rubidium polarization across the sample cell.

An analytical discussion of the temperature sensitivity of the NMR gyro bias due to quadrupolar frequency shift in ^{131}Xe is presented. That frequence shift is demonstrated to be a mechanism for the temperature dependence of the gyro bias and the temperature turning point (temperature at which temperature sensitivity of gyro bias becomes zero). Results indicate that cells with low wall surface adsorption energy provide a smaller range of temperature sensitivity of NMR gyro bias.

Studies of Corning 1720 glass NMR cells, both rubidium hydride coated and non coated, are presented and compared with results for similarly prepared Pyrex cells. Hydride coated cells of both types are found to exhibit similar properties. At 80°C ^{129}Xe relaxation times are similar, and both types of cells exhibit similar ^{131}Xe magic angle behavior. Relaxation time studies for uncoated cells at close to 80°C show longer transverse relaxation times for ^{129}Xe in 1720 glass than in Pyrex. The opposite trend is seen for ^{131}Xe relaxation, but the effect is not as large as for ^{129}Xe.

Accession For

NTIS GRA&I	☒
DTIC TAB	☐
Unannounced	☐
Justification	

By

Distribution/

Availability Codes

| Dist | Avail and/or Special |

A

DTIC
COPY
INSPECTED
2

404720

TABLE OF CONTENTS

Paragraph	Title	Page

GUIDANCE & CONTROL SYSTEMS
5500 Canoga Avenue, Woodland Hills, California 91365

FSCM 06481

TABLE OF CONTENTS (cont)

FSCM 06481

GUIDANCE & CONTROL SYSTEMS
Litton 5500 Canoga Avenue, Woodland Hills, California 91365

LIST OF ILLUSTRATIONS

GUIDANCE & CONTROL SYSTEMS
Litton 5500 Canoga Avenue, Woodland Hills, California 91365

LIST OF ILLUSTRATIONS (cont)

GUIDANCE & CONTROL SYSTEMS
Litton 5500 Canoga Avenue, Woodland Hills, California 91365

LIST OF ILLUSTRATIONS (cont)

GUIDANCE & CONTROL SYSTEMS
5500 Canoga Avenue, Woodland Hills, California 91365

LIST OF TABLES

SECTION I

PROGRAM DESCRIPTION

1.1 INTRODUCTION

Since 1968, Litton Guidance and Control Systems has been carrying out research aimed at development of a new low cost magnetic resonance gyro. In 1977, a basic research program under the auspices of AFOSR Contract No. F49620-77-C-0047 was begun and has subsequently resulted in fundamental contributions to the gyro program.

The nuclear magnetic resonance gyro is based on the principle that a nuclear moment, when placed in a magnetic field, will precess about the field direction with a characteristic frequency; and when the system itself is rotated about the field direction, the apparent frequency of precession will change. In the latest version of the *Litton Demonstration Model Gyro* (DMG), two isotopes of xenon having different gyromagnetic ratios and hence different precession frequencies in a given field, are used. This allows a gyro mechanization not requiring precise knowledge of precession field strength. Both isotopes of xenon are polarized through spin exchange with an optically pumped rubidium metal vapor. The optically pumped rubidium is also mechanized as a magnetometer.

The successful development of a gyro using noble gas nuclei as the working substance requires methods to contain the substances and, inasmuch as possible, control the polarization and relaxation characteristics. The major emphasis of AFOSR sponsored research has been on developing an understanding of fundamental atomic and molecular physics of systems consisting of noble gases, alkali metals, and their environment. In particular a great deal of research, both theoretical and experimental, has been directed

toward understanding factors in noble gas nuclear moment polarization and relaxation. These factors include not only spin exchange processes but also cell boundary interactions, diffusion through buffer gases, spacial distribution of alkali polarization, and external field gradient effects. The research carried out in 1981-82 has concentrated on approaches to sorting out boundary effects from other factors and has included both new experimental techniques and new cell boundary treatment.

1.2 SUMMARY OF CONTRACT PROGRESS MADE FROM FEBRUARY 1977 TO JANUARY 1981

Sections II through VI of this report describe progress made in 1981-82. Here progress made from 1977 to 1981 under the auspices of AFOSR contract number F49620-77-C-0047 is summarized. The extended description of these results can be found in the Annual Technical Reports prepared under this grant for the Air Force Office of Scientific Research for the periods 1977-78, 1978-79, 1979-80, and 1980-81.

In 1977-78, extensive theoretical groundwork was laid. In particular, it was shown that the spin exchange between an alkali valence electron and a noble gas nucleus, the frequency shift of the noble gas nuclear energy levels, and the frequency shift of the alkali Zeeman levels in the presence of the polarized noble gas nuclei are all ramifications of the alkali atom noble gas nucleus spin exchange interaction. Predictions made from the theoretical model were born out experimentally in later contract years. For example, the theory predicted that the magnetic field experienced by the noble gas nucleus due to the alkali atom polarization would be different for different noble gases but approximately the same for different isotopes of the same noble gas. Experiments demonstrating this were reported in the AFOSR Annual Report for 1980-81 in which combinations of ^{83}Kr and ^{129}Xe were compared with combinations of ^{131}Xe and ^{129}Xe. Refinements and extensions for both experimental and theoretical results of

considering frequency shift effects are presented in Sections III and IV of this report.

Also in 1977-78, experimental surveys of ^{129}Xe, ^{131}Xe, and ^{83}Kr relaxation rates were made for a variety of cell sizes and materials, but typically 15ml pyrex cells were used. At the same time, gas phase mechanisms for both transverse and longitudinal relaxations were considered. These mechanisms included the noble gas-noble gas direct dipolar interaction, the quadrupolar interaction (applicable to ^{131}Xe and ^{83}Kr), the noble gas-nitrogen molecule interaction for both dipolar and quadrupolar cases, and interactions of the noble gases with the rubidium vapor. Molecular forming collisions were discussed briefly as well as field gradient effects. It was concluded that the dominating gas phase relaxation interaction was the noble gas-alkali atom spin exchange interaction. For the large sample cells (15ml) it was concluded that the cell wall interactions were not important.

In 1978-79, more subtle effects began to be investigated. A model for the contribution of RbXe Van der Waals molecules to spin exchange as a function of varying buffer gas pressure was developed. Also the groundwork was laid for the theoretical understanding of the quadrupolar relaxation of noble gas nuclei. Subsequently ^{131}Xe T_2's as long as 80 sec were observed for the first time in 15ml cells. The theoretical analysis coupled with experimental results for ^{83}Kr was published in a paper in the Physical Review. This analysis lead to the identification of magic angle behavior of quadrupolar relaxation in cells with a symmetry axis. Figures 1-1 and 1-2 reproduced from the contract Annual Report for 1978-79 (Figures 3-1 and 3-2 of that report) illustrate this behavior. It can be seen that by judiciously orienting the NMR sample cell, one can obtain a relatively long exponential decay.
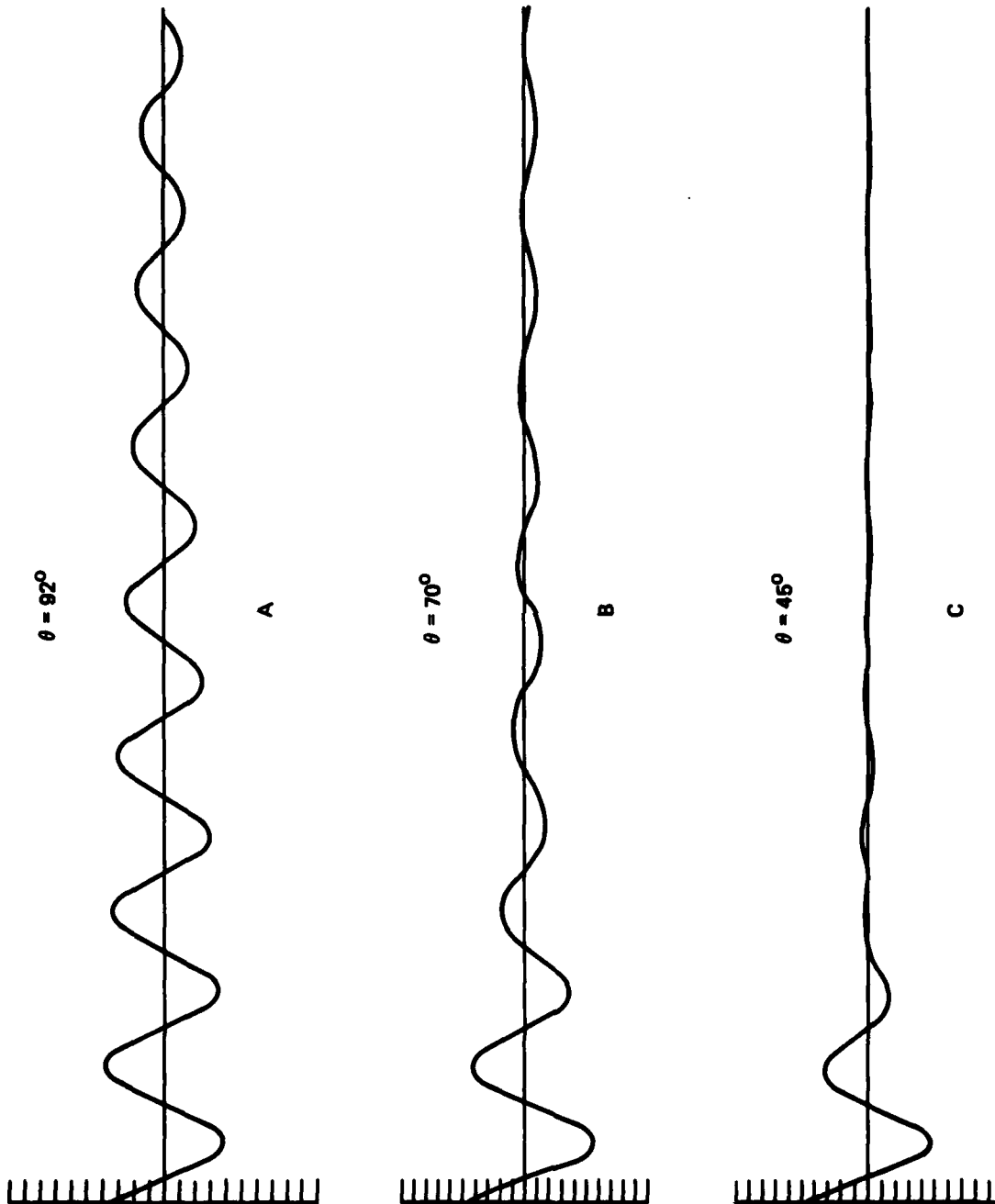
Figure 1-1. Kr Decay Signal Showing Relative Amplitude Versus Time for a 500 Second Data Run. θ Indicates the Relative Orientation of the Cell in the Apparatus.
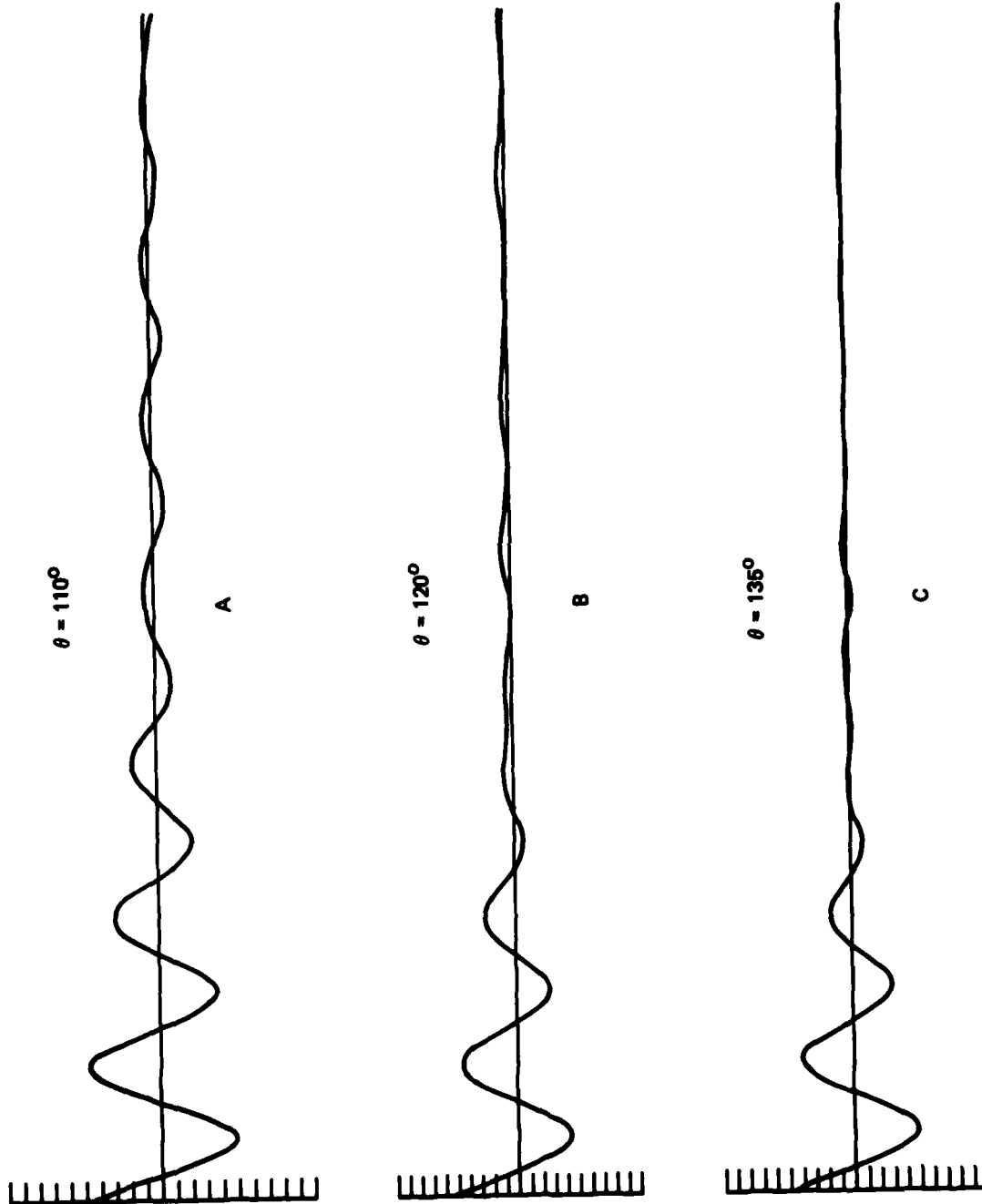
Figure 1-2. Kr Decay Signal Showing Relative Amplitude Versus Time for a 500 Second Data Run. θ Indicates the Relative Orientation of the Cell in the Apparatus.

In the particular case shown here, rubidium was in a specific location on the cell wall. It was found that the "magic angle" orientation depended on how and where the Rb was distributed on the walls. It was further discovered that by driving the rubidium to the tip off region of the cell, one would produce the typical $(1-3\cos^2\theta)$ magic angle dependence with $\theta \approx 55^\circ$ for the symmetry axis through the cell tip. (The magic angle is defined as the angle between the symmetry axis and the magnetic field such that $(1 - 3\cos^2\theta)$ is zero.) This important advance made quadrupolar polarization and relaxation effects much more subject to the manipulation of the experimentalist.

Calendar year 1979-80 work was highlighted by the submission and subsequent publication of two papers, one in the Physical Review and the other in Physical Review Letters. The first of these described a measurement of $^{87}Rb - ^{129}Xe$ spin exchange cross section in which the alkali polarization was forced to zero during the measurement so that there was no dynamic polarization coupling of the alkali electron with the noble gas nucleus during the decay. This was accomplished by blocking the light during most of the decay and simply allowing it to pass periodically for detection purposes. The detection beam, then, was used only to determine initial and final amplitudes from which the noble gas transverse relaxation rate could be determined. With this modification, good agreement with the then existing model was obtained.

The second paper published in 1980 described a measurement of the Rb-^{131}Xe spin exchange cross section. As the ^{131}Xe has a quadrupolar nucleus (spin 3/2) it differs markedly from ^{129}Xe (spin 1/2). Because of the dominance of quadrupolar relaxation for ^{131}Xe, the effects of walls and buffer gases, i.e., anything that can lead to electron cloud distortions and, hence, an electric field gradient at the nucleus, are much greater. The ^{131}Xe relaxation is then not so strongly dominated by the Rb-Xe spin

exchange interaction. Thus, as the Rb-^{131}Xe spin exchange cross section is perhaps an order of magnitude smaller than the Rb-^{129}Xe spin exchange cross section, a more efficient means for studying ^{131}Xe was sought.

In a collaboration with a group at the University of Southern California, the problem of the small signal amplitude was over-come by pumping the system with a dye laser tuned to the D_1 rubid-ium resonance line. In this way, increased alkali polarization was attained over a much wider temperature range than had been possible previously. As the ^{131}Xe relaxation rate is much less sensitive to temperature than the ^{129}Xe relaxation rate, such a temperature range was needed in order to fit the data to a reason-able model.

Research year 1980-81 saw several significant advances. A paper describing the magic angle quadrupolar behavior of ^{131}Xe, both theoretically and experimentally, was accepted for publication in the Physical Review, and a rubidium hydride cell wall coating, which increased the ^{131}Xe magnetic moment, decreased the quadru-polar relaxation effect, and increased the reproducibility of magic angle behavior was discovered. This launched a series of experiments on hydride treated cells and resulted in two patent applications. Some typical results for hydride coated cells are presented in Sections V and VI of this report.

1980 also saw experimental verification that NMR gyro bias tem-perature and light sensitivity is smaller by a factor of ≥30 using the ^{129}Xe-^{131}Xe combination rather than the ^{83}Kr-^{129}Xe com-bination of noble gases which had been used previously. The improved ^{131}Xe polarization and relaxation times brought about by theoretical understanding of quadrupolar relaxation and the experimentally determined benefits of RbH cell wall treatment allowed use of ^{129}Xe-^{131}Xe cells of 1 ml size in the Litton Demonstration Model Gyro (DMG). Further work in 1980 identified

GUIDANCE & CONTROL SYSTEMS
5500 Canoga Avenue, Woodland Hills, California 91365

experimentally the temperature at which the temperature sensitivity of the gyro bias becomes identically zero for the ^{129}Xe-^{131}Xe cells.

Thus, the groundwork laid in the theoretical and experimental efforts carried out under auspices of AFOSR Contract F49620-77-C-0047 resulted not only in important scientific advances but also in very practical NMR gyro applications. Today important progress is being made in research aimed at understanding the basic atomic and molecular processes in the NMR cell physics. The main body of this Final Report (Sections II through VI) describes in detail the current status of the program and our most recent advances.

1.3 PUBLICATIONS RESULTING FROM WORK CARRIED OUT UNDER AFOSR CONTRACT NO. F49620-77-C-0047

This contract has resulted in the four publications listed here. In addition, one more publication based on the material presented in Section III of this report is in preparation.

"Spin Dephasing of Kr^{83}," by C.H. Volk, J.G. Mark, and B.C. Grover, Phys. Rev. A 20, 2381 (1979)

"Measurement of the Rb-^{131}Xe Spin-Exchange Cross Section in ^{131}Xe Relaxation Studies," by C.H. Volk, T.M. Kwon, and J.G. Mark, Phys. Rev. Lett. 44, 136 (1980)

"Measurement of the ^{87}Rb-^{129}Xe Spin-Exchange Cross Section," by C.H. Volk, T.M. Kwon, and J.G. Mark, Phys. Rev. A 21, 1549 (1980)

"Quadrupole Nuclear Spin Relaxation of ^{131}Xe in the Presence of Rubidium Vapor," by T.M. Kwon, J.G. Mark, and C.H. Volk, Phys. Rev. A 24, 1894 (1981).

1.4 PATENT APPLICATIONS AND DISCLOSURES

Work carried out under AFOSR Contract No. F49620-77-C-0047 resulted in a patent disclosure based on the use of rubidium

hydride cell wall treatments. This disclosure resulted in two patent applications being filed with the U.S. Patent Office:

"Improved Magnetic Resonance Cell and Method for Its Preparation," by T.M. Kwon and W.P. Debley.

"Improved Magnetic Resonance Cell," by T.M. Kwon and C.H. Volk.

The first of these pertains to the improved noble gas polarization and relaxation through use of the RbH coating while the second involves the benefit of driving the rubidium deposit to the tip off region of the cell.

In addition, Dr. T.M. Kwon has made a patent disclosure, "Improved Temperature Sensitivity of NMR Gyro Bias," based on information presented in Section IV of this report.

1.5 OBJECTIVES AND STATUS OF CURRENT PROGRAM

For the project year 1981-82 it was proposed to study cell wall coating and fabrication materials and to study the effect of cell wall temperature on quadrupolar interaction. In particular, it was proposed to determine whether controlled deposition of uniform rubidium hydride coatings could be accomplished through use of "clean glass" substrates; and, if so, whether it would lead to control of wall effects associated with ^{131}Xe relaxation. In addition it was proposed to study the quadrupolar wall effect by designing and performing experiments in which the spin exchange process is carefully controlled while the wall temperature is varied.

Section II discusses the design of the experiment which controls the spin exchange process and presents some results showing increased signal to noise made possible by this technique. Wall effects are addressed in Sections V and VI. Section V presents

GUIDANCE & CONTROL SYSTEMS
5500 Canoga Avenue, Woodland Hills, California 91365

FSCM 06481

results of a study of Corning 1720 glass cells which were pre-
pared by cleaning the surface at high temperatures prior to
rubidium hydride deposition while Section VI discusses alkali
hydride chemistry, the interaction of alkali metals and hydrides
with glass surfaces, and the effect of alkali hydride coated
surfaces on magic angle behavior for ^{131}Xe. Sections III and IV
represent unanticipated advances which took place in this contract
year. The material presented in Section III grew out of un-
expected observations made in the course of the double oven
experiment described in Section II and represents the first obser-
vations of noble gas nuclear magnetic resonance relaxation due
to internal field gradients arising from spacial variation of
alkali polarization across the sample cell. Section IV is an
interpretation of the significance of the results of Section III
for gyro operation. This represents yet another important
development for gyro operation coming out of the AFOSR basic
research program.

1.6 PROFESSIONAL PERSONNEL ASSOCIATED WITH PROGRAM

The principal investigator for this program has been Dr. Tae M.
Kwon, who has been succeeded by Dr. Ann T. Nicol as of September
1981. All sample cells were prepared by Mr. William P. Debley,
who was also closely involved with the design and implementation
of the double oven apparatus. Mr. James Eddingfield has been
responsible for taking many data and maintaining the research
apparatus. Dr. Nicol is also pleased to acknowledge useful dis-
cussions with Dr. Kwon and with Dr. Edward Kanesberg and Dr. Leo
Lam.

SECTION II

NOBLE GAS POLARIZATION AND RELAXATION AT CONSTANT
ALKALI METAL VAPOR DENSITY

2.1 INTRODUCTION

A recurring challenge in the study of noble gas nuclear orienta-
tion and relaxation in the presence of an alkali metal vapor is
the proper breakdown of contributions to relaxation from various
mechanisms. Such mechanisms can include spin exchange relaxation
between the noble gas atoms and the alkali metal atoms, relaxation
due to diffusion through buffer gas, relaxation due to field
inhomogeneity of internal or external origin, and relaxation on
the walls of the vessel. As all these mechanisms, with the pos-
sible exception of the externally generated field inhomogeneity,
can exhibit a strong temperature dependence a way to sort out
these various contributions to relaxation is needed. One ap-
proach, described here, is to hold constant the alkali metal
vapor density within the sample cell thereby minimizing changes
in spin exchange relaxation as a function of temperature. (This
can also have an effect on the internally generated field
inhomogeneities, and that topic is addressed in Section III.)

The transverse relaxation rate, T_2^{-1}, for a system of noble gas
atoms polarized through spin exchange with the electronic spin
of optically pumped alkali vapor atoms can be modeled by:

$$\frac{1}{T_2} = N_A \, \sigma_{ex} \, \bar{V}_{rel} + f(T) \tag{1}$$

where $T_{ex}^{-1} = N_A \, \sigma_{ex} \, \bar{V}_{rel}$ is the spin exchange rate where N_A is
the number density of the alkali metal in the gas phase, σ_{ex} is
the alkali metal-noble gas spin exchange cross section, and $\bar{V}_{rel}$
is the alkali atom-noble gas atom relative velocity. For our

purposes it is convenient to lump any molecular formation into
the spin exchange term. This point is discussed more fully in
paragraph 3.4 of this report. Other temperature dependent terms
in equation (1) are incorporated into $f(T)$. Theoretical results
have shown that the spin exchange cross section is inversely pro-
portional to the relative velocity squared[1] and thus

$$N_A \, \sigma_{ex} \, \overline{V}_{rel} \, \alpha \, \frac{N_A}{\overline{V}_{rel}} \quad . \tag{2}$$

As

$$\overline{V}_{rel} = \left(\frac{8 \, RT}{\pi \, \mu} \right)^{1/2} \tag{3}$$

it is evident that

$$N_A \, \sigma_{ex} \, \overline{V}_{rel} \, \alpha \, \frac{N_A}{\sqrt{T}} \quad . \tag{4}$$

For rubidum the experimental number density in cm^{-3} is given
by [2].

$$\log_{10} N_{Rb} = -4560/T + 30.98 - 2.45 \log_{10}T \quad . \tag{5}$$

From these expressions it is evident that the first term of
equation (1) has a rather complicated temperature dependence. By
holding the rubidium vapor density constant one major source of
the temperature dependence of equation (1) would be eliminated.

At the outset of the experiments described here it was hoped that
by removing the temperature dependence inherent in equation (5)
it would be possible to modify the temperature dependence of
equation (1) sufficiently to characterize underlying parameters

associated with wall relaxations. Substantial progress has been made toward that goal while unanticipated difficulties with equipment design and cell shape and size have been dealt with. This section describes the experimental apparatus and the cell shape modifications and presents some results for several experimental cells.

2.2   DESIGN OF EXPERIMENTAL APPARATUS AND CELL SHAPE MODIFICATION

The new apparatus, a double oven arrangement, is designed to be compatible with the usual optical pumping – NMR experimental setup and is shown schematically in figure 2-1. The purpose of this arrangement is to make it possible to hold the rubidium density constant while varying the actual wall temperature of the sample cell. To do this, two ovens, independently controlled, are employed. One oven, called the tip heater, surrounds the tip-off area of the cell where the excess rubidium resides. The second oven, called the wall heater, is arranged cylindrically around the body of the cell to allow for passage of light. A third heater surrounding the entire cell cylindrically is available for carrying out conventional experiments without requiring removal of the cell.

Because of the small cell size (1-3 ml) the temperature difference between the tip and wall body is not readily controlled by heater settings, but rather it depends on the thermal conductance of the cell itself. In order to maintain as large a temperature difference as possible it was found experimentally that teardrop shaped cells are preferable to spherical cells. This permits a relatively massive amount of glass in the colder tip region and has resulted in differences as large as 35° between the tip and wall regions. Also, during operation of the apparatus, a flow-controlled forced air nozzle is directed at the tip. This aids in maintaining the steady-state temperature difference. Otherwise, as the whole
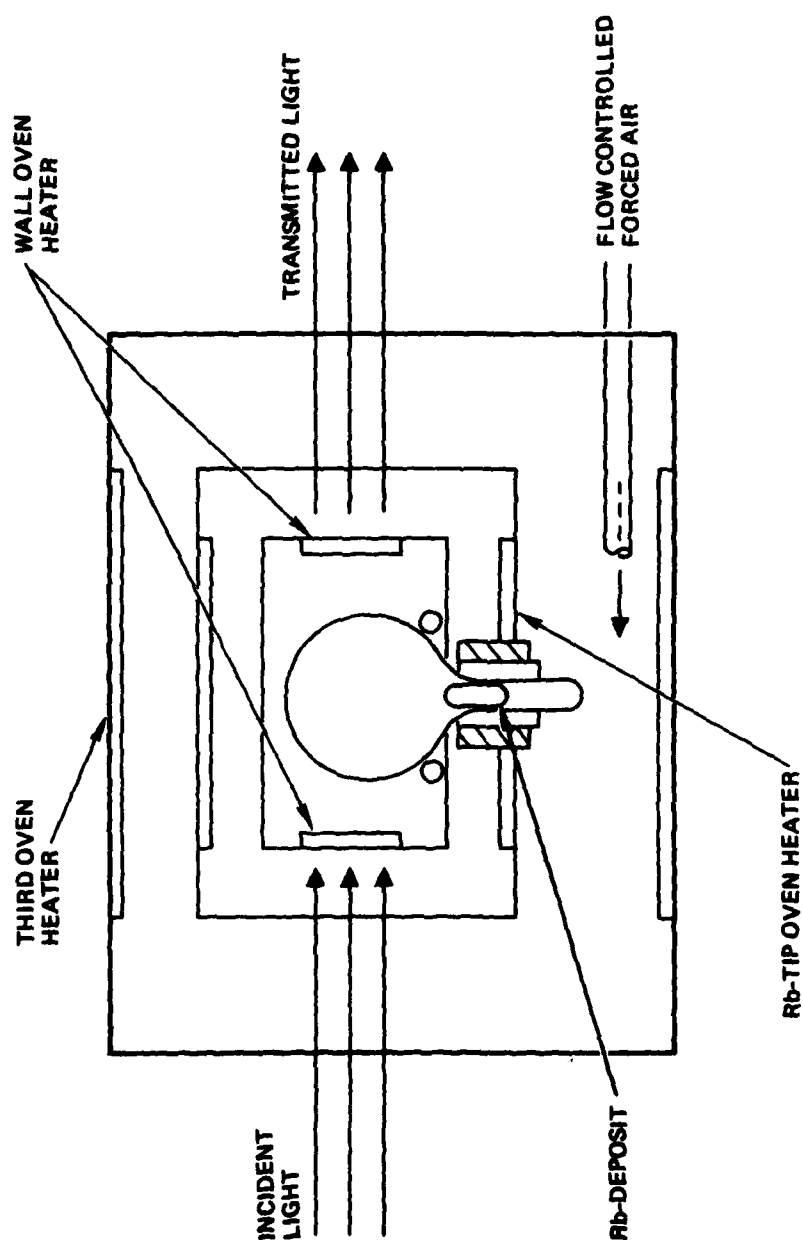
Figure 2-1. Double Oven Apparatus

oven assembly is fairly well insulated, the whole cell tends toward a uniform temperature.

An important question is the accurate control and calibration of a system for observing the rubidium number density. As the rubidium density is a known function of temperature, an ideal situation would have the rubidium density controlled by the tip oven temperature. Because of the cell size and the non-trivial effect of the thermal conductance of the glass, such a control is impractical; and another method had to be devised. A schematic representation of the entire experimental set-up, shown in figure 2-2, suggests that the transmitted light can be used to monitor the rubidium density. To do this, a large magnetic field gradient is applied perpendicular to the optical axis. This has the effect of destroying any rubidium polarization, i.e., $<S_z> = 0$. The transmitted light voltage is then monitored as a function of cell wall and tip temperatures. A typical calibration curve obtained in this way is shown in figure 2-3. A calibration run takes about twelve hours and is carried out by first heating the entire oven assembly to a high temperature, usually between 80° and $90^\circ C$. Thermocouples placed near the tip and wall read out temperature. The heater is then turned off and temperatures and photo detector voltages are recorded by the computer while the entire system cools slowly to room temperature. Ideally the calibration curve should be such that the wall and tip temperatures are the same throughout the cooling process, and this is what is observed unless the apparatus is cooled too rapidly. A calibration curve is routinely taken at the start and finish of a series of double oven experiments. It should be emphasized that, in spite of this calibration, the actual wall body temperature, as measured by attached thermistors, can vary by greater than ten degrees from near the top to the bottom of the cell.
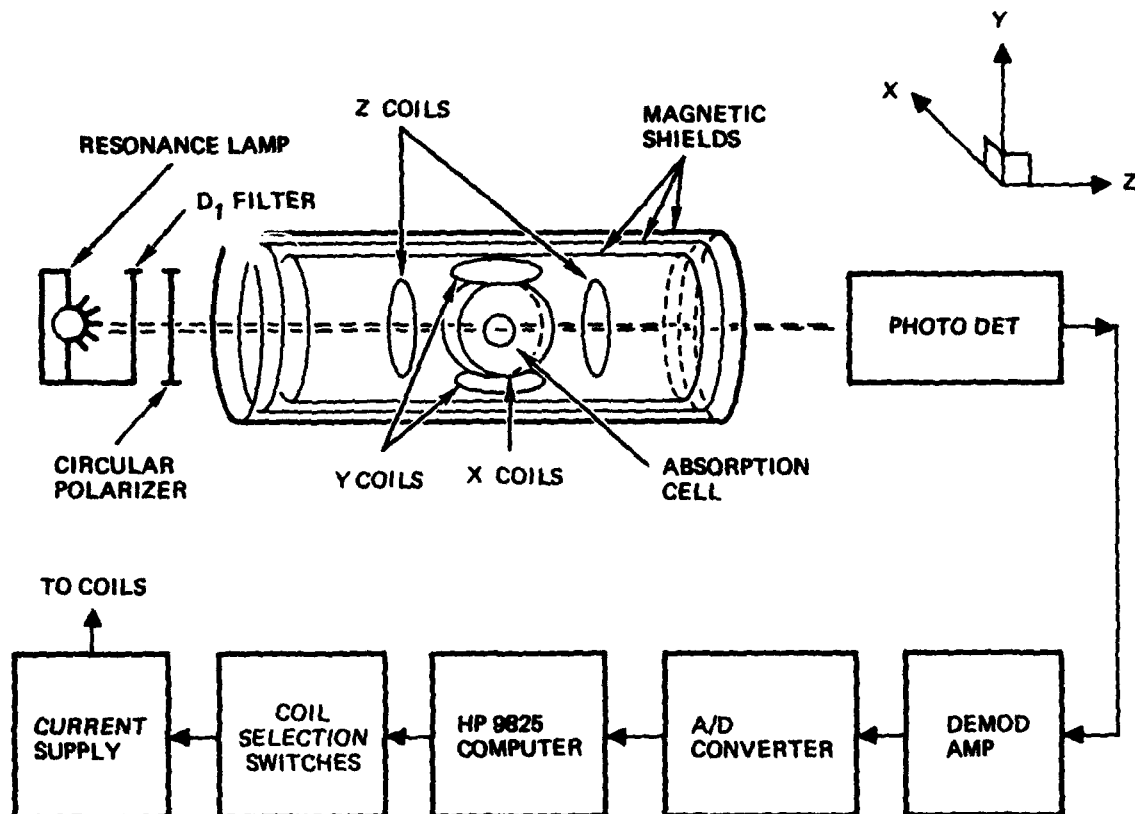
Figure 2-2.   Schematic Representation of the
Experimental Apparatus
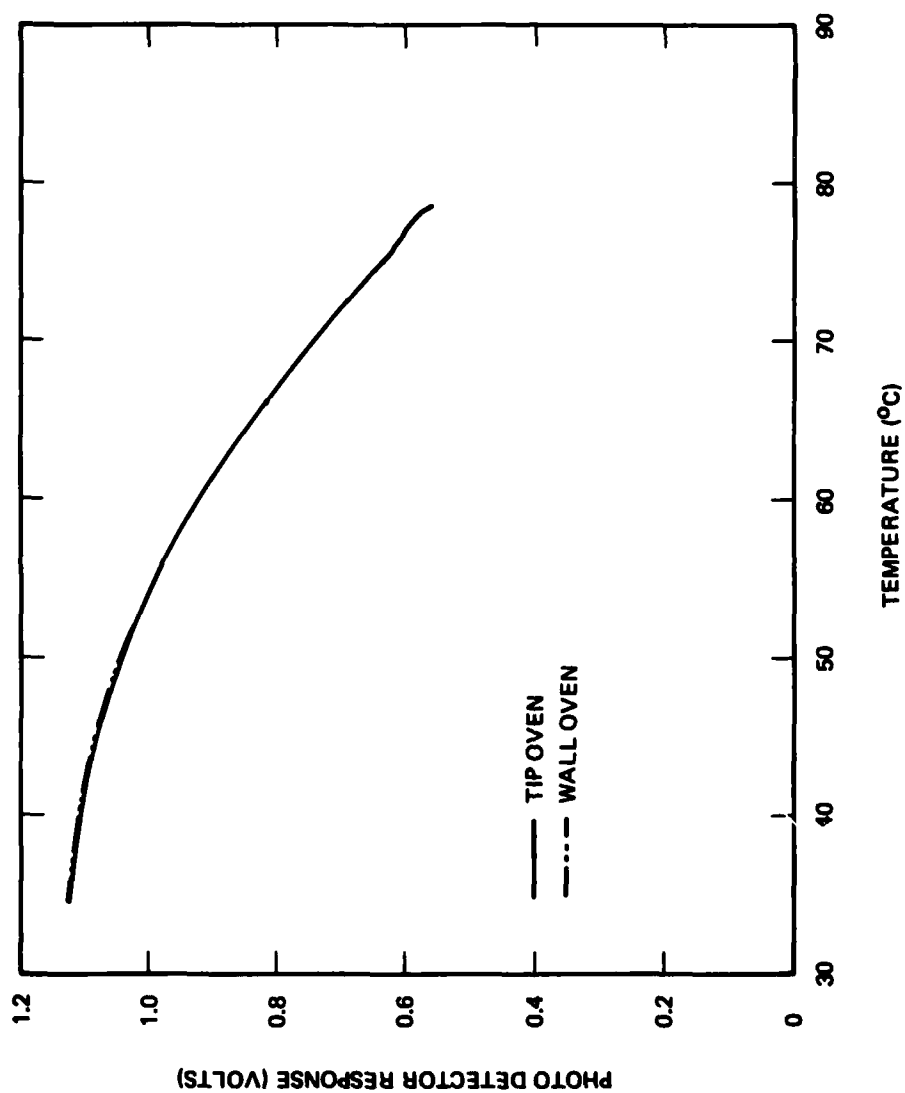
Figure 2-3. Rubidium Density Control Calibration Curves

GUIDANCE & CONTROL SYSTEMS
Litton 5500 Canoga Avenue, Woodland Hills, California 91365

Having established a calibration curve under a given set of
conditions (specific cell in place, resonance lamp and photo
detector bolted down, resonance lamp operating at a uniform
level) it is possible to carry out the double oven experiment of
interest. A program written for the HP-9825 aids in setting the
desired DC light level. The steady-state temperature condition
is arrived at in 1-2 hours and the system is ready for an ex-
periment. To date, the types of experiments carried out in the
double oven apparatus have been the normal transverse relaxation
time experiment and the pump time experiment.

The normal transverse relaxation time experiment, described in
detail in Section III, has the precession axis normal to the
light beam. The pump time experiment measures the longitudinal
relaxation time by monitoring initial amplitude of the free in-
duction decay in the normal experiment versus time of polariza-
tion, t . The data are fitted to the functional form

$$A(t) = A^{\infty} (1-e^{-t/T_p}) \tag{6}$$

where $A(t)$ is the observed initial amplitude for polarization
time, t. A^{∞} is the asymptotic amplitude and T_p is called the
pump time. Values of A^{∞} and T_p are obtained as parameters by
fitting the data to the form of equation (6). Knowledge of T_p,
the total longitudinal relaxation time, and of T_2, the transverse
relaxation time, are important for gyro operation.

When the experiments are carried out, the computer which runs
the experiment and records the data also records, as part of
those data, the D.C. light voltage. As already discussed, the
zero polarization light intensity, referred to as D.C.$\perp$, is a
measure of the rubidium density. With the field parallel to the

light the steady state polarization, DC $\parallel$, is obtained. The dif-
ference, DC $\parallel$ - DC $\perp$, is a measure of the rubidium polarization.

As the pump time experiments are carried out over a period as
long as 14 hours and at specific steady state temperature set-
tings, a record of any fluctuations in the DC light level over
such time is available in the recorded data. It was discovered
during the course of the pump time experiments that fluctuations
in D.C. light can be a serious source of error in certain cir-
cumstances. The observed light level can change with change of
resonance lamp characteristics, degradation of circular polar-
izers, aging of the cell, or a faulty photodetector. For our
setup it appears that the major challenge is control of the
resonance lamp. Changes in D.C. light level can render the
calibrations meaningless. Fortunately, for the fluctuations en-
countered, an insulation package proved sufficient to damp the
light fluctuations resulting from room temperature changes. The
recorded light levels could be used to assess the reliability of
each run. Subsequent to this series of experiments the entire
resonance lamp assembly was renovated and tuned to a level
where thermal insulation from room temperature fluctuations
was unnecessary.

2.3 EXPERIMENTAL RESULTS AND DISCUSSION

Following double oven studies directed toward equipment design
and testing, program goals were addressed. The original goal of
this research was to establish the contribution of wall effects
to the transverse relaxation of ^{129}Xe and ^{131}Xe. As a starting
point cells containing no ^{131}Xe were investigated in the double
oven apparatus. Figures 2-4, 2-5, and 2-6 show some results for
a pyrex cell containing excess rubidium, 1.0 torr ^{129}Xe, and as
buffer gases, 40 torr N_2, 100 torr He, and 10 torr H_2.

Litton GUIDANCE & CONTROL SYSTEMS
5500 Canoga Avenue, Woodland Hills, California 91365

^{129}XE NMR SIGNAL

RUBIDIUM AT 52 C

WALL TEMP: 53.5 C
T_2 : 342 SEC

WALL TEMP: 86.4 C
T_2 : 551 SEC

RELATIVE SIGNAL

0   100   200   300   400   500

TIME (SEC)
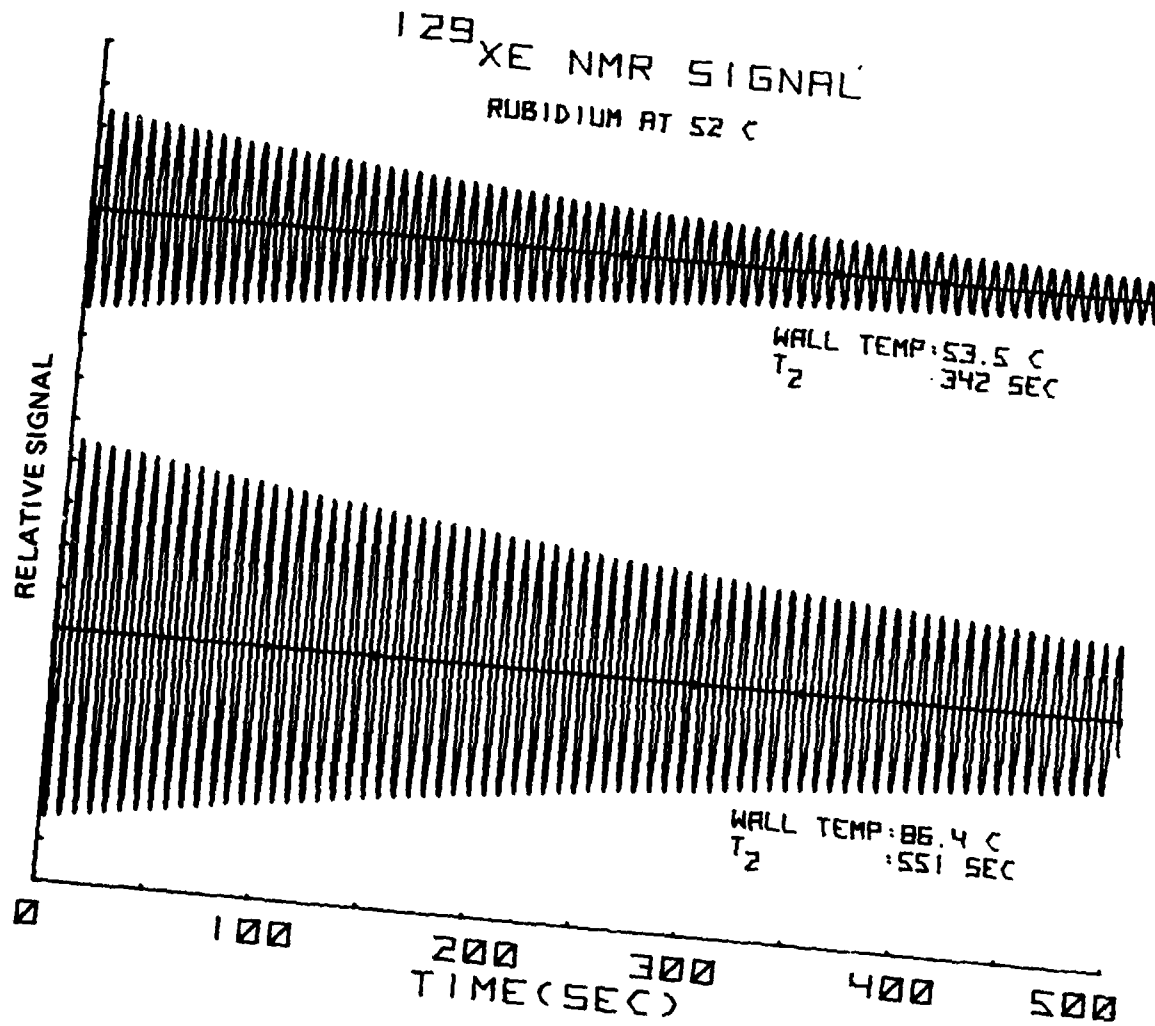
Figure 2-4. Improved Signal to Noise Using Double Oven Apparatus. Traces are 129Xe signal for effective rubidium density temperature of 52°C.

■ **GUIDANCE & CONTROL SYSTEMS**
5500 Canoga Avenue, Woodland Hills, California 91365

FSCM 06481
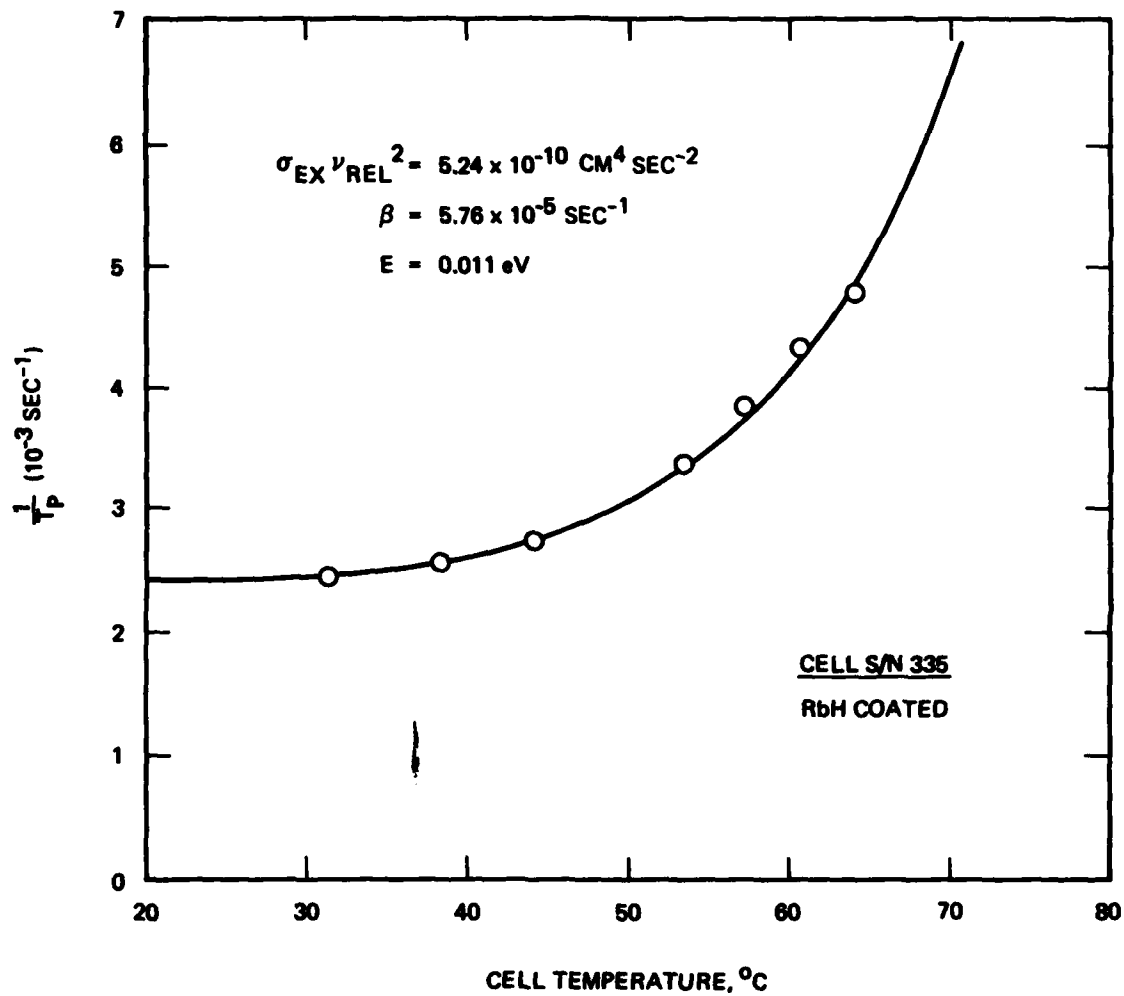
Figure 2-5. Pump Time Relaxation Rate of ^{129}Xe versus Cell Temperature
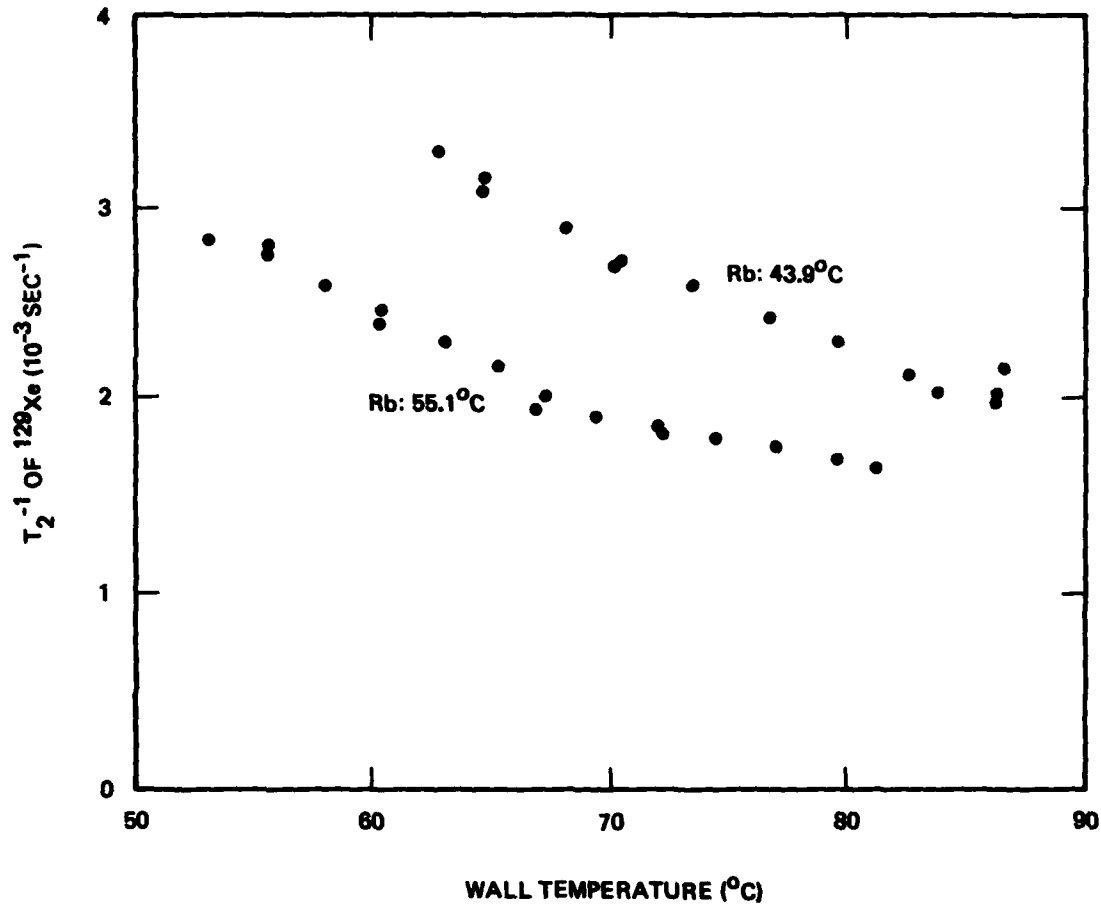
Figure 2-6. Temperature Dependence of ^{129}Xe Transverse
Relaxation Rate at Constant Rubidium Density.
The data are presented for effective rubidium
density temperatures of 43.9 and 55.1°C.

GUIDANCE & CONTROL SYSTEMS
Litton 5500 Canoga Avenue, Woodland Hills, California 91365

In fact, the main purpose for adding the hydrogen gas is to form a rubidium hydride wall coating which appears to provide desired wall characteristics and about which more information is needed. As the temperature dependence for the ^{129}Xe is largely controlled by the first term of equation (1) it was expected that the effect of holding the rubidium density constant while varying the wall temperature would be dramatic.

Of course, there must be some temperature dependence of the wall relaxation itself; and for a spin 1/2 nucleus such as that of ^{129}Xe, that relaxation rate can be modeled by[3]

$$\frac{1}{T_2 \text{ wall}} = \beta \, e^{2E/kt} \quad . \tag{7}$$

Here E is the adsorption energy, k is the Boltzman constant, T is the cell wall temperature, and β is a parameter shown to be:

$$\beta = (\frac{S}{V}) \, \frac{\overline{V}_{129}}{2} \, (\gamma \, \overline{H}_\ell \, \tau_s^{\,o})^2 \quad . \tag{8}$$

Here (S/V) is the microscopic wall surface to volume ratio, γ is the gyromagnetic ratio of the noble gas, $\overline{H}_\ell$ is the effective local magnetic dipolar field at the wall surface, $\overline{V}_{129}$ is the ^{129}Xe velocity and $\tau_s^{\,o}$ is the high temperature sticking time which is on the order of 10^{-13} sec. In the event that f(t) has the form of the wall relaxation rate and the rubidium density is held constant, equation (1) becomes:

$$\frac{1}{T_2} = \frac{X_1}{\sqrt{T}} + X_2 \, \sqrt{T} \, e^{2E/kT} \tag{9}$$

where X_1 and X_2 are constants.

The temperature dependence of equation (9), although present in both terms, is in sharp contrast to a form including the temperature dependence of equation (5) which would provide an additional factor in the first term of equation (9) of the form

$$X'T^{-2.45} 10^{-4560/T}$$

Where X' is a constant.

Figure 2-4 shows an example of the improvement in signal-to-noise which can be obtained using the double oven technique. Illustrated are typical free induction decay spectra for the cell described. These traces are for a rubidium density corresponding to a temperature of 52°C. The upper trace is for uniform wall and tip temperature and exhibits a decay time of 342 sec while the lower trace taken at elevated wall temperature exhibits a decay time of 551 sec and a larger initial amplitude. This represents an important advance, for although the apparent initial amplitude of the noble gas polarization can increase and then decrease as a function of temperature, in fact the relaxation times are seen to decrease with temperature due to the strong influence of the spin exchange term in the relaxation rate. Both improved amplitude and longer decay times are desired for optimizing gyro cells, and both have been improved in this experiment as figure 2-4 demonstrates.

Figure 2-5 shows the results of a pump time experiment taken over a limited temperature range for the same cell. In this particular case the wall and tip temperature are the same, and this is not a double oven experiment. These data show, however, the typical temperature dependence for the relaxation. In this case it is found that $T_2 \cong T_p$. The parameters listed in figure 2-5 are the results of a fit to the functional form of equation (1)

with $f(t)$ as given by equation (7) and are typical of results obtained in such systems. More results of this type are presented in Section V. The important point here is to compare figure 2-5, showing typical non double oven temperature dependence with figure 2-6 showing the results of the double oven experiment. Figure 2-6 plots transverse relaxation rate versus cell wall temperature for two different values of rubidium density corresponding to whole cell temperatures of 55.1°C and 43.9°C. Note that the values of the transverse relaxation rates are confined to a band of about 1.3×10^{-3} to 3.3×10^{-3} sec^{-1} corresponding to a range of 55°C or lower in figure 2-5. Also note in figure 2-6 that from wall temperatures of about 60°C on up, longer relaxation times have been achieved by using the double oven technique. Comparison of figures 2-5 and 2-6 presents a good understanding of what the double oven technique promises to provide for sorting out effect of wall relaxation. Because of complications in separating effects other than wall relaxation and taking into consideration the admittedly large errors in assigning the wall temperatures attempts to provide a fit to the data in figure 2-6 have been inconclusive. Some of the complications are discussed in the next section of this report, and work aimed at separating various other relaxation mechanisms is in progress.

Finally some double oven results, showing the same sort of effect for ^{131}Xe as for ^{129}Xe are presented here. Figures 2-7, 2-8, 2-9, and 2-10 show some results for a cell containing excess rubidium, 0.2 torr ^{129}Xe, 0.8 torr ^{131}Xe, 100 torr He, 40 torr N_2, and 10 torr H_2. Each figure represents a breakdown of the original data taken with a particular set of conditions. The top trace is the reconstructed ^{131}Xe signal from the computer analysis of the raw data while the lower trace is that for ^{129}Xe. Both transverse and longitudinal relaxation times are indicated.
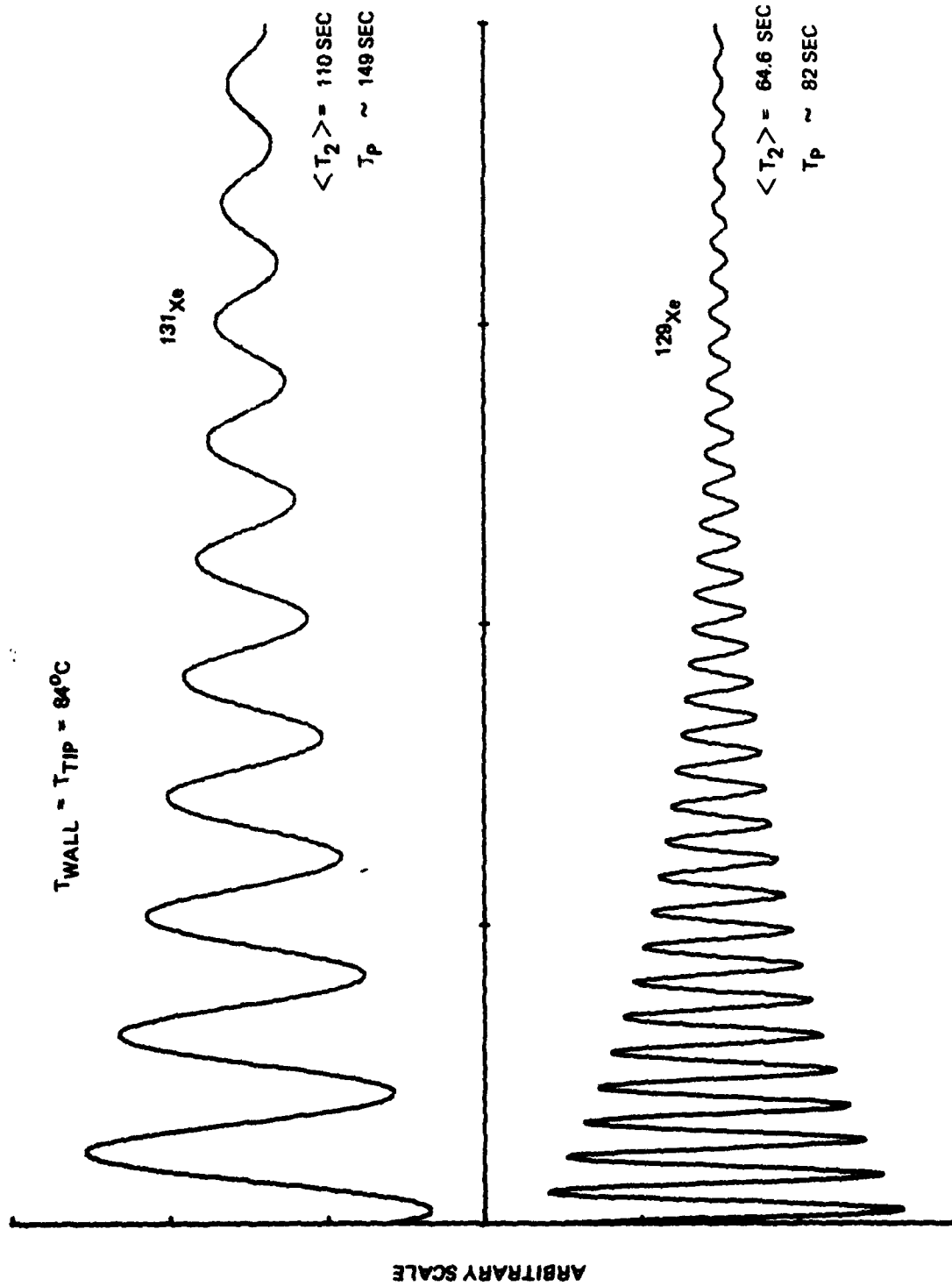
Figure 2-7. Typical Decay Traces for ^{131}Xe and ^{129}Xe when the Entire Cell is at Elevated Temperature

$T_{WALL} = T_{TIP} = 56.1^{\circ}C$

^{131}Xe

$\langle T_2 \rangle = 102$ SEC

$T_P \sim 181$ SEC

^{129}Xe

$\langle T_2 \rangle = 150$ SEC

$T_P \sim 172$ SEC

ARBITRARY SCALE
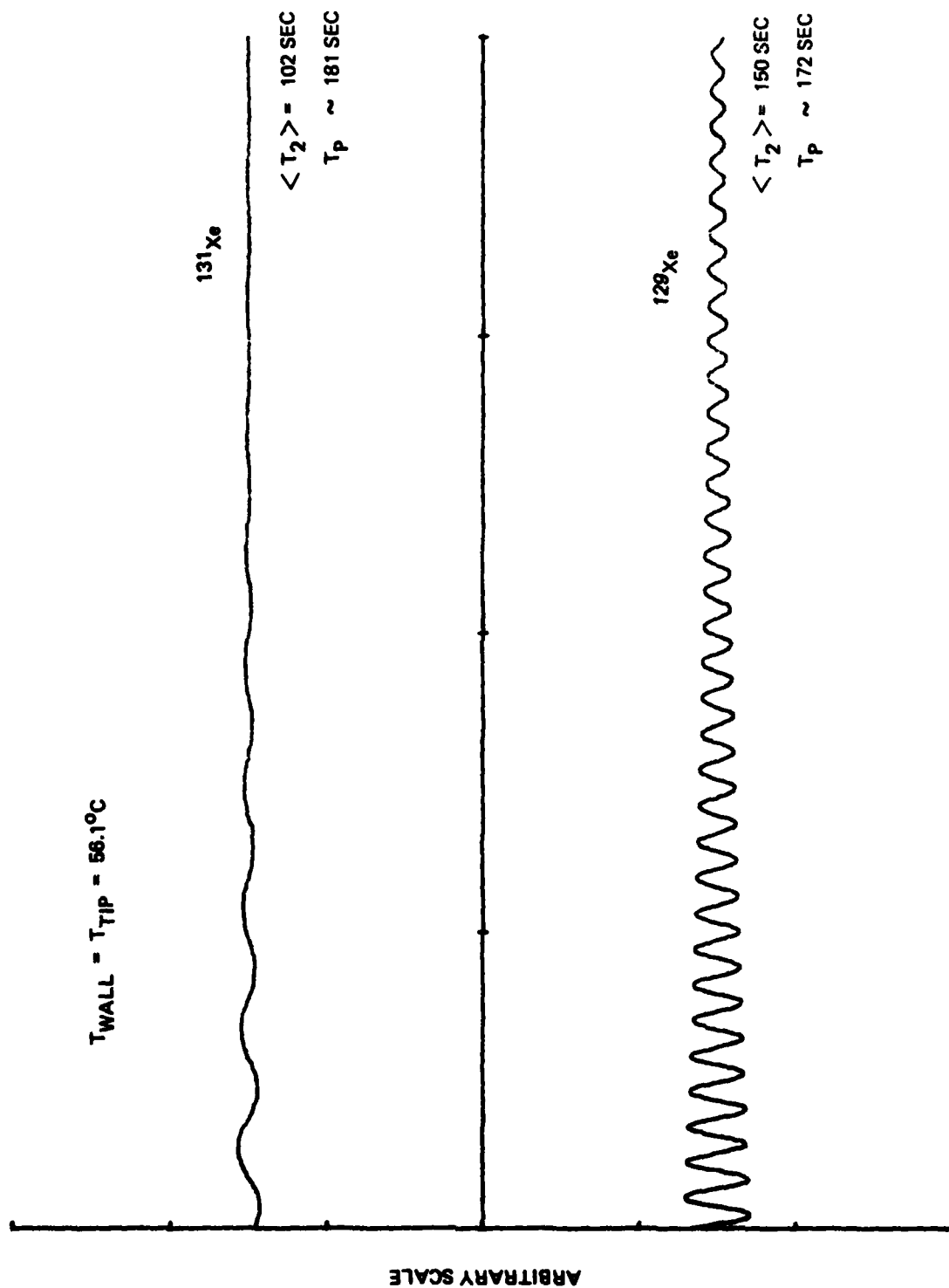
Figure 2-8. Typical Free Induction Decay Traces for ^{131}Xe and ^{129}Xe for a Case in which Entire Cell is at a Relatively Low Temperature
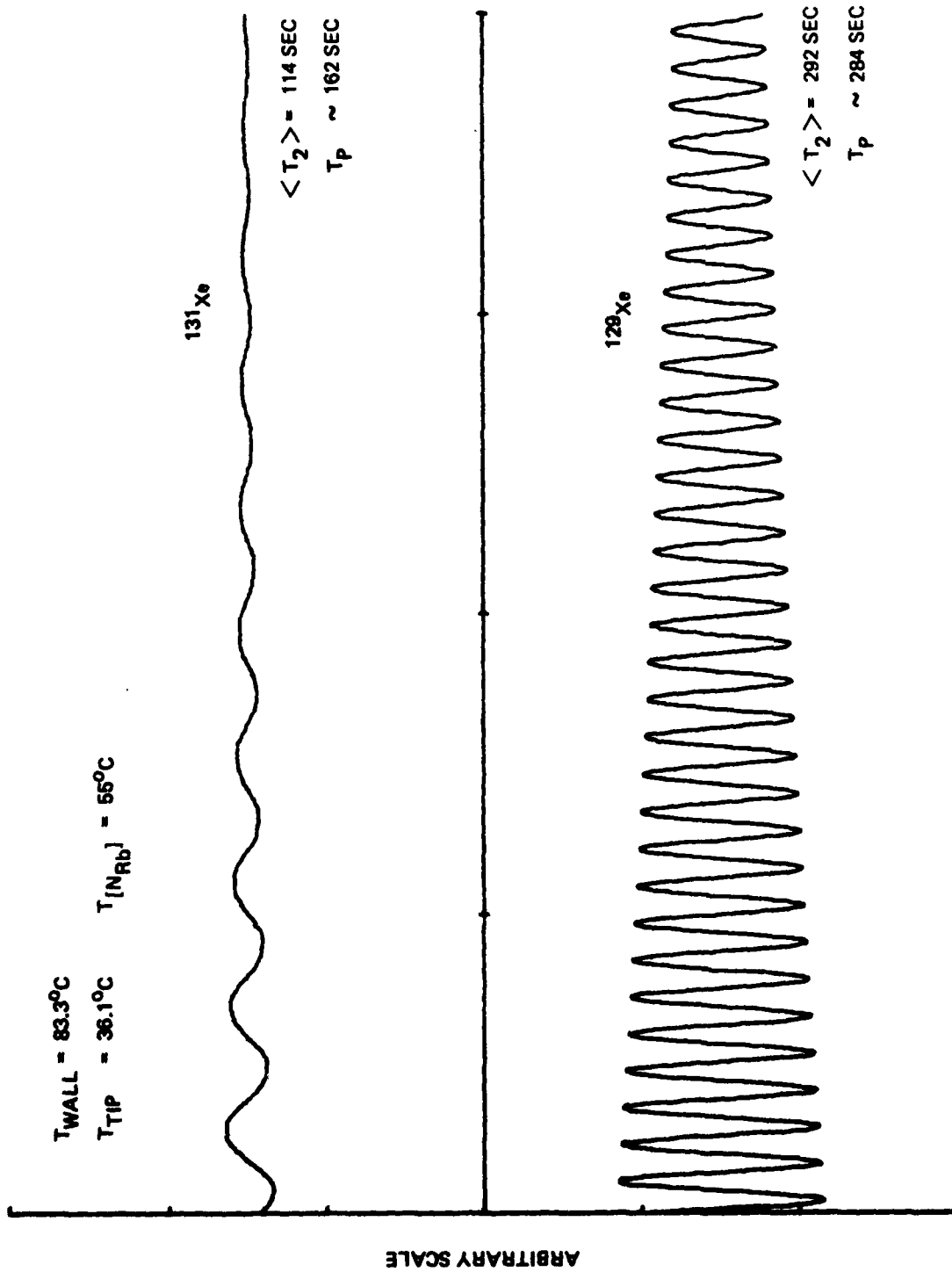
Figure 2-9. Typical Decay Traces for ^{131}Xe and ^{129}Xe at Elevated Wall Temperature in Double Oven Experiment
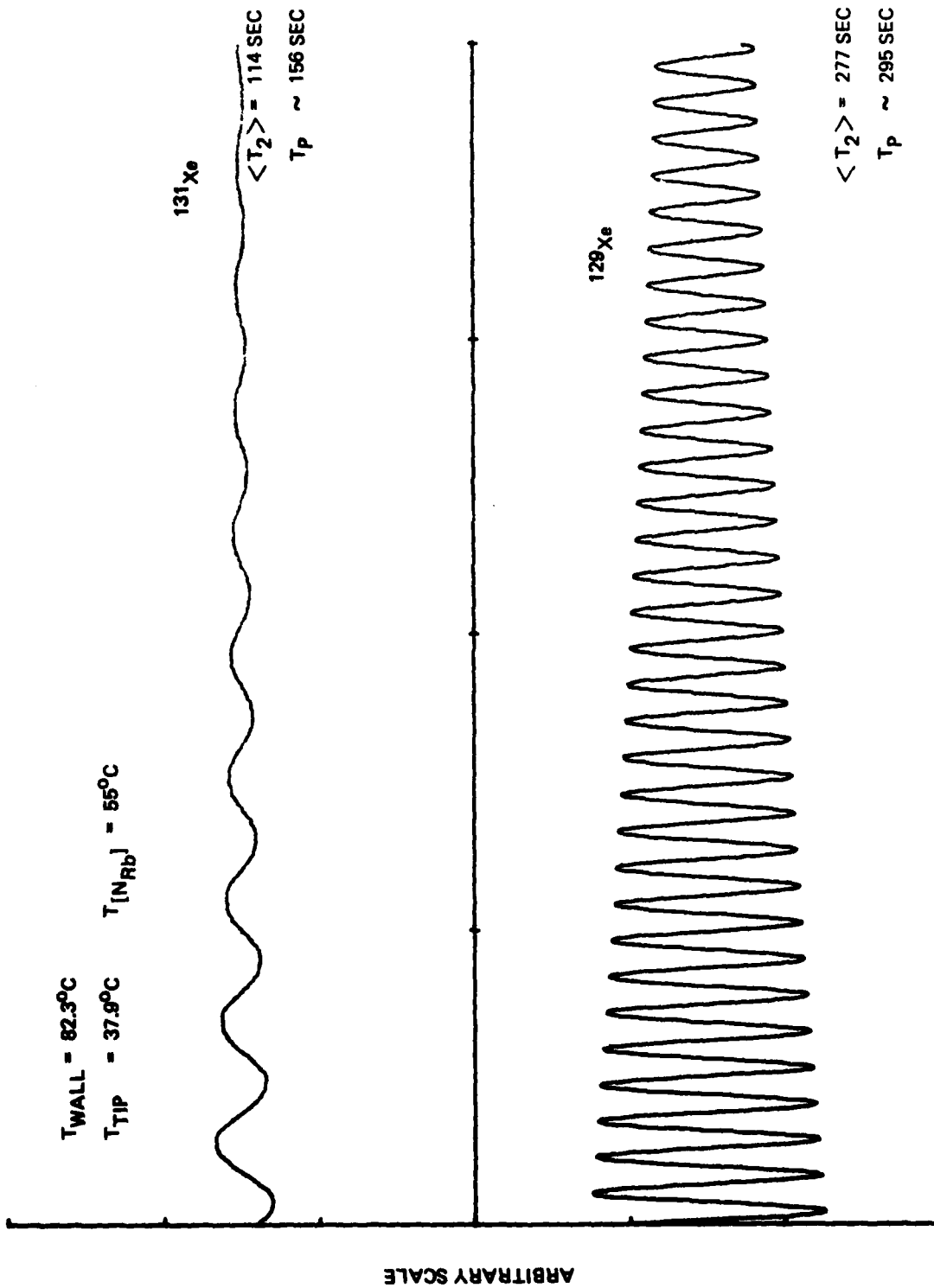
Figure 2-10. Typical Decay Traces in Double Oven Experiment
(Compare with figure 9)

GUIDANCE & CONTROL SYSTEMS
Litton 5500 Canoga Avenue, Woodland Hills, California 91365

Because of D.C. light fluctuations over the course of these experiments an error as large as 20% should be assigned to values of T_p. Figures 2-7 and 2-8 represent typical non-double oven experiments. Figures 2-8, 2-9, and 2-10 are on the same scale. Experimental details precluded putting figure 2-7 on that same scale. Nevertheless, the experimentally observed initial amplitudes for figure 2-7 are greater than in figure 2-8 as is typical of spectra at those different temperatures. Figures 2-9 and 2-10 represent double oven runs in which the rubidium density corresponds to about $55^{\circ}C$, but the wall temperature is $82-84^{\circ}C$. Figures 2-9 and 2-10 demonstrate the reproducibility of the double oven experiment. Either of those figures in comparison with figure 2-8 shows an improvement in signal-to-noise for both isotopes of xenon just as figure 2-4 demonstrates for ^{129}Xe alone. For the samples studied here, however, the temperature variation of ^{131}Xe transverse and longitudinal relaxation time is not large whether or not the rubidium density is held constant (cf. Section V). Furthermore, in the samples studied it is observed that $T_p > T_2$ for ^{131}Xe whether ordinary or double oven experiment is applicable while, within experimental error, $T_p \cong T_2$ for ^{129}Xe for both types of experiment.

The difference in pump time versus T_2 for ^{131}Xe, known to be relaxation due to quadrupolar interaction[4], can be interpreted as a geometrical effect due to the nonspherical nature of the sample cell. The somewhat smaller improvement in signal strength for ^{131}Xe as compared with ^{129}Xe in the double oven experiment is consistent with the temperature dependent relaxation results presented in Section V. For this particular cell the relaxation rate is fairly insensitive to spin exchange effects over the temperature range investigated.

GUIDANCE & CONTROL SYSTEMS
Litton 5500 Canoga Avenue, Woodland Hills, California 91365

FSCM 06481

In summary, significant progress has been made in refining the double oven technique. Initial experimental results are extremely encouraging, and a stage has been reached where it should be possible to use this technique to characterize non-spin exchange relaxation mechanisms.

2.4 CONSIDERATIONS FOR FUTURE WORK

The double oven technique can be used to help characterize wall relaxation for a series of new cell coatings. Several new kinds of surfaces such as mixed alkali hydride on glass surfaces and very high purity water-free quartz with or without hydride coatings are to be investigated.

The ability to achieve higher wall temperatures for a given rubidium density, i.e., a greater wall-tip temperature difference may aid in producing more accurate wall parameters. A wall-tip difference of 55° has more recently been accomplished through cooling the air blown over the tip.

2.5 BIBLIOGRAPHY

1. R.M. Herman, Phys, Rev. 137, A1062 (1965).

2. C.J. Smithells, Metals Reference Book (Butterworths, London, 1962), Vol. 2, p. 655.

3. W.A. Fitzsimmons, L.L. Tankersley, and G.K. Walters, Phys. Rev. 179, 156 (1969).

4. T.M. Kwon, T.G. Mark, and C.H. Volk, Phys. Rev. A 24, 1894 (1981).

GUIDANCE & CONTROL SYSTEMS
Litton 5500 Canoga Avenue, Woodland Hills, California 91365

FSCM 06481

SECTION III

NOBLE GAS NUCLEAR SPIN RELAXATION AND FREQUENCY SHIFTS IN ^{87}Rb - ^{129}Xe OPTICAL PUMPING EXPERIMENTS

3.1 INTRODUCTION

Frequency shifts due to alkali atom polarization in spin-exchange optical pumping experiments for electron-alkali atom systems have been observed experimentally[1,2,3] and treated theoretically[3]. In those experiments, electron-alkali atom spin exchange was demonstrated to be a dominant mechanism for electron spin relaxation and hence the major contribution to electron resonance line width. The spin exchange collisions resulted also in an observed frequency shift of the resonance line depending on the use of right or left circularly polarized light for optical pumping. The theory predicts no change in linewidth as a function of sense of light polarization, however, and none was reported.

In this Section, frequency shift experiments for which the relaxation, and hence linewidth, of ^{129}Xe (nuclear spin 1/2) involved in spin exchange with an alkali atom changes as a function of sense of light polarization are reported. It is shown that this additional relaxation cannot be explained on the basis of spin exchange (including any molecular formation), cell wall relaxation, or buffer gas relaxation. Rather the anomalous relaxation effects result from field gradients experienced by the noble gas as a result of non-uniform alkali metal polarization across the sample cell. In order to demonstrate this effect, two different types of transverse relaxation experiments were performed. In the first type of experiment the axis of quantization defining the longitudinal direction for the precession of nuclear spins was chosen normal to the optical

pumping light direction. In the second type of experiment the axis of quantization was chosen along the light axis as is typical of frequency shift experiments. In the first type of experiment, referred to here as normal, no frequency shift or relaxation change as a function of choice of sense of light polarization is observed. By contrast, in the second type of experiment definite frequency shifts were observed as a function of choice of σ^+ or σ^- circularly polarized light, and the relaxation times were found to be different for the two different polarizations. Frequency shifts and/or relaxation times are reported not only as a function of polarizers, but also as functions of light intensity and externally applied gradient fields. Experimental results are interpreted as demonstrating that the unusual ^{129}Xe relaxation in the frequency shift experiment arises from non-trivial field gradients along the pump light direction due to ^{87}Rb polarization gradients across the sample cell.

3.2 THEORY

The theory of spin exchange collisions and resulting relaxation and frequency shift effects have been documented[1-7]. The theoretical approach is summarized here. The Hamiltonian for the alkali-noble gas system can be written as the sum of three terms in the spin variables.

$$H = -\hbar\,\omega_S S_Z - \hbar\,\omega_I I_2 + \left[\hbar\,\gamma(R)\,\underset{\sim}{I}\cdot\underset{\sim}{S}\right] \tag{1}$$

where S refers to the electronic spin state of the alkali metal atom (spin 1/2), I refers to the noble gas nuclear spin (1/2 for ^{129}Xe), and ω_S and ω_I are appropriate angular frequencies. The strength of the scalar interaction between spins I and S, following Herman[8], is given by

$$\gamma(R) = \frac{16\pi}{3} \, g_N \, \mu_N \, \mu_0 \, u_1 \, (B)^2 \, \eta(R)^2 / \hbar \tag{2}$$

where g_N is the nuclear g factor, μ_N the nuclear magneton and μ_0 the Bohr magneton. The factor $\left[u_1 (B)\right]^2$ represents the probability density for the alkali electron at a distance from the alkali nucleus equal to the internuclear separation while $\left[\eta(R)\right]^2$ is an exchange enhancement factor. As the scalar interaction drops off rapidly with R, the internuclear separation, we can divide the Hamiltonian into a time independent part given by the first two terms of equation (1) and a time dependent part given by the scalar interaction term. Starting with a basis set of the eigenfunctions of $\underset{\sim}{I}^2$, I_z, $\underset{\sim}{S}^2$, S_z for the free (non-interacting) spins one can, using a density matrix approach, calculate the time development of the spin system[3,5]. This provides explicit expressions for the spin exchange relaxation time as embodied in the third term of equation (1). Specifically, expressions for $<\dot{I}_z>$, the time rate of change of the expectation value of the longitudinal polarization, and $<I^{\pm}>$, the analogous rate of change of the transverse magnetization, are obtained[5-7]. As described previously[9], assuming a mean time between collisions, τ_A, to be much greater than the average collision duration, τ_D, and performing a time average over collision duration one obtains

$$<\dot{I}_z> = T_{ex}^{-1} \left(<I_z> - <S_z>\right) \tag{3}$$

where

$$T_{ex}^{-1} = \left(\frac{1}{2\,\tau_A}\right)\left(\frac{\gamma_{ave}^2 \, \tau_D^2}{1 + \gamma_{ave}^2 \, \tau_D^2}\right) \tag{4}$$

where γ_{ave} is an interaction strength averaged over the collision. This particular derivation is valid for two or three body collisions under the stated assumptions.

Equation (3) includes only the spin exchange (allowing for long τ_D as in molecular formation) relaxation. Note that a term $T_1^{-1} <I_z>$ must be included to account for other relaxation mechanisms. Then a steady state solution to (3) provides

$$<I_z^o> = \frac{T_p}{T_{ex}} <S_z^o> \text{ where } T_p^{-1} = T_1^{-1} + T_{ex}^{-1}. \quad T_p \text{ is called the}$$

pump time, and $<I_z^o>$ and $<S_z^o>$ refer to steady state polarization.

Similarly, the results of the density matrix calculation provide expressions relating to the transverse magnetization. Specifically the equation of motion for $<I^+>$ or $<I^->$ is required. Making the same sort of average over collision duration as described for the longitudinal case, Major[5] obtained

$$<\dot{I}^+> = \frac{-1}{\tau_A} \left[\frac{(\frac{1}{2}) \gamma^2_{ave} \tau_D^2}{1 + \gamma^2_{ave} \tau_D^2} - i <S_z> \frac{\gamma_{ave} \tau_D}{1 + \gamma^2_{ave} \tau_D^2} \right] <I^+> - \frac{1}{T_2'} <I^+> \quad (5)$$

Here T_2', a transverse relaxation from sources other than spin exchange has already been included. We recognize the first term in equation (5), as $-T_{ex}^{-1}$. Rewriting (5) as

$$<\dot{I}^+> = -\left(\frac{1}{T_{ex}} + \frac{1}{T_2'} \right) <I^+> - i \, \Delta\omega <I^+> \quad (6)$$

it is at once apparent that integration of (6) will provide a time dependence of $<I^+>$ damped by a rate $T_2^{-1} = T_{ex}^{-1} + T_2'^{-1}$

and oscillating at a frequency $\Delta\omega$. Equation (6) was obtained without reference to any external fields. An external field, H_z^o, along the longitudinal direction would appear additively in the imaginary part of equation (6)[10] so that the actual

oscillation frequency would be $\dfrac{\omega_z^o}{\gamma} + \Delta\omega$. The source of the

frequency shift is evident in the expression for $\Delta\omega$. Note, however, that it will be necessary to invoke a non-spin exchange relaxation, T_2', to explain changes in relaxation with differing incident light polarization and intensity. Nothing in equations (5) or (6) predicts that the observed transverse relaxation time should change as a function of sign of alkali metal atom polarization.

3.3 EXPERIMENTAL

Shown in figure 3-1 is the experimental arrangement designed to measure the magnetic field experienced by the noble gas nuclei due to spin exchange interaction with optically oriented alkali metal atoms. This apparatus has been described in detail previously[9], and the basic modification made here is that the pumping light can be made left or right hand circularly polarized through use of one of two different polarizers placed in front of the pump light beam. The two polarizers used in this experiment have been tested and found to transmit nearly equal intensity of rubidium D_1 light. The polarized light intensity was measured to be 92% for one polarizer and 96% for the other.

Both types of experiments described here are performed by first polarizing the noble gas nuclear moments along the Z direction. This is shown schematically in figure 3-2a. The rubidium atom magnetic moments are oriented by the absorption of left or right hand circularly polarized rubidium D_1 light, and the ^{129}Xe nuclei are polarized through spin exchange with the rubidium.
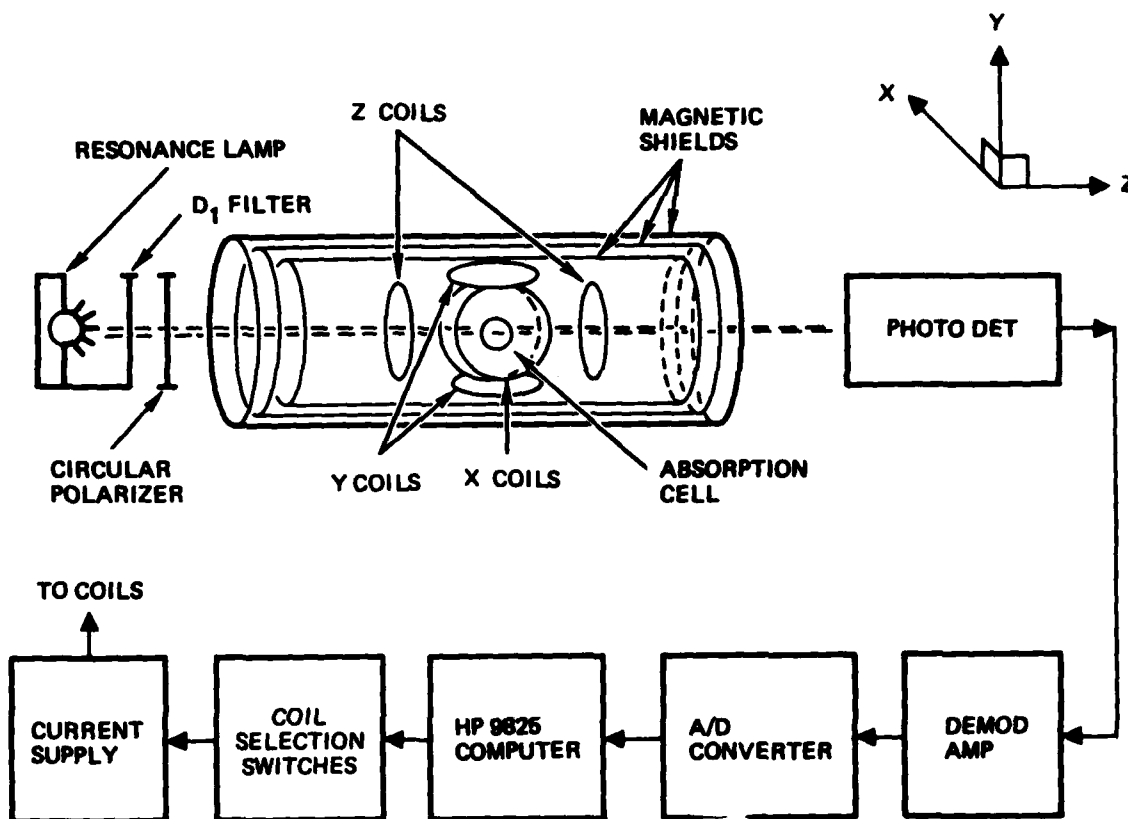
Figure 3-1. Schematic Representation of the Experimental
Apparatus (Note that choice of coordinate system
differs from reference 9.)
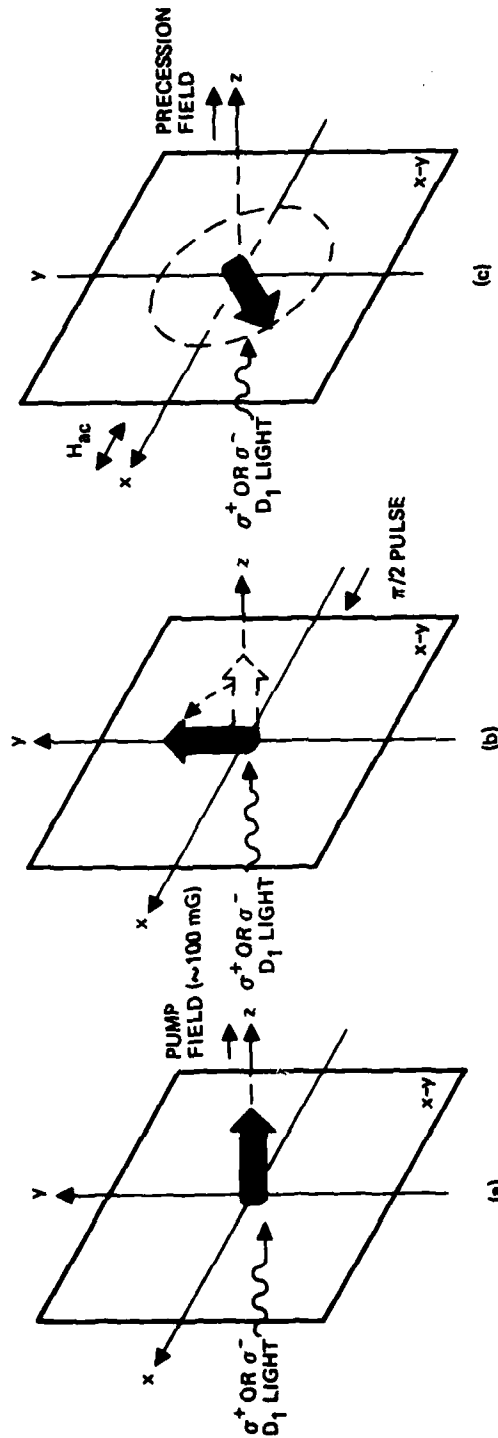
Figure 3-2. Magnetic Field Arrangement for (a) the Longitudinal Pumping of the Noble Gas Nuclear Spin Polarization, (b) Application of $\pi/2$ Pulse, and (c) the Precession of the Polarized Nuclear Spins

The pumping takes place in the presence of a longitudinal magnetic field of approximately 100 mG along the z-axis. The noble gas polarization, I_z, is found to follow the usual pumping law:

$$<I_z(\tau)> = <I_z^O> \{1 - \exp (\tau/T_p)\} \tag{7}$$

The spin system is pumped for a time sufficient to build up the desired magnetization, typically up to ten minutes. For the normal experiment the pump field is then turned off and a precession field is at the same time applied along the y-axis causing the magnetization to precess in the x-z plane. In order to observe the precessing nuclear spin polarization the rubidium vapor is mechanized as a magnetometer which detects magnetic field variations along the x-axis due to the precessing spin system. The form of the observed signal has been shown to be[9]

$$S(\tau) = S^O \exp (\frac{-\tau}{T_2}) \sin (\Omega\tau + \psi) \tag{8}$$

where S^O is the initial amplitude, T_2 is the total transverse decay time, Ω is the precession frequency and ψ is the initial phase. The data are analyzed using a Kalman filter technique which provides as parameters the frequency, phase, transverse relaxation rate, and initial amplitude.

For the second type of experiment, referred to here as frequency shift, the spin system is first pumped as indicated in figure 3-2a using either left or right hand circularly polarized light. After magnetization is established along z the pump field is

turned off and a 90° pulse is applied along x which rotates the magnetization onto the y-axis as illustrated in figure 3-2b. Then a precession field is applied along the z-axis (figure 3-2c). The magnetization precesses in the x-y plane and is observed along x as in the normal type of experiment. Analysis of the observed time development of the spin system again provides initial amplitude, relaxation rate, frequency, and phase. The experiment is then repeated for the other sense of pump light polarization. In this experiment it has been shown that the optically oriented rubidium vapor acts either to increase or decrease the effective precession field experienced by the noble gas ensemble depending on the circular polarizers used in the experiment[7], and it is this experiment which should be compared with the electron resonance results[1-3].

The sample cell used in this study is a 0.7" diameter teardrop shaped cell made of pyrex glass. The cell was baked overnight at 300°C under high vacuum and then filled with 1.0 torr 80% enriched ^{129}Xe, 40 torr N_2, 100 torr He, 10 torr H_2 and an excess of rubidium metal. The sample cell was selected from one of several cells prepared in this way and sealed off with a working flame thermally isolated from the cell body. The rubidium metal was then driven into the tip-off area, and the cells were cured in an oven at 80°C for at least two weeks prior to use.

3.4 RESULTS AND DISCUSSION

Displayed in figure 3-3 are data taken using the normal experiment which exhibit the non-linear relaxation behavior which led to this investigation. Previously it has been assumed that the total transverse decay rate, T_2^{-1}, can be expressed as[9]
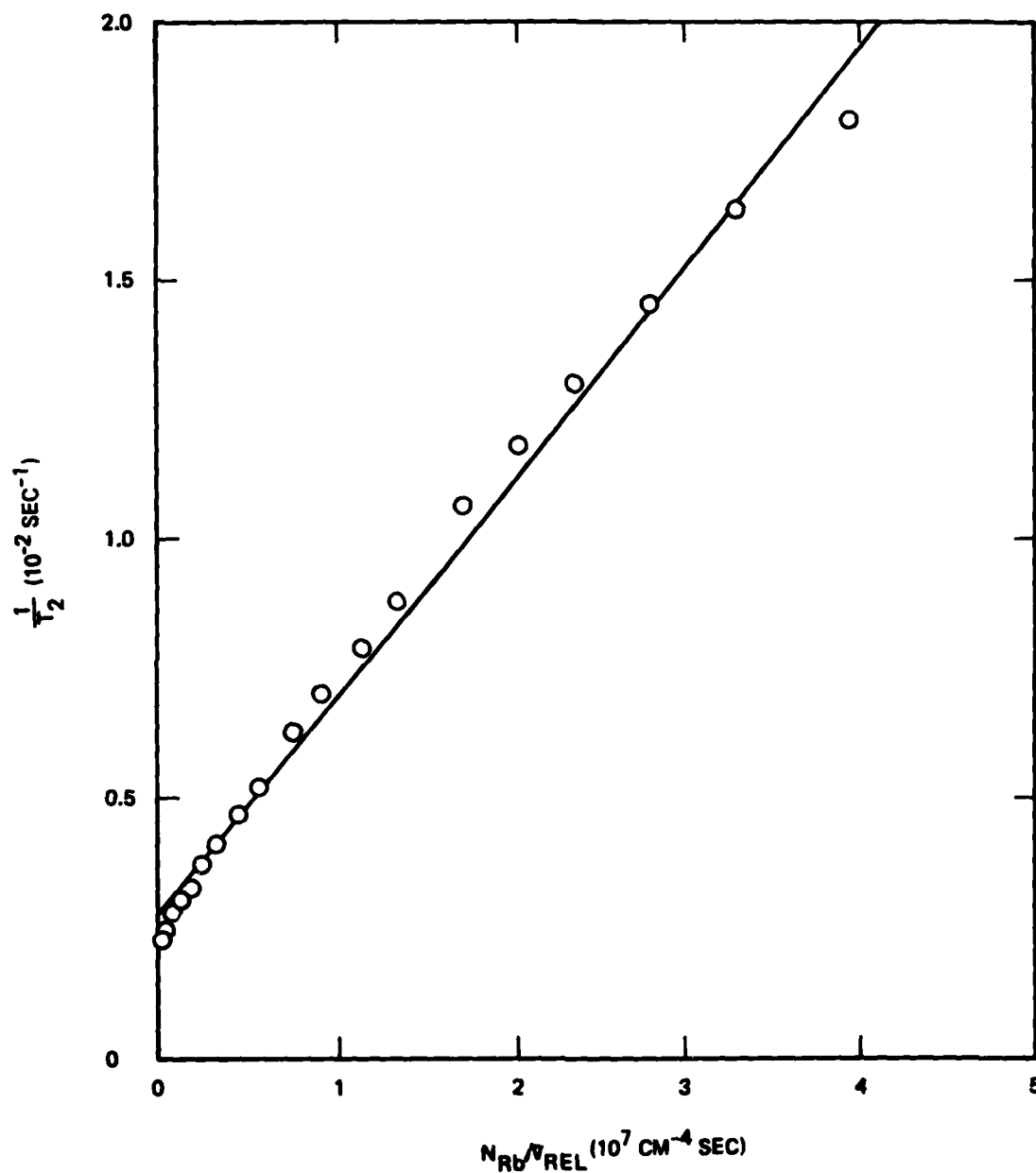
Figure 3-3.   Transverse Decay Rate of ^{129}Xe versus
$N_{Rb}/\bar{v}_{rel}$.   The solid line represents a linear
least-squares fit of the experimental data. A
systematic deviation of the data from the
linear fit can be clearly seen.

$$T_2^{-1} = T_{ex}^{-1} + (T_2')^{-1}$$

$$= N_{Rb}\, \sigma_{ex}\, \bar{v}_{rel} + (T_2')^{-1} \qquad (9)$$

where N_{Rb} is rubidium density, σ_{ex} is spin exchange cross section and $\bar{v}_{rel}$ is the rubidium-noble gas relative velocity. As the spin exchange cross section is inversely proportional to the relative velocity squared[8], a plot of $N_{Rb}/\bar{v}_{rel}$ should, in this model, provide a straight line with slope $\sigma\bar{v}_{rel}^2$ and intercept $(T_2')^{-1}$. Such a linear fit is indicated in figure 3-3. The data displays an obvious deviation from linear behavior. Shown in figures 3-4 and 3-5 are the same data plotted in two different ways and fit with the functional form

$$T_2^{-1} = f(T)\,(C_1 + C_2\, e^{C_3/T}) + C_4 \qquad (10)$$

where

$$f(T)\ \alpha\ \frac{N_{Rb}\,(T)}{\bar{v}_{rel}} \qquad (11)$$

and $N_{Rb}(T)$ is given by[11]

$$\log_{10} N_{Rb} = -4560/_T + 30.98 - 2.45\,\log_{10}T \quad . \qquad (12)$$

The C_i's are constants. In this formulation C_4 represents the zero rubidium density intercept while the first term in paren-thesis in equation (10) represents the spin exchange. The second term in parenthesis represents some other type of relaxa-tion. Note that if this term is replaced by a non-integral
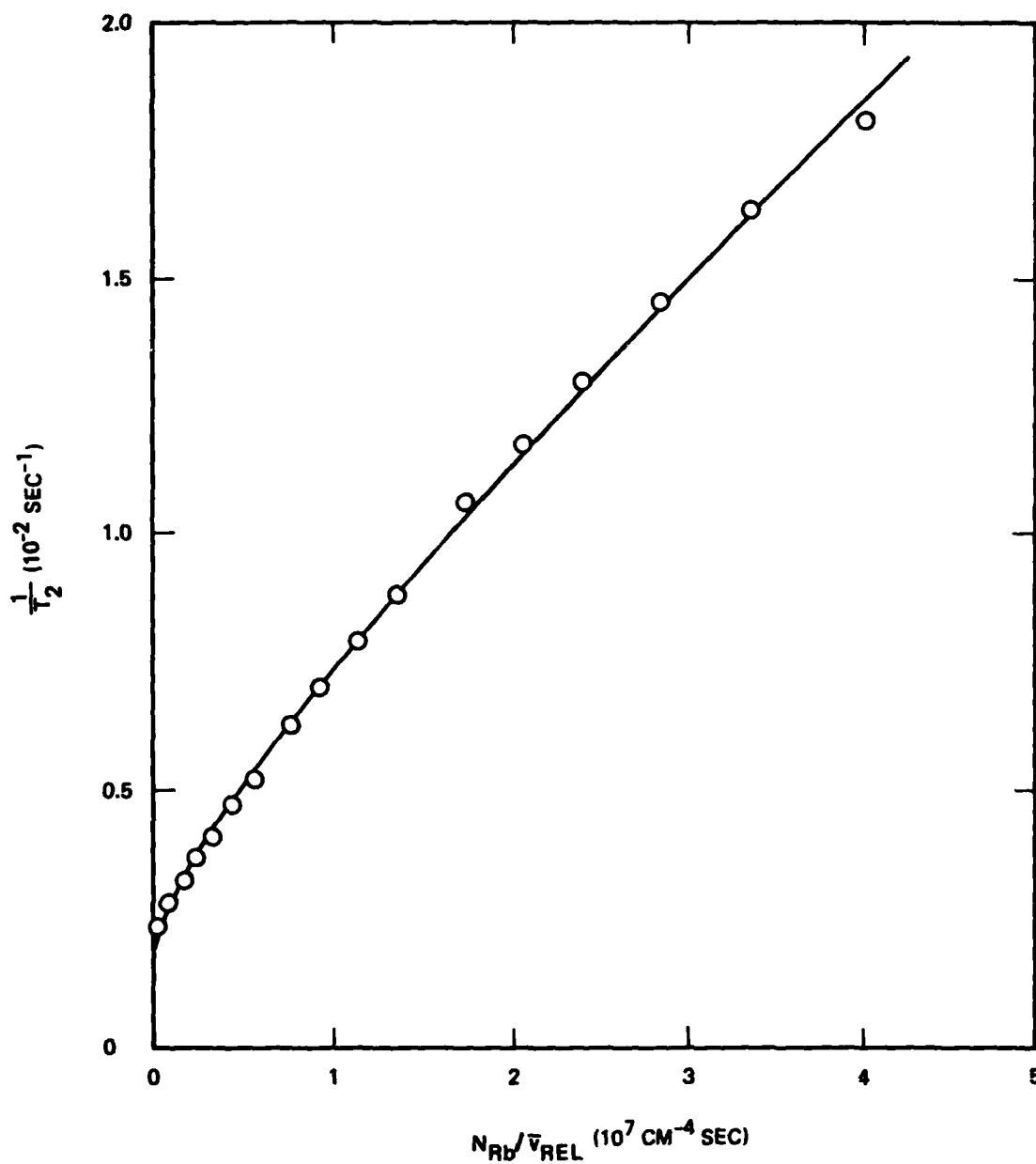
Figure 3-4. Transverse Decay Rate of ^{129}Xe versus
$N_{Rb}/\bar{v}_{rel}$. The solid line represents the least
squares-fit to the functional form of
equation (10) in the text.
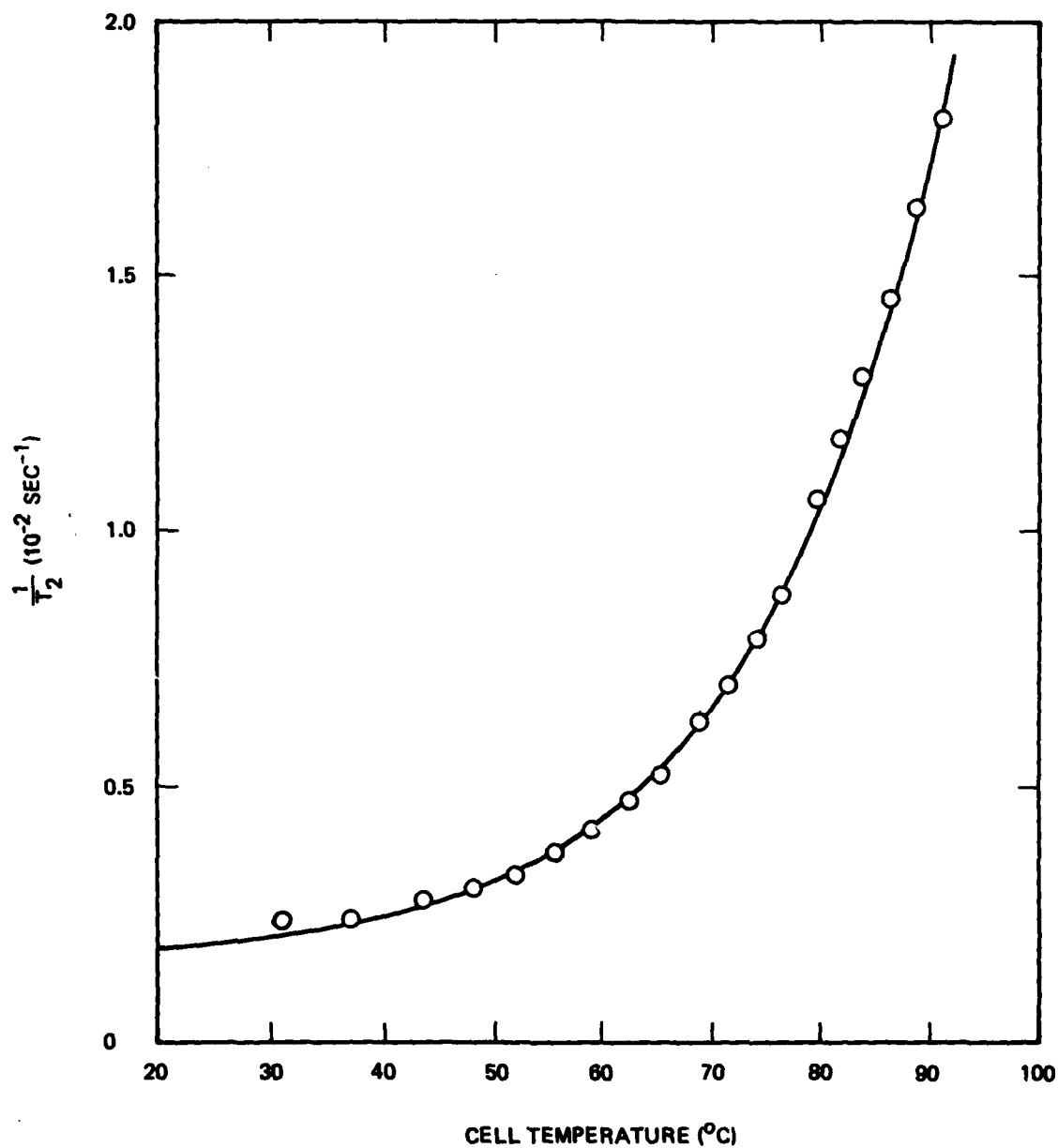
Figure 3-5. Transverse Decay Rate of ^{129}Xe versus Cell
Temperature. The data and the least squares fit
presented in figure 3-4 are replotted as a
function of cell temperature.

3-13

temperature dependence such at $T^{1.75}$ (typical of relaxation due to diffusion through a buffer gas) it is possible to get an equally good fit to the data of figure 3-3. The important point is that equation (10) implies the existence of some relaxation mechanism, other than spin exchange, but also strongly dependent on alkali metal density. Thus wall relaxation which is temperature dependent, but does not depend on alkali metal density[12] must be excluded. Relaxation mechanisms which must be considered include relaxation due to molecular formation and relaxation due to inhomogenous rubidium magnetic field experienced by the noble gas nucleus. It has been demonstrated that molecular formation is an important mechanism[13] and should be considered separately. Because of the dependence on rubidium density, in the approach taken here Rb-Xe molecular formation relaxation is incorporated into the spin exchange term; and it is then desirable to probe possible field gradient effects which were, in the past, assumed due to external gradients alone and characterized by the intercept of equation (10). Previously relaxation due to internal field gradients had been dismissed, but that was in cases where alkali metal vapor density was low and cell volume was large[6].

Prior to looking at relaxation in the frequency shift experiment we will look at the frequency shifts themselves and their implications as far as internal field gradients are concerned. It has been shown[7] that as the spin exchange collision rate, τ_A^{-1}, can be written as $\pi(\bar{d})^2 N_{Rb} \bar{v}_{rel}$ where $\bar{d}$ is the mean interaction distance, and the binary collision duration can be taken as $\tau_D = \bar{d}/\bar{v}_{rel}$, it is possible using equations (2) and (5), to write an expression for the additional field due to rubidium polarization as

$$\Delta H = \frac{16 \pi^2}{3} (\overline{d})^3 N_{Rb} \mu_0 \overline{u_1 (B)}^2 \overline{\eta (R)}^2 <S_Z> . \quad (13)$$

This expression was derived for exchange processes of the binary type under the assumption that $\gamma_{ave} \tau_D \ll 1$ and does not take into consideration any molecular forming, three body collisions. However, it has been shown that a molecular forming collision will produce a frequency (or field) shift proportional to the product of the molecular formation rate and the rubidium polarization[7]. In the concentration ranges considered here the molecular formation rate would be expected to be proportional to the alkali metal density so one would predict a total field or frequency shift proportional to $N_{Rb} <S_Z>$, and the inclusion of molecular formation in the spin-exchange interaction for the purposes of these experiments is justified.

In the frequency shift experiment, then, a precession field is applied along the z-axis (figure 3-2) and the optically oriented rubidium vapor acts directly either to increase or decrease the effective precession field as experienced by the noble gas ensemble, depending on the circular polarizers used in the measurement. The precession frequency of the ensemble of the noble gas nuclei is, correspondingly, increased or decreased such that

$$\omega_A \approx -\gamma (H_0 - \Delta H) \quad (14a)$$

$$\omega_B \approx -\gamma (H_0 + \Delta H) \quad (14b)$$

where H_0 is the magnetic field applied externally and ΔH is the additional field experienced by the noble gas nuclei due to the spin exchange interaction. The subscripts A and B refer to the

two different circular polarizers. By measuring the precession frequencies, ω_A and ω_B, ΔH is obtained.

The dependence of the precession frequency at a constant rubidium density as a function of light intensity, and hence polarization, is displayed in figure 3-6. The symmetric nature of the frequency shift about the central frequency is apparent in accordance with the simple picture presented in equation (14) and the theoretical prediction outlined in equations (5), (6) and (13). Incidentally, note that the equations do not predict a frequency shift for the normal experiment. This can be understood by considering that for the normal experiment equation (5) is subject to a coordinate transformation with the imaginary term S polarization then directed along y. As there is no $<S_y>$ polarization developing along y no frequency shift is predicted in the normal experiment and none is observed experimentally. Relaxation effects, however, present a more complicated picture.

In figure 3-7 are shown relaxation time data from the same experiment as shown in figure 3-6. There is a clear dependence of relaxation time on polarization light intensity and polarizer in the frequency shift experiment. Figure 3-8 shows that there is also a dependence on alkali metal density for both types of experiment. We note several trends. In the frequency shift experiment the relaxation rate increases as the pump light intensity increases for a given polarizer. This is demonstrated not only in figure 3-7 but also in figures 3-8 and 3-9. However, this effect is not observed in the normal experiment (figure 3-8). Although not shown, the relaxation as a function of rubidium density and/or light intensity using polarizer B is not seen to be different from the results for polarizer A in the normal experiment. In addition, in the frequency shift experiment the relaxation rate increases when the sense of the pumping light polarization is changed from A to B for the same light

GUIDANCE & CONTROL SYSTEMS
5500 Canoga Avenue, Woodland Hills, California 91365
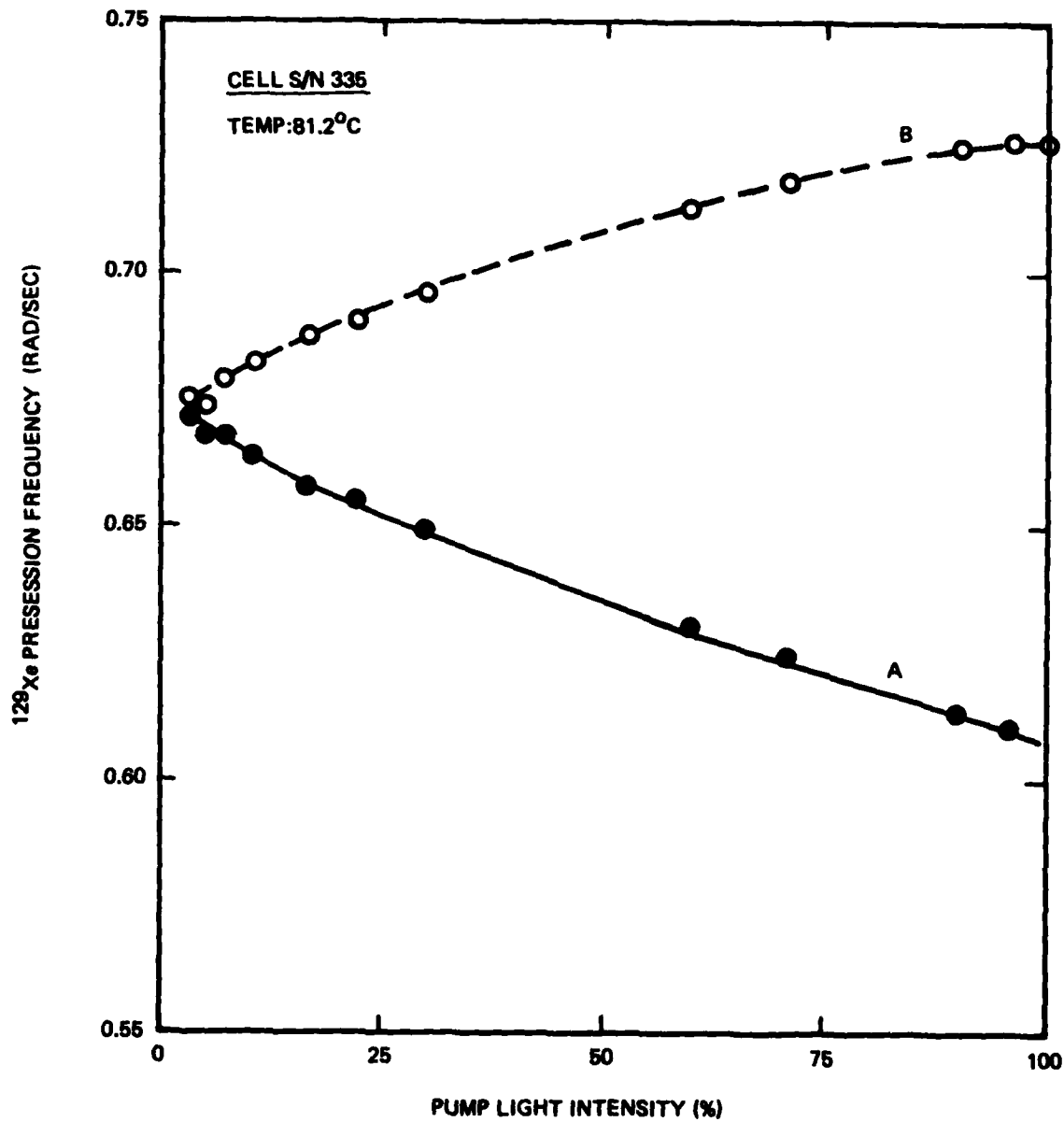
Figure 3-6. ^{129}Xe Precession Frequency versus Rb Pump Light
Intensity as a Function of the Circular Polarizers.
The polarizer A and B refer to σ^{+} and σ^{-} pump
light, respectively.
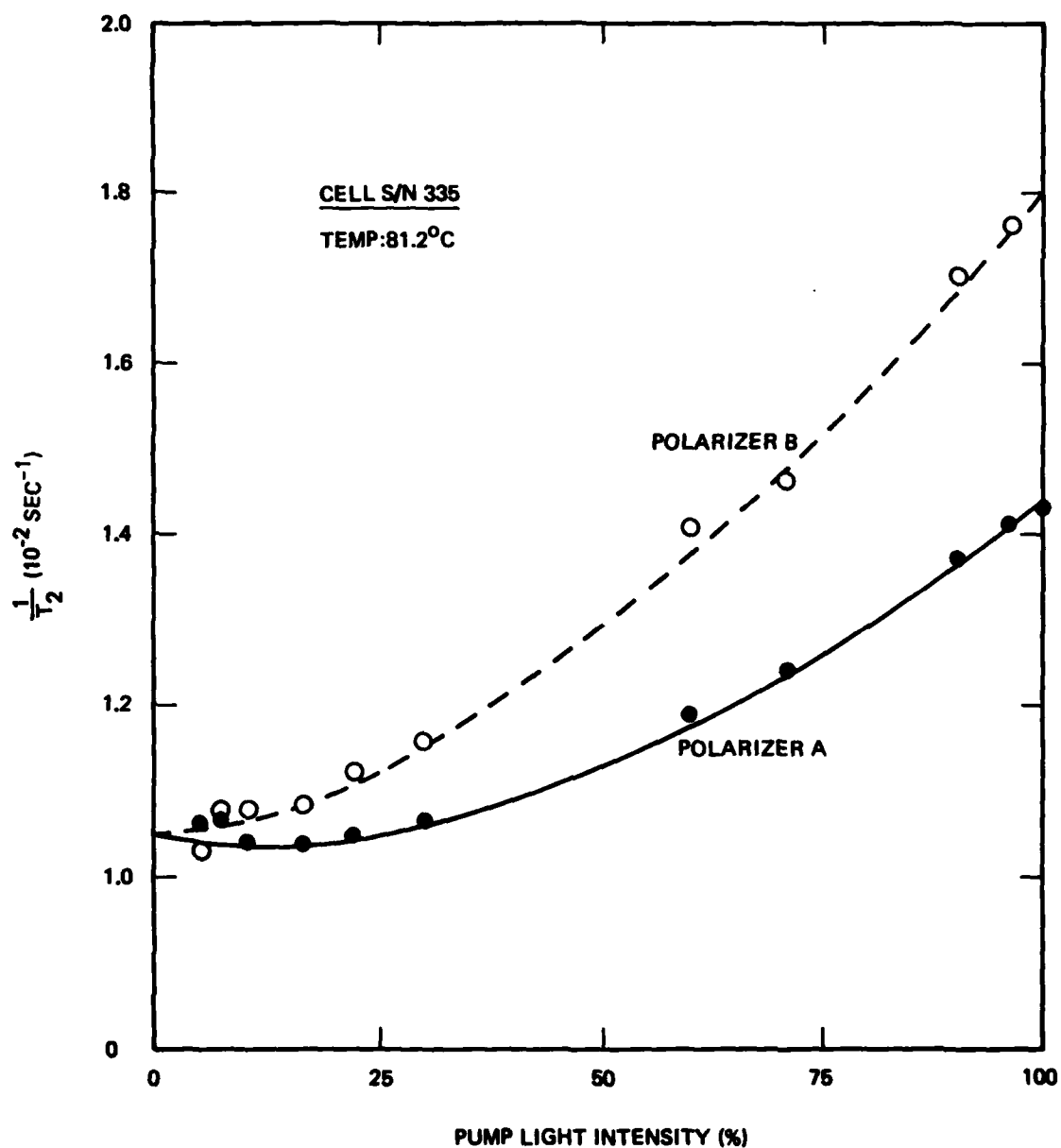
Figure 3-7. Frequency Shift Experiment Showing Transverse
Relaxation Rate of ^{129}Xe versus Rb Pump Light Intensity as a
Function of the Circular Polarizers. The polarizer
A and B refer to σ^+ and σ^- pump light, respectively.
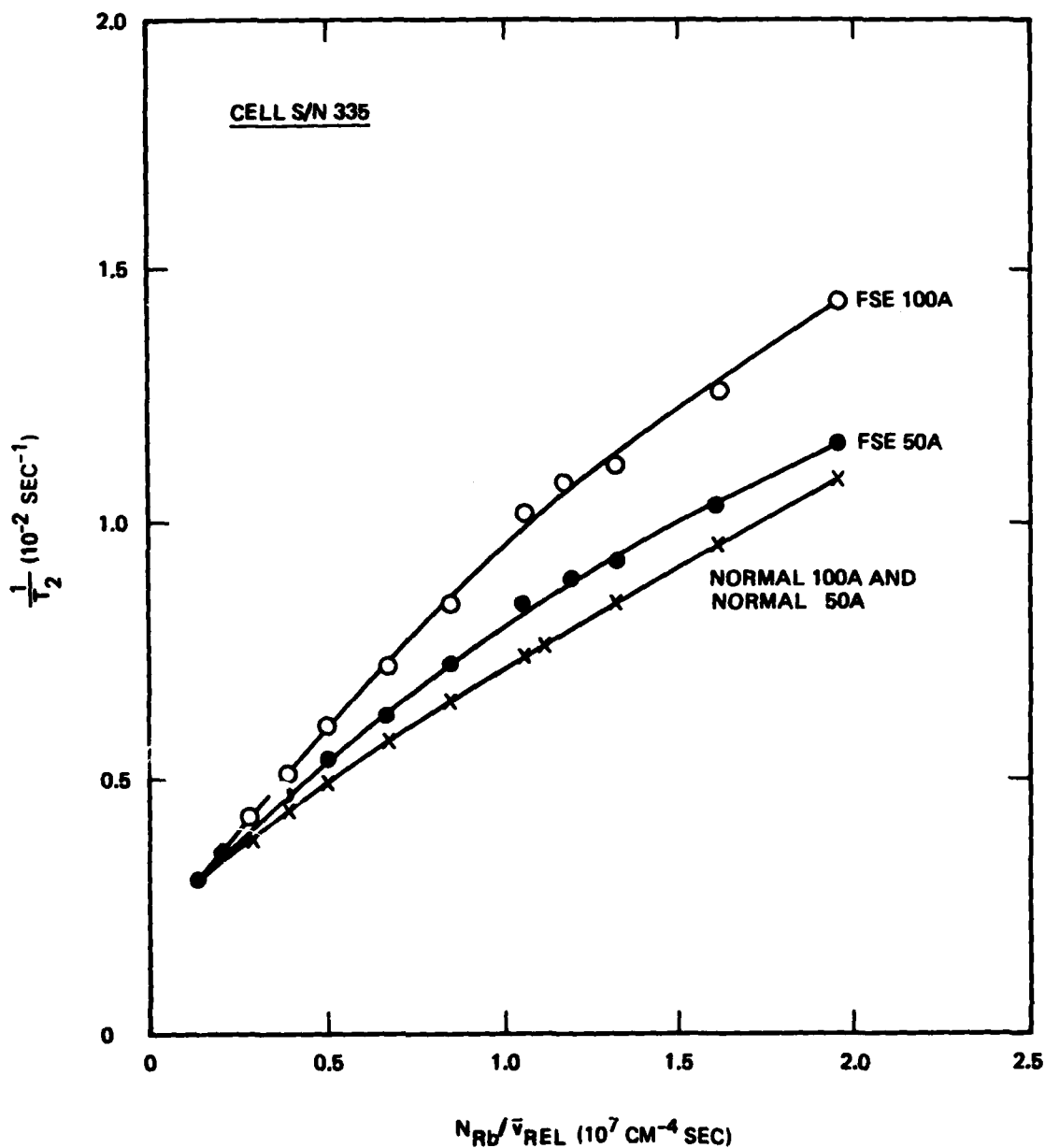
Figure 3-8. Transverse Relaxation Rate of ^{129}Xe versus $N_{Rb}/\bar{v}_{rel}$ as a Function of Pump Light Intensity and the Measurement Mode. Designation 100A refers to 100% light through polarizer A and 50A refers to 50% light through A. "Normal" refers to the normal experiment while FSE stands for frequency shift experiment.

GUIDANCE & CONTROL SYSTEMS
Litton 5500 Canoga Avenue, Woodland Hills, California 91365

FSCM 06481
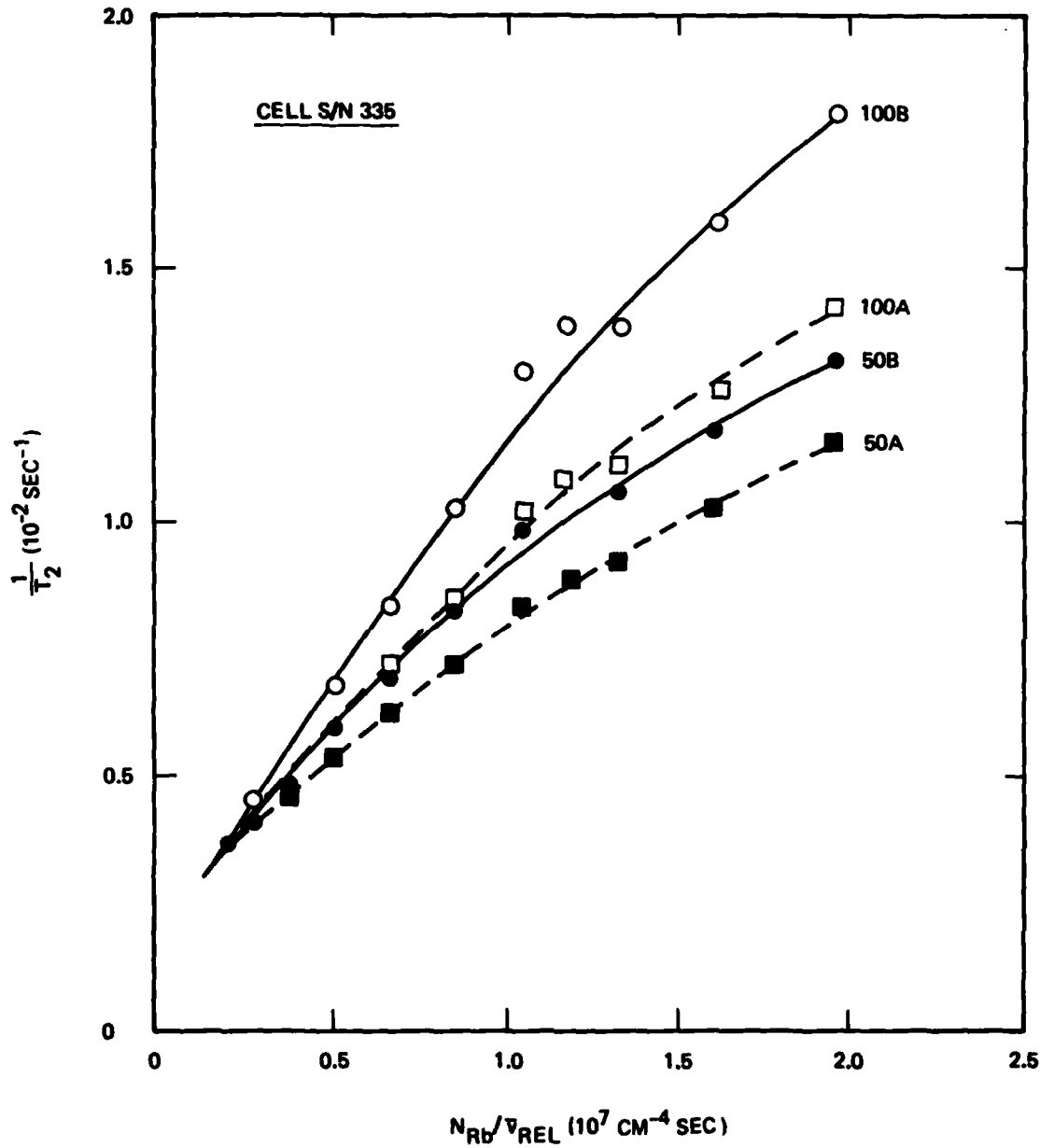
Figure 3-9.   Transverse Relaxation Rate of ^{129}Xe versus
$N_{Rb}/\bar{v}_{rel}$ as a Function of Pump Light Intensity for
A and B Polarizers in the Frequency Shift
Experiment.   Use of A and B polarizers
correspond to σ^+ and σ^- pump light,
respectively.

intensities indicating a dependence of relaxation time on the sense of the rubidium magnetization. These observations suggest that the unexpected trends in ^{129}Xe relaxation in the frequency shift experiments are due to rubidium field gradients experienced by the noble gas. Relaxation due to mechanisms such as molecular formation, diffusion through buffer gas, or wall effects would not be expected to depend on light intensity or sense of rubidium polarization. Further note that the relaxation time is always shorter in frequency shift experiments than in normal experiments, but that all relaxation rates converge to one value at low rubidium densities.

The origin of field gradients across a sample cell can be understood by considering the spacial distribution of rubidium polarization, S_z, across the cell. Legowski[14] has reported results of a calculation of cesium polarization spacial dependence in buffered spherical cells. He has solved, by numerical analysis, the equation for an alkali polarization $<S_z>$ given by

$$\frac{d <S_z>}{dt} = D \nabla^2 <S_z> - k <S_z> + P (1-2 <S_z>) \tag{15}$$

where D is the diffusion constant, k represents the depolarization rate due to collisions with the buffer gas, and p is the pump rate. The boundary condition for equation (15), assuming efficient wall relaxation, is $S_z = 0$ at the wall surface. The calculation predicts an axially symmetric polarization distribution across the sample cell with, for low buffer gas pressure, the peak polarization at the cell center. Higher buffer gas pressure results in a sharp gradient along the optical axis in the region of the cell closest to the incident light. Thus, one would expect that in the rubidium-xenon system the ^{129}Xe

would experience a spread of effective magnetic fields across the sample cell with an attendant decrease in relaxation time. This will be true whether the field gradient is internally generated or externally applied.

For the type of systems studied here the transverse relaxation rate due to magnetic field gradients has been shown to be[15]

$$\frac{1}{T_2} = \frac{1}{3}\left(\frac{G_\perp}{H_0}\right)^2 \bar{v}_{rel}^2 \frac{\tau_c}{1 + \omega_0^2 \tau_c^2} + \gamma^2 D_0 G_{||}^2 \tau_v^2 \qquad (16)$$

where $\bar{v}$ is the relative velocity described earlier, τ_c is the average time between collisions of the noble gas nucleus with anything, H_0 is the precession field and ω_0 is the corresponding frequency. D_0 is the diffusion coefficient for noble gas atoms through the cell, τ_v is the wall to wall diffusion time and γ is the noble gas gyromagnetic ratio. $G_\perp$ is the average transverse field gradient and is equal to $\Delta H_\perp/\ell$ where $H_\perp$ is perpendicular to the axis of quantization and ℓ is the cell diameter. $G_{||}$ is equal to $\Delta H_z/\ell$ where z defines the direction of the quantization axis. Equation (16) is derived for the case of fairly high buffer pressure where $\tau_c/\tau_v \ll 1$. Furthermore, for small gradients where $(G_\perp/H_0)^2 \ll 1$ the first term of (16) can be ignored and we have

$$\frac{1}{T_2} \cong \gamma^2 D_0 G_{||}^2 \tau_v^2 \qquad (17)$$

As shown in (17) the transverse relaxation rates due to the field gradient are expected to be independent of the sign of the gradient. The observed dependence of T_2 on the sense of polarization, therefore, is interpreted to imply the existence of an

additional external field gradient, $G_{||}{}^{ext}$. If we call the
internal field gradient $G_{||}{}^{int}$ we have

$$G_{||} = G_{||}{}^{ext} \pm G_{||}{}^{int} \tag{18}$$

where the $+$ and $-$ sign correspond to σ^+ and σ^- circularly polar-
ized light. From equations (17) and (18) we can write

$$\frac{1}{T_2} = \gamma^2 D (G_{||}{}^{ext} \pm G_{||}{}^{int})^2 \tau_v{}^2 + C \tag{19}$$

where C represents all relaxation rates (including spin exchange)
other than relaxation due to field gradients.

In order to verify the validity of equation (19) the transverse
relaxation rate in the frequency shift experiment was measured
at $81.2^{\circ}C$ as a function of external magnetic field gradient.
The field gradient was generated by a coil designed to help
compensate for non uniformity of the applied field along the z-
axis. In the measurement reported here that coil was used
simply to generate external gradients.

The results of this experiment are shown in figure 3-10. The
horizontal axis is given in terms of current through the gradient
coil and the vertical axis represents relaxation rate in the
frequency shift experiment. Data shown are for 100% light in-
tensity and for both light polarizations. The lines drawn
through the data points represent least squares fits to the
functional form of equation (19) under the assumption that the
applied field gradient is proportional to the current. The
minima of the two curves are different depending on whether the
rubidium field gradient adds to or subtracts from the applied
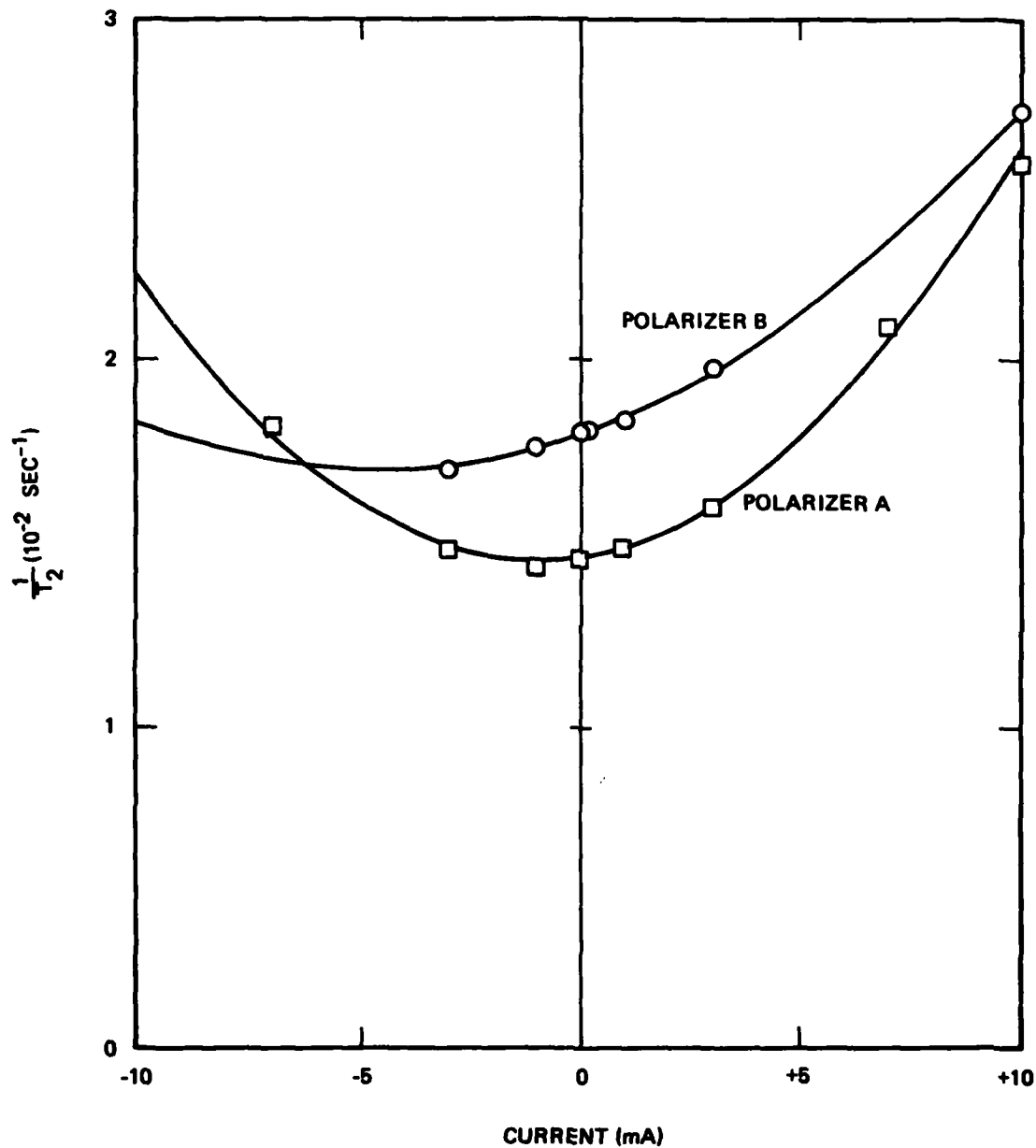
Figure 3-10.   Transverse Relaxation Rate for ^{129}Xe in the
Frequency Shift Experiment versus Current in the Field
Gradient Coils (see discussion in text)

gradient and is further shifted by any already existing external
field gradients. Neither the actual field gradient applied nor
the minimum value of such a gradient can be measured directly
in the present experimental apparatus. Nevertheless, the results
shown in figure 3-10 are strong evidence for the effect of the
rubidium field gradient.

One additional point can be made concerning the internally gen-
erated field gradient relaxation. The normal type of experiment
shows no transverse relaxation rate dependence on change of
circular polarizer or light intensity although it does not dis-
play completely linear behavior with $N_{Rb}/\bar{v}_{rel}$. For the normal
experiment $G_{\parallel}$ is along y in the coordinate frame defined for
the frequency shift experiment while one component of $G_{\perp}$ is
along z. Assuming that the major field gradient effect is along
the optical axis, equation (16), for the normal experiment,
would assume the form

$$\frac{1}{T_2} = \frac{1}{3}\left(\frac{G^{ext} \pm G^{int}}{H_0}\right)^2 \bar{v}_{rel}^2 \frac{\tau_c}{1 + \omega_0^2 \tau_c^2} + \gamma^2 D_0 G_y^2 \tau_v^2 \tag{19}$$

The fact that a polarizer or light intensity effect is not seen
suggests that the first term on the right hand side of equation
(19) is small in the normal experiment. It does not rule out
the possibility of the existence of the second term as a mech-
anism for relaxation. The gradient perpendicular to the optical
axis, although present, is not sensitive to changes of light
intensity or polarization. As the initial amplitudes of the
free induction decay of the noble gas have not been seen to vary
with variation in external applied field gradients in the
frequency shift experiment described here, it may be possible

that pump time experiments will aid in sorting out field gradient effects. The T_1 contribution to relaxation due to a field gradient is given by[15]

$$\frac{1}{T_1} = \frac{2}{3}\left(\frac{G_\perp}{H_0}\right)^2 \overline{v}^2 \frac{\tau_c}{1 + \omega_0^2 \tau_c^2} \qquad (20)$$

In the pump time experiment the axis of quantization is along z during the establishment of magnetization, so $G_\perp$ in equation (20) corresponds to Gy of equation (19). As the right hand side of equation (20) is a term expected to be much smaller than the last term of equation (19) a comparison of T_p^{-1} with T_2^{-1} in the normal experiment should lead to characterization of the importance of field gradient relaxation effects in the normal experiment. This assumes, of course, that other relaxation mechanisms contribute equally to T_2 and T_p. Pump time experiments to probe for such possible differences are currently being carried out in our laboratory.

In summary, the relaxation of ^{129}Xe nuclear moments due to the spacial variation of the optically pumped rubidium field has been observed. The nuclear spins experience the magnetic field through spin exchange collisions with the alkali metal atoms, and as the noble gas experiences different effective fields in different regions of the sample cell the nuclear magnetic resonance linewidth is subject to an internally generated inhomogenous broadening or, equivalently, decreased dephasing time. This relaxation becomes significant at high alkali number density, especially in highly buffered sample cells.

3.5 CONSIDERATIONS FOR FUTURE WORK

It has been proposed to model theoretically for several cell geometries the contribution of the alkali metal polarization to the nonuniformity of the magnetic field experienced by the noble gas nuclei. Cells can be prepared based on the theoretical predictions and can be tested experimentally. Results will help assess the importance of internally generated field inhomogeneities under various conditions.

3.6 BIBLIOGRAPHY

1. S.J. Davis and L.C. Balling, Phys. Rev. A6, 1479 (1972).

2. L.C. Balling and F.M. Pipkin, Phys. Rev. 136, A46 (1964).

3. L.C. Balling, R.J. Hanson, and F.M. Pipkin, Phys. Rev. 133 A607 (1964).

4. H.G. Dehmelt, Phys. Rev. 109, 381 (1958).

5. F.G. Major, Litton Subcontract Report No. WC376807 (unpublished).

6. C.H. Volk, B.C. Grover, and E. Kanegsberg, AFOSR, Annual Technical Report, Contract No. F49620-77-C-0047 (1978).

7. T.M. Kwon, AFOSR, Contract No. F49620-77-C-0047 (1981).

8. R.M. Herman, Phys. Rev. 137, A1062 (1965).

9. C.H. Volk, T.M. Kwon, and J.G. Mark, Phys. Rev. A21, 1549 (1980).

10. See, for example, C.P. Slichter, _Principles of Magnetic Resonance_ (Springer-Verlog, New York, 1978) pp. 32-35.

11. C.J. Smithells, _Metals Reference Book_ (Butterworths, London, 1962), Vol 2, p. 655.

12. W.A. Fitzsimmons, L.L. Tankersley, and G.K. Walters, Phys. Rev. 179, 156 (1969).

GUIDANCE & CONTROL SYSTEMS
Litton 5500 Canoga Avenue, Woodland Hills, California 91365

13. T.A. McClelland, Thesis, Columbia University (1981).

14. S. Legowski, Bull. de L'Academic Palonaise des Sciences, $\underline{14}$, 525 (1968).

15. S.P. Dovgopol, V.P. Putyrskii, and S.L. Votyakov, Opt. Spectrosc. $\underline{35}$, 596 (1973).

GUIDANCE & CONTROL SYSTEMS
Litton 5500 Canoga Avenue, Woodland Hills, California 91365

SECTION IV

TEMPERATURE SENSITIVITY OF NMR GYRO BIAS DUE TO QUADRUPOLAR FREQUENCY SHIFT IN ^{131}Xe

4.1 INTRODUCTION

An experimental observation[1] in a ^{129}Xe - ^{131}Xe cell has shown that there exists a cell temperature at which the temperature sensitivity of the gyro bias becomes identically zero. Such a cell temperature will be termed hereafter "Temperature turning point (TTP)" for our convenience. The experimental results are summarized in figures 9 and 11, Sec. III of AFOSR Report, 1981[1]. The two figures are reproduced here, and referred to as figures 4-1 and 4-2, respectively. Notice in figure 4-2 that, at the cell temperature of $\sim 79^\circ$C, the gyro bias goes through a minimum, i.e., TTP $\sim 79^\circ$C. This Section is an analysis in which the frequency shift due to nuclear quadrupole inter-action is shown to be the probable mechanism for the TTP.

4.2 APPARENT RUBIDIUM FIELD

In this section the experiment from which figures 4-1 and 4-2 were obtained is described briefly. A more detailed descript·· ·· was given in Section III. A reiteration aids in the develo··· ··t of the discussion.

The physics research station was set up for a frequency shift experiment (FSE) (H_0 parallel to pumping axis) at n = 0. The precession of the noble gas nuclear spin was accomplished by applying a precession field ($H_0 \sim 100$ µG) along the optical axis. The optically polarized rubidium vapor in this scheme, then, acts either to directly increase or decrease the effective pre-cession field as experienced by the noble gas ensemble, depending on the sense of polarization of the rubidium D_1 light. Both
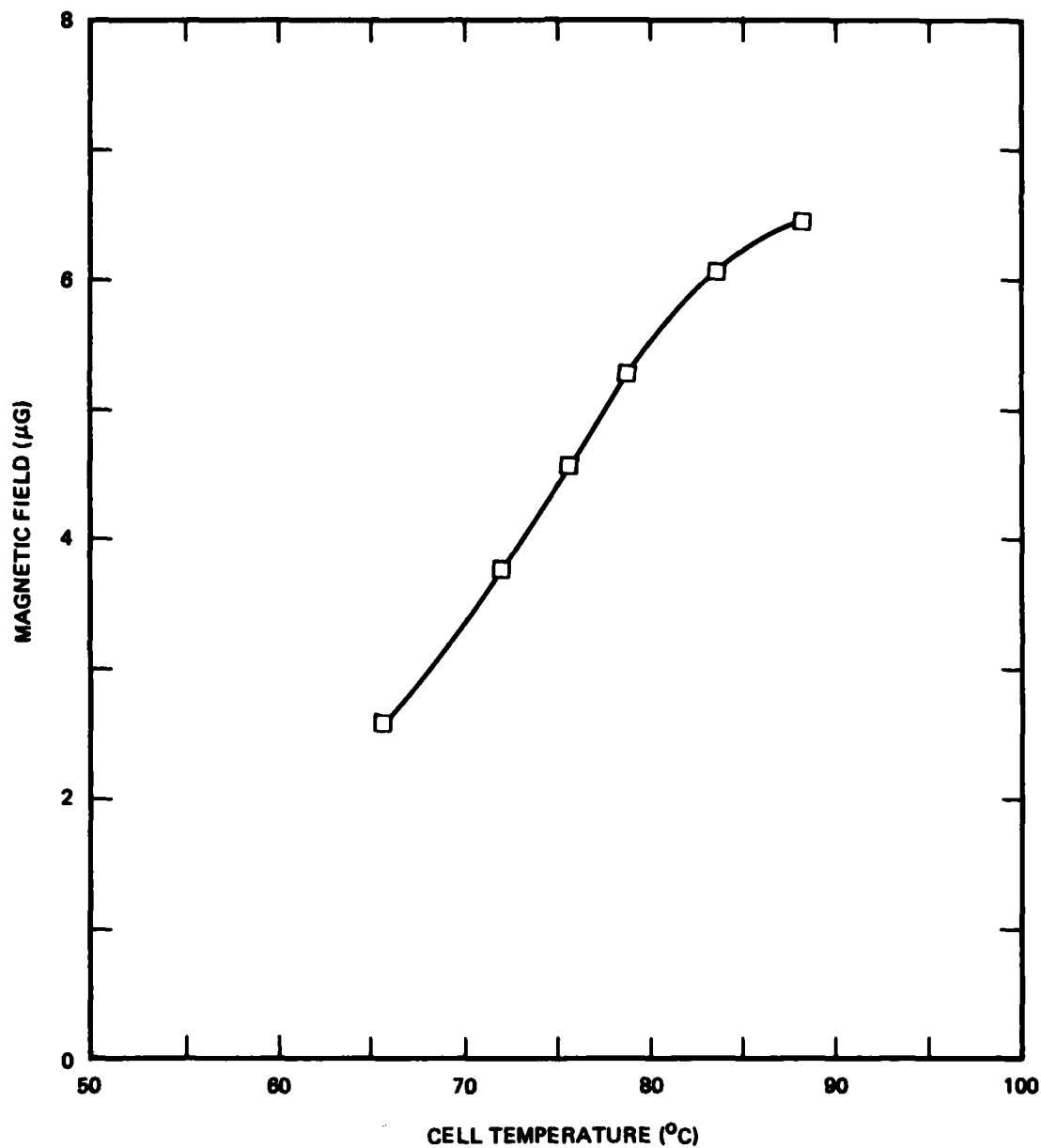
Figure 4-1. The Magnetic Fields Experienced by both ^{129}Xe and ^{131}Xe Nuclei as a Function of the Sample Cell Temperature. The difference in the fields experienced by the two nuclear species are too small to be seen clearly in the plot.
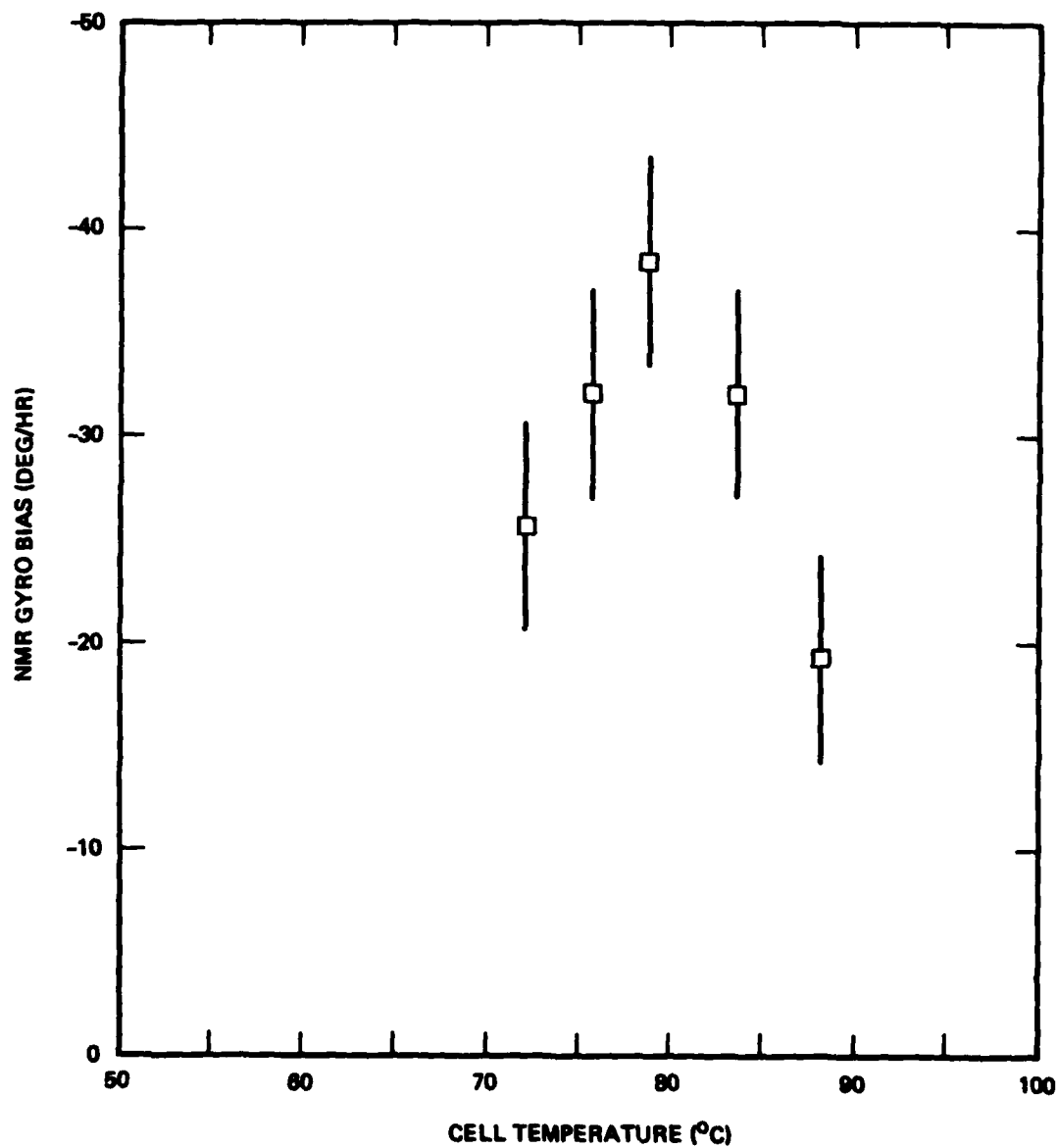
Figure 4-2.   NMR Gyro Bias versus the Cell Temperature for
the Cell (1-75) with the ^{129}Xe and ^{131}Xe Pair of
Isotopes.   The large error bars are due to the
computational error.

4-3

left and right hand circular polarizers were used. The amount
of circularly polarized light transmitted was measured to be
92% for one polarizer and 96% for the other. The precession
frequency, ω, of the ensemble of the noble gas is correspond-
ingly increased or decreased such that

$$\omega_1 = -\gamma (H_0 + H^*) \qquad (1a)$$

$$\omega_2 = -\gamma (H_0 - H^*) \qquad (1b)$$

where H_0 is the magnetic field applied externally along the pre-
cession axis. H^* is the apparent rubidium field experienced by
the noble gas due to the spin exchange interaction. γ is the
nuclear gyromagnetic ratio of the noble gas. The subscripts,
1 and 2, refer to the two different circular polarizers. From
these, H^* is readily obtained by measuring the precession
frequencies, ω_1 and ω_2.

Figure 4-1 is the plot of the apparent rubidium field experienced
by ^{129}Xe and ^{131}Xe versus the cell temperature. The differences
of the apparent rubidium fields experienced by the two nuclear
species are too small to be seen clearly in the figure. This
represents experimental verification of the prediction of the
theory of spin exchange that two nuclear isotopes of the same
noble gas atom experience essentially the same rubidium field.
Nevertheless, there existed very small differences between the
two apparent fields in the order of a few hundredths of one
microgauss. These differences were of the same order of magni-
tude as, if not marginally beyond, the experimental uncertainties.
Such differences are shown by the error bars in figure 4-2. The
vertical axis is scaled to represent the NMR gyro bias, Ω_a, given
by

GUIDANCE & CONTROL SYSTEMS
Litton 5500 Canoga Avenue, Woodland Hills, California 91365

$$\Omega_a = \frac{\gamma_a \gamma_b}{\gamma_b - \gamma_a} (H_a{}^* - H_b{}^*) \qquad (2)$$

where the subscripts, a and b, refer to ^{129}Xe and ^{131}Xe nuclei, respectively, and the γ's are the gyromagnetic ratios.

4.3 QUADRUPOLE INTERACTION

The apparent rubidium field should be distinguished from the true rubidium field in the presence of any frequency shift other than that due to the true rubidium field. For the case of ^{131}Xe there exists a frequency shift due to its nuclear quadrupole interaction. The precession frequency of ^{131}Xe, ω_b, at the magic angle, θ, has been shown to be:

$$\omega_b = \omega_b{}^o + \frac{54 \, \bar{\alpha}^2}{\omega_b{}^o} \sin^2 \theta \cos^2 \theta \qquad (3)$$

where $\omega_b{}^o$ is the nuclear Larmor frequency given by:

$$\omega_b{}^o = | - \gamma_b (H_0 \pm H_{Rb}) | \qquad (4)$$

where H_0 and H_{Rb} are the applied field and the true rubidium field experienced by ^{131}Xe nucleus. $\bar{\alpha}$ is the strength of the quadrupole interaction averaged over the wall collision parameters, and is shown to be:

$$\bar{\alpha} = \left(\frac{\tau_s}{\tau_s + \tau_v} \right) \frac{e^2 \, Qq}{4I \, (2I-1)} \qquad (5)$$

where τ_s and τ_v are the "sticking" time and the time between collisions with the wall, respectively, and are given by:

GUIDANCE & CONTROL SYSTEMS
Litton 5500 Canoga Avenue, Woodland Hills, California 91365

$$\tau_s = \tau_0 \, e^{E/kt} \tag{6}$$

$$\tau_v = 4V/Av \tag{7}$$

where τ_0 is 10^{-12} sec, E is the adsorption energy, V is the cell volume, A is the surface area, and v is the kinetic velocity of the xenon atoms.

Following the experimental procedures described in paragraph 4.2, the apparent rubidium field seen by ^{131}Xe can be shown to be:

$$H_b^* = H_{Rb} - \frac{54 \, \bar{\alpha}^2 \, H_{Rb}}{\gamma_b^2 \, (H_0^2 - H_{Rb}^2)} \sin^2 \theta \cos^2 \theta \tag{8}$$

In the case of ^{129}Xe, the apparent rubidium field is taken to be identical to the true rubidium field, i.e.,

$$H_a^* \equiv H_{Rb} \tag{9}$$

Substituting equations (8) and (9) into equation (2), we get:

$$\Omega_a = \frac{\gamma_a \, \gamma_b}{(\gamma_b - \gamma_a)} \frac{54 \, \bar{\alpha}^2 \, H_{Rb}}{\gamma_b^2 \, H_0^2} \sin^2 \theta \cos^2 \theta \left[1 - \left(\frac{H_{Rb}}{H_0} \right)^2 \right]^{-1} \tag{10}$$

Taking $\left[1 - (H_{Rb}/H_0)^2 \right]^{-1} \approx 1$, and substituting equations (6) and (7) into (10) with the condition of $\tau_s \ll \tau_v$, the NMR gyro bias becomes:

$$\Omega_a = C_o \, T \, e^{E/kT} \, H_{Rb} \qquad (11)$$

where,

$$C_o = \left(\frac{\gamma_a \, \gamma_b}{\gamma_b - \gamma_a}\right) \frac{54}{\gamma_b^2 H_0^2} \left[\frac{\tau_0}{4\,(V/A)} \sqrt{\frac{8R}{\pi m}} \frac{e^2}{4I} \frac{Qq}{(2I-1)}\right]^2 \qquad (12)$$

$$x \, \sin^2 \theta \, \cos^2 \theta$$

The true rubidium field, H_{Rb} in equation (11) is a function of the pump light intensity, the nature of buffer gas in the cell, the cell geometry, and the spin exchange interaction strength. Figure 4-1 is the temperature dependence of H_{Rb} for the sample cell under the particular measurement conditions.

The strength of the electric field gradient, $[eq]$ in equation (12), has been shown to arise from the distorted electronic orbitals of xenon atoms during collisions with the cell wall, and is considered to be characteristic of noble gas atoms. If $[eg]$ is taken to be insensitive to the cell temperature, equation (12) becomes independent of the temperature. The temperature dependence of the NMR gyro bias is shown explicitly in equation (11). Note here that the gyro bias decreases as the external field increases. The field, however, does not alter the functional form of the temperature dependence of the gyro bias including the cell temperature at which TTP takes place, if any. From the following numerical values

$$\gamma_a = -7.40 \times 10^3 \text{ rad/sec/gauss} \tag{13a}$$

$$\gamma_b = 2.19 \times 10^3 \text{ rad/sec/gauss} \tag{13b}$$

$$H_0 = 1.09 \times 10^{-4} \text{ gauss} \tag{13c}$$

$$k = 8.62 \times 10^{-5} \text{ eV/}^\circ\text{k} \tag{13d}$$

$$\theta = 55 \qquad \text{deg} \tag{13e}$$

$$I = 3/2 \tag{13f}$$

and estimating from published data[2] and from reasonable surface energies

$$\left[\frac{\tau_0}{4(V/A)} \sqrt{\frac{8R}{\pi m}} \, e^2 \, Qq \right]^2 \approx 1.6 \times 10^{-9} \text{ (rad/sec)}^2/^\circ\text{k} \tag{14}$$

Equations (13a) through (14) substituted into equation (12) give

$$C_0 \approx 0.8 \text{ (deg/hr)/(gauss} \cdot {}^\circ\text{k)} \tag{15}$$

Figure 4-3 is the plot of NMR gyro bias given by equations (11) and (15) versus the cell temperature as a function of the wall adsorption energy. In this plot, the actual data shown in figure 4-1 are used for $H_{Rb}(T)$. Figure 4-3 should be compared with the experimental data in figure 4-2.

Lack of sufficient data points together with the large error bars in figure 4-2 precludes fitting the data to the functional form of equation (11). However, figure 4-3 clearly demonstrates the temperature dependence of the gyro bias and the very existance of the TTP. Emphasized in figure 4-3 is the occurrence of the TTP at 79°C for E = 0.16 eV with the gyro bias of
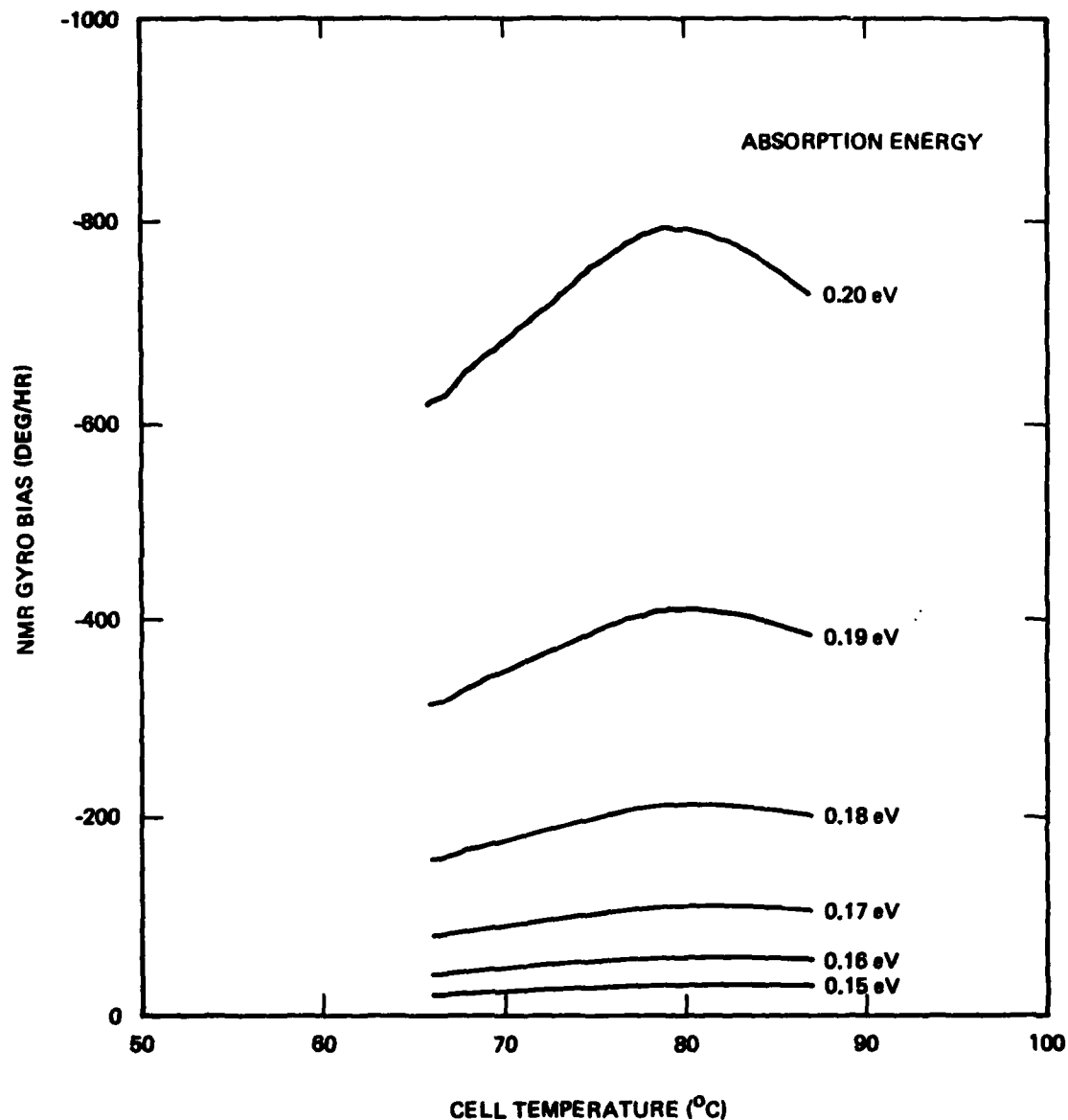
Figure 4-3.   NMR Gyro Bias versus Cell Temperature for
Various Cell Boundary Surface Energies

45 deg/hr, whereas experimental data in figure 4-2 shows TTP at 79°C with the gyro bias of 39 deg/hr. In a separate experiment $E = 0.13$ eV in a different cell has been observed.

The TTP's and the gyro bias at the TTP are shown in figures 4-4 and 4-5 as a function of the wall adsorption energy. Figure 4-6 gives the slopes of the selected curves shown in figure 4-3, (d Ω_a/dT), as a function of the cell temperature. The slope represents the temperature sensitivity of the NMR gyro bias.

4.4 SUMMARY

The frequency shift in ^{131}Xe due to the nuclear quadrupole moment has been demonstrated to be a mechanism for the temperature dependence of the NMR gyro bias and the occurrence of the TTP. The numerical values of wall adsorption energy, TTP, and the gyro bias at TTP are in excellent agreement with the previous results even though comprehensive data analysis was not possible at the present time due to the lack of sufficient data points and the large error bars.

Dr. Tae M. Kwon is making a patent disclosure based on the idea of adjusting the cell operating condition to the temperature turning point as a means of improving the temperature sensitivity of the NMR gyro bias.

4.5 CONSIDERATIONS FOR FUTURE WORK

The importance of finding low surface energy coatings has been demonstrated. Efforts are currently under way to (1) refine techniques for investigating wall effects and (2) devise new surface treatments.

GUIDANCE & CONTROL SYSTEMS
Litton 5500 Canoga Avenue, Woodland Hills, California 91365
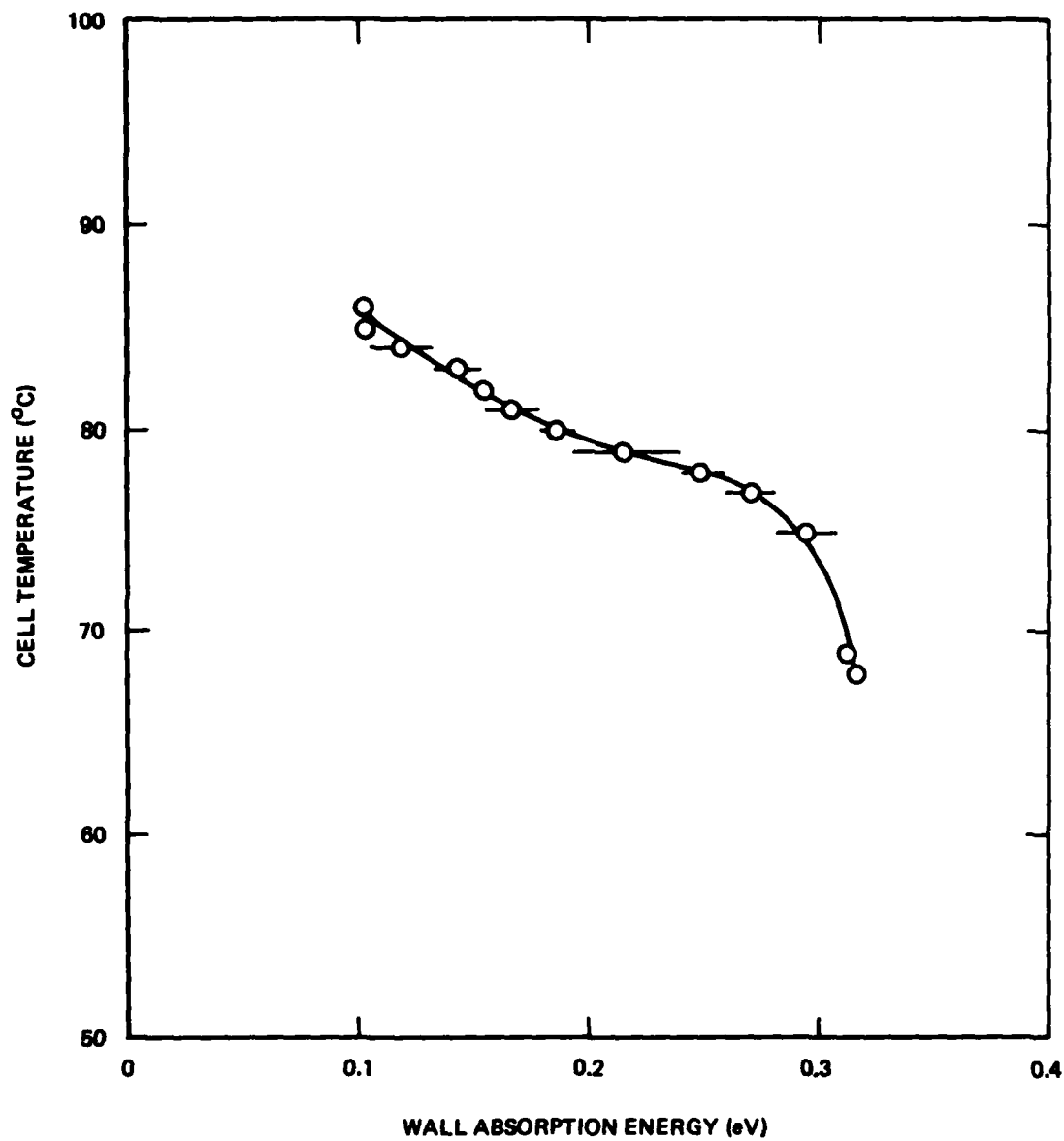
Figure 4-4. Cell Temperature versus Wall Adsorption
Energy (See discussion in text)

Figure 4-5.   NMR Gyro Bias versus Wall Adsorption Energy
(See discussion in text)

Figure 4-6.   Temperature Sensitivity of NMR Gyro Bias
as a Function of Cell Temperature
(See discussion in text)

GUIDANCE & CONTROL SYSTEMS
Litton 5500 Canoga Avenue, Woodland Hills, California 91365

4.6 BIBLIOGRAPHY

1. T.M. Kwon, AFOSR, Annual Technical Report, Contract No. F49620-77-C-0047 (1981).

2. T.M. Kwon, J.G. Mark, and C.H. Volk, Phys. Rev. A $\underline{24}$, 1894 (1981).

SECTION V

STUDIES OF CELLS PREPARED USING CORNING 1720 GLASS

5.1 INTRODUCTION

One specific task proposed for 1981-82 was to study the effect
of "clean glass" on the reaction $2 Rb + H_2 \rightarrow 2 RbH$. It was pro-
posed that, by providing a clean surface for deposition of the
metal hydride, the improved relaxation effects associated with
the use of alkali hydrides might be further enhanced. Corning
1720 glass is an alkali resistant aluminosilicate glass which
can be heated to higher temperatures than Pyrex. It was decided
to prepare a series of teardrop shaped cells from this material
in the same way that Pyrex cells are prepared but, prior to
filling, the 1720 glass cells were baked out on the vacuum line
at an elevated temperature (greater than $600^\circ C$ as compared with
$350^\circ C$ for Pyrex) in order to remove as many surface waters and
hydroxyls as possible. Three batches of teardrop shaped 1720
glass cells were prepared using the same proportions of buffer
gas. Each batch consisted of four cells, two containing
hydrogen and two free from hydrogen. The total xenon pressure
was 1 torr. Two batches were prepared with ^{129}Xe only and one
with both xenon isotopes in a mix of 0.2 torr of ^{129}Xe and 0.8
torr of ^{131}Xe. The results for cells of this type are to be
compared with similar cells prepared using Pyrex glass.

5.2 EXPERIMENTAL METHODS

The experimental NMR methods reported on here have been described
in detail in Section III. Cells were screened at around $80^\circ C$
using the normal T_2 experiment and certain of those were selec-
ted for more detailed study. As an initial step, the tempera-
ture dependency of the transverse relaxation rates was observed

GUIDANCE & CONTROL SYSTEMS
5500 Canoga Avenue, Woodland Hills, California 91365

for three cells of one of the batches containing no ^{131}Xe. Subsequently, detailed temperature dependent pump time as well as selected double oven experiments were carried out on two cells containing both isotopes of xenon, one with and one without hydrogen. A list of cells and experiments carried out is presented in table 5-I. Where feasible, data were fit to relaxation models. Resulting 1720 glass cell parameters are discussed and compared with results for Pyrex cells.

^{129}Xe, having a spin 1/2 nucleus and thus no quadrupole moment and also a larger Rb-Xe spin exchange cross section, provides better signal to noise than the ^{131}Xe. Studies of ^{131}Xe alone are further complicated by the presence of residual amounts of ^{129}Xe in the purified product. Thus, initial studies of Corning 1720 glass were designed for cells containing only the ^{129}Xe noble gas species.

For Batch A of 1720 cells prepared containing 1.0 torr ^{129}Xe, 100 torr He, 40 torr N_2, and either no hydrogen or 10 torr hydrogen, the rubidium in the two hydrogen containing cells reacted completely during the curing period. Transverse times for the non-hydrogen cells, numbers 341 and 344, were determined at around 80°C only and found to be 140 and 138 seconds respectively. Because of the loss of rubidium in the first batch, a second batch was prepared containing much more rubidium and the same gas mix. In Batch B, both non-hydride cells and one hydride cell survived the curing process and became the subject of a normal transverse relaxation experiment carried out on the non-computer controlled apparatus and, in addition, selected frequency shift and pump time experiments were carried out. Finally, an extended series of experiments using the computer controlled apparatus was carried out on the Batch C cells containing both xenon isotopes.

TABLE 5-I. LIST OF CORNING 1720 GLASS TEARDROP CELLS AND EXPERIMENTS

Batch	Cell No.	Hydride Surface Coating	Xe Isotope Present		Experiments Performed				
			129	131	T2 at Close To 80°C	Normal $T_2(T)$	$T_p(T)$	Frequency Shift	Double Oven
A	341		x		x				
	342*	x	x						
	343*	x	x						
	344		x		x				
B	359		x		x	x			
	360		x		x	x			
	361	x	x		x	x	x	x	
	362*	x	x		x				
C	367		x	x	x	x	x		
	368		x	x	x				
	369	x	x	x	x				
	370	x	x	x	x	x	x		x

*Rubidium in these cells reacted completely during oven curing period.

5.3 RESULTS AND DISCUSSION

In presenting the results for the 1720 cells where temperature dependence of ^{129}Xe is reported, one of two models is used in fitting the data. In the simpler model, a line drawn through the data points represents a least squares fit to the form

$$\frac{1}{T_2} = N_{Rb}\, \sigma_{ex}\, \bar{v}_{rel} + \frac{1}{T_2'} \quad . \tag{1}$$

Where N_{Rb} is the rubidium number density, σ_{ex} represents the spin exchange cross section, $\bar{v}_{rel}$ is the rubidium - xenon relative velocity, and T_2' is a temperature independent relaxation time. As[1]

$$\sigma_{ex} \; \alpha \; \frac{N_{Rb}}{\bar{v}_{rel}^2} \tag{2}$$

prior to the initiation of wall effect studies, it was customary to fit the relaxation rate data to a straight line of slope $(\sigma_{ex}\, \bar{v}_{rel}^2)$ and intercept corresponding to a temperature independent relaxation rate $1/T_2'$.[2]

In the second model, a temperature dependent wall relaxation rate such as discussed in Section II is assumed. In that case, the relaxation rate can be expressed by

$$\frac{1}{T_2} = (\sigma\bar{v}^2)\, \frac{N_{Rb}}{\bar{v}} + X_2\, \sqrt{T}\, e^{(2E/kT)} \tag{3}$$

where $(\sigma\bar{v}^2)$, X_2, and E are parameters. In some cases, the data discussed here, being taken earlier than some other data, were

fit to the form of equation (1) rather than (3). In the case where (3) is used, results of a fit to equation (1) are presented also. This permits comparison with previously published results for pyrex cells[2] as well as more recent results from this laboratory.

In figures 5-1 through 5-3 are presented the first temperature dependent transverse relaxation studies for teardrop shaped Corning 1720 glass cells, numbers 359, 360, and 361. These results are presented as a graph of relaxation rate versus rubidium density divided by velocity with the data fit to the form of equation (1). The parameters are presented with the figures. Although not plotted on the same scale, these results show a trend toward the same relaxation rate at close to $100^{\circ}C$, however, with different slope and intercept. At higher temperatures, the non-hydride coated cells appear similar to each other as compared with the hydride coated cell. For example, at close to $80^{\circ}C$, numbers 159 and 160 exhibited T_2's of 139 and 138 seconds respectively while T_2 for number 361 was about 85 seconds. At lower temperatures, all three cells were different. For example, at close to $50^{\circ}C$, cell number 359 (non-hydride) exhibited a T_2 of about 350 seconds, cell number 360 (non-hydride) exhibited a T_2 of about 460 seconds, and cell number 361 (hydride) exhibited a T_2 of about 170 seconds. This initial study suggested that, for ^{129}Xe, the surface relaxation might be more effective on hydride coated cells than on simply heat treated 1720 glass.

At the same time that the 1720 glass teardrop shaped cells were being studied, a series of experiments on a Pyrex cell of similar shape and fill were being carried out on the computer controlled research apparatus. Those studies, already discussed in the section on frequency shift experiments, were suggesting that, in
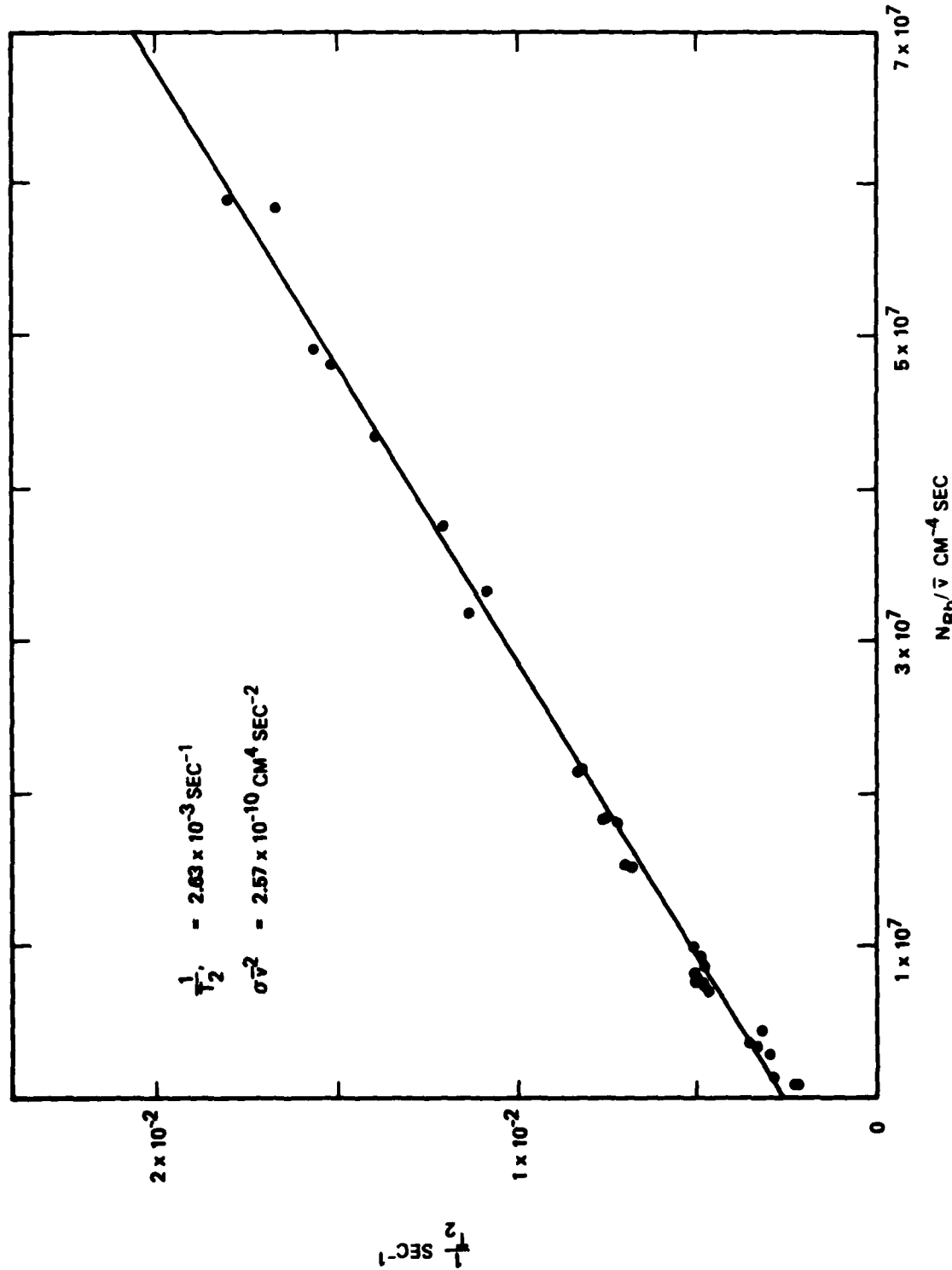
Figure 5-1. ^{129}Xe Relaxation Rate versus $N_{Rb}/\overline{v}$ for Cell No. 359

$\dfrac{1}{T_2'} = 2.63 \times 10^{-3}$ SEC^{-1}

$\sigma\overline{v}^2 = 2.57 \times 10^{-10}$ CM^4 SEC^{-2}

$\dfrac{1}{T_2}$ SEC^{-1}

$N_{Rb}/\overline{v}$ CM^{-4} SEC
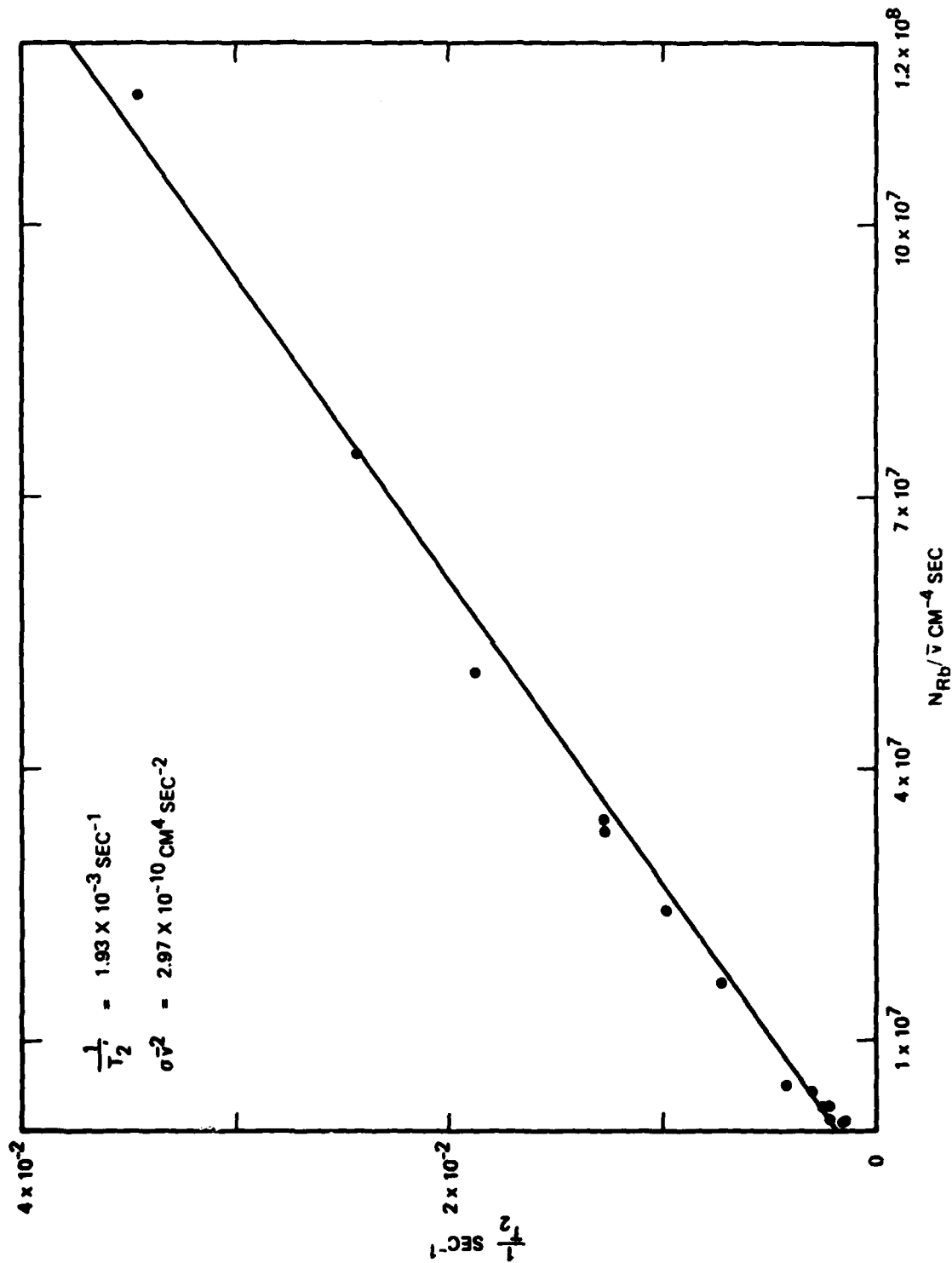
Figure 5-2. ^{129}Xe Relaxation Rate versus $N_{Rb}/\bar{v}$ for Cell No. 360
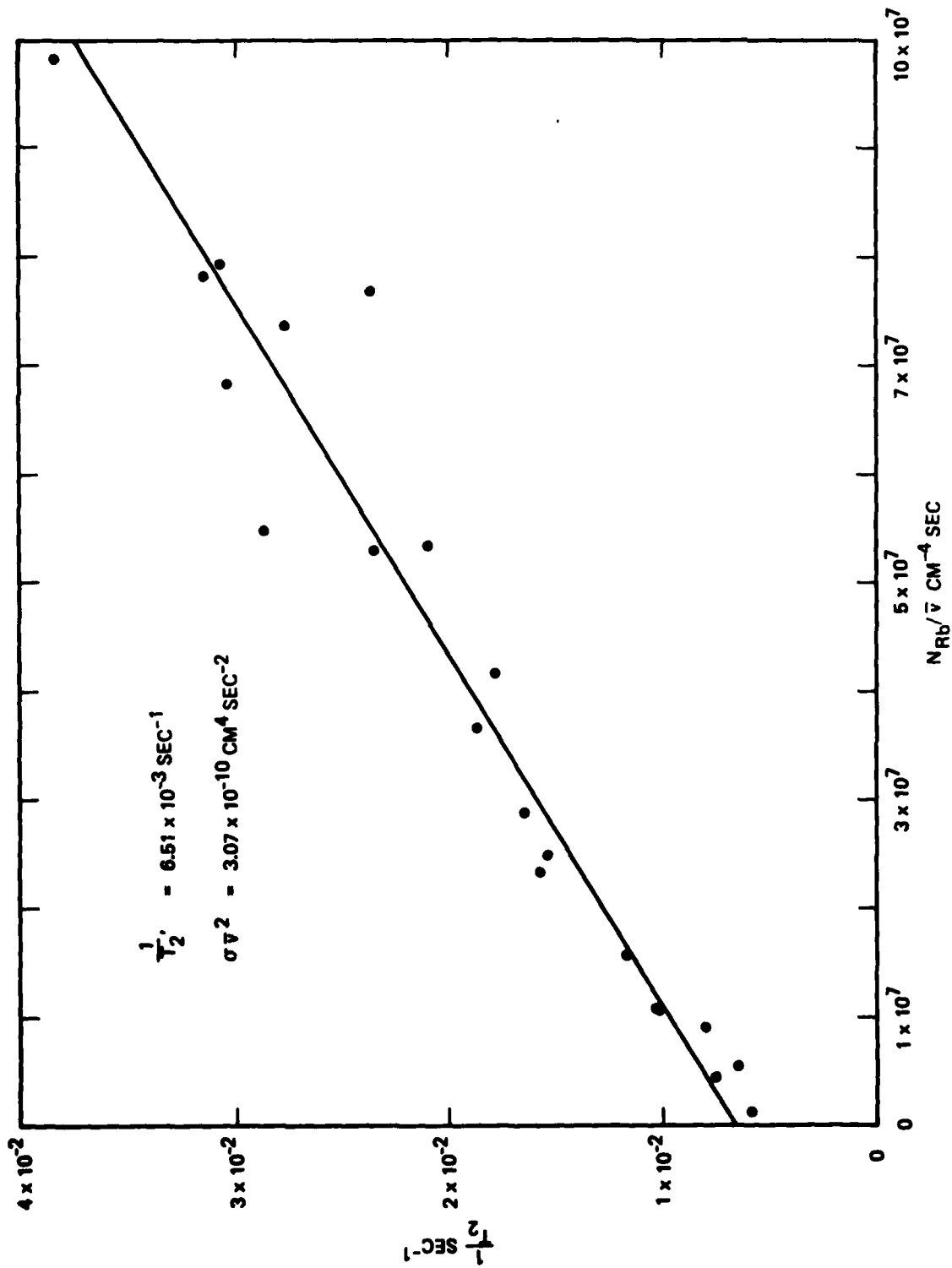
Figure 5-3. ^{129}Xe Relaxation Rate versus $N_{Rv}/\bar{v}$ for Cell No. 361

addition to wall relaxation effects, it might be necessary to take into consideration effects due to internally generated magnetic field gradients, and a series of pump time measurements as a function of temperature were being conducted on that cell. As discussed in Section III, a field gradient along the precession axis can contribute to T_2 but not to the pump time, T_p. Although there was a clearly demonstrated gradient along the pump light direction, the existence of such a gradient along the perpendicular direction had not been detected and was being looked for. As a cross check for such effects in 1720 glass cells in a fairly high temperature region where the one hydride cell still exhibits definite differences from the non-hydride cells, some frequency shift experiments followed by two pump time experiments were run on the hydride cell. The results of the pump time experiments are displayed in figures 5-4 and 5-5, along with the calculated pump time, T_p, and the measured transverse relaxation time, T_2, at the indicated temperatures. Within experimental error, those two numbers are the same. The frequency shift experiments, as with the pyrex cells, exhibited different relaxation times depending on whether the effective precession field was increased or decreased.

The conclusion from these results is that 1720 glass cells behave much as pyrex cells except that, as discussed more thoroughly in Section VI, the relaxation times for ^{129}Xe in non-hydrided cells may be longer in 1720 cells than in Pyrex cells although the number of batches investigated has been small.

Finally, Batch C was examined in some detail. These cells contained 0.2 torr ^{131}Xe, 0.8 torr ^{129}Xe, and the same mix of buffer gases as for the previous sets of 1720 glass cells. Transverse relaxation data for all four at close to 80°C were

T_P = 48.7 SEC

T_2 (90°C) = 53.6 SEC

TIME (SEC)

INITIAL ^{129}Xe POLARIZATION AMPLITUDE (ARBITRARY UNITS)
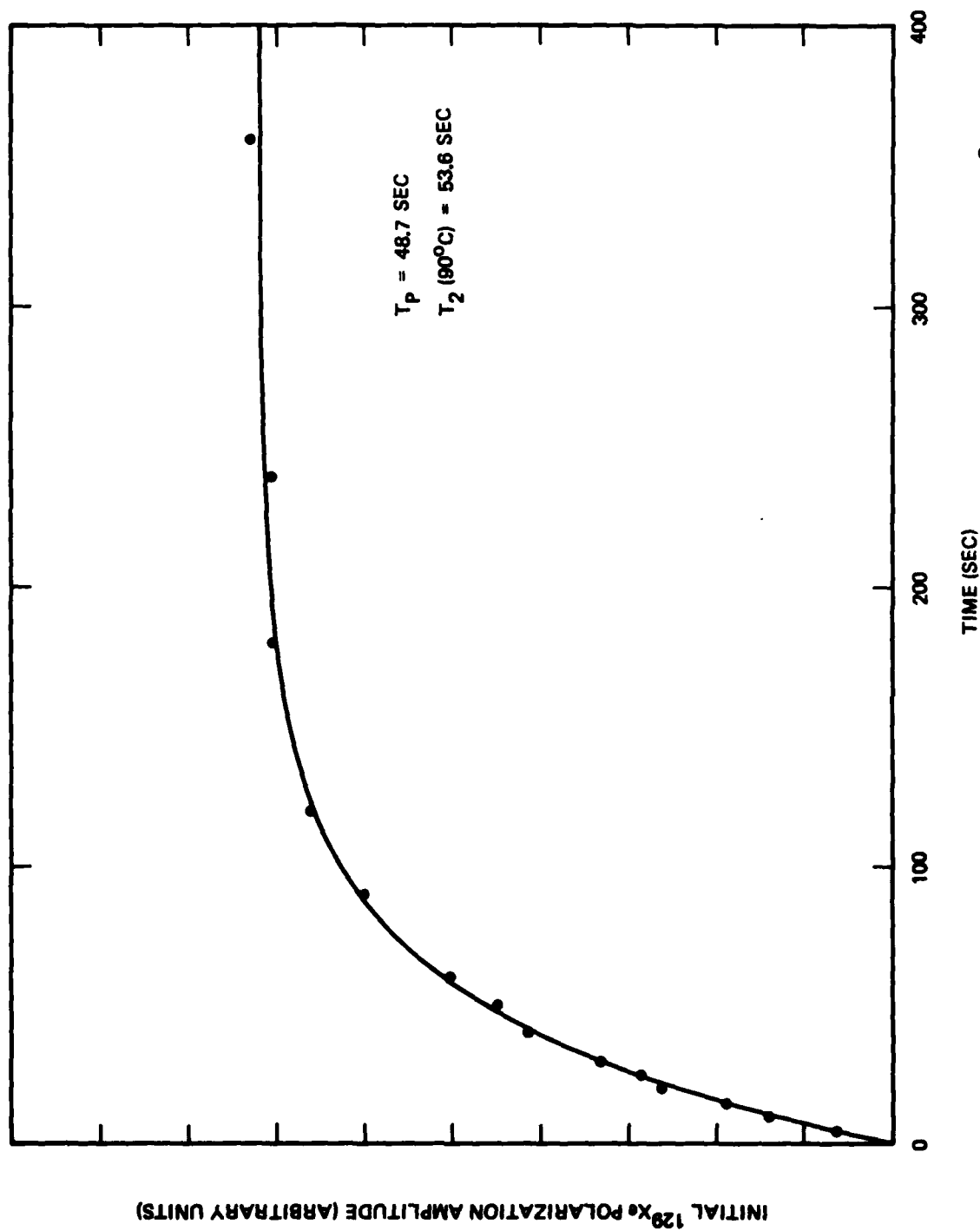
Figure 5-4. Pump Time Experiment for Cell No. 361 at 89.4°C
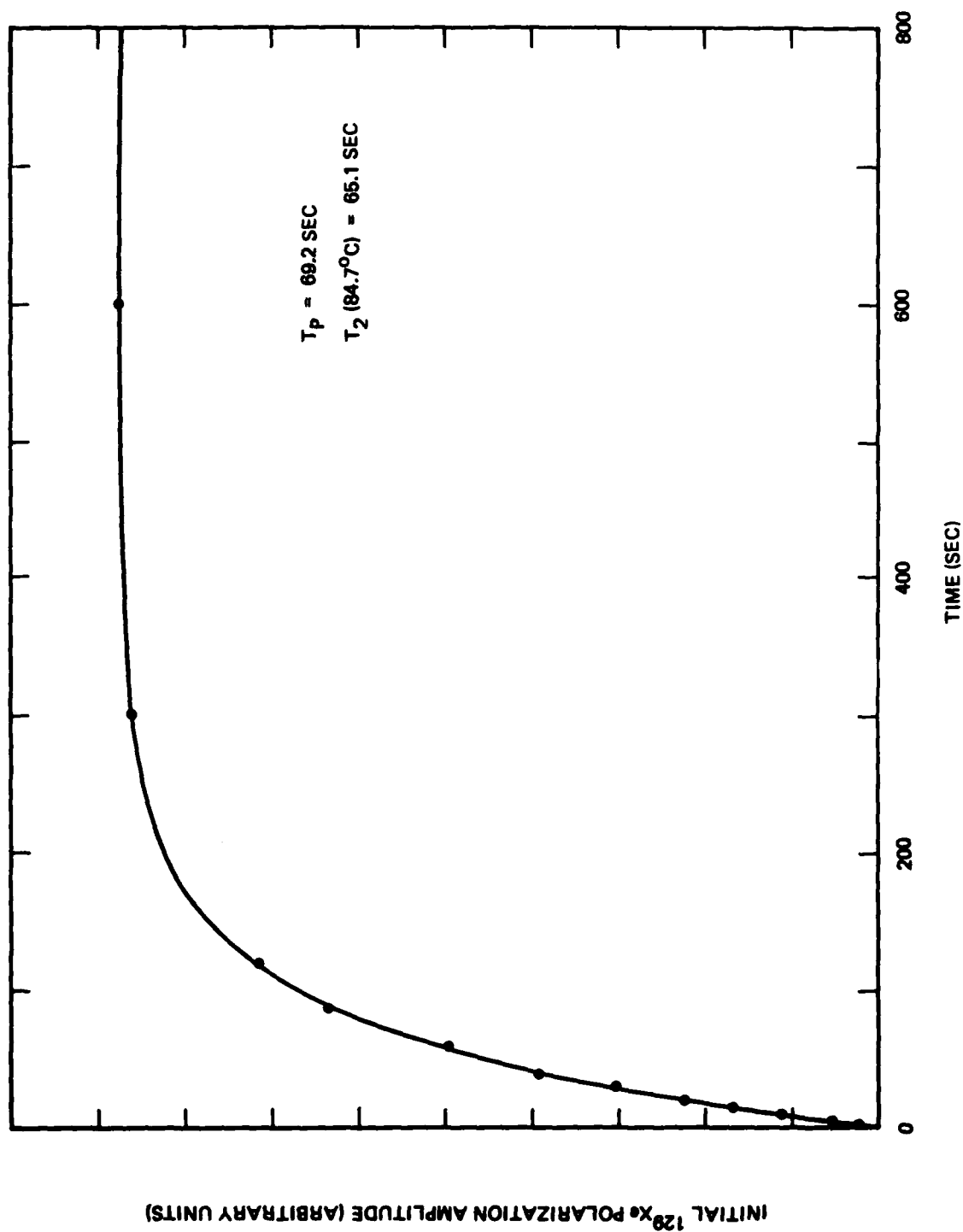
Figure 5-5. Pump Time Experiment for Cell No. 361 at 84°C

taken. The cells without hydride, numbers 367 and 368, showed T_2's for ^{129}Xe of 155 and 162 seconds respectively and T_2's for ^{131}Xe of 47.5 and 45.8 seconds respectively. By contrast, the two hydrided cells, numbers 369 and 370, showed ^{129}Xe transverse relaxation times of 98.4 and 97.3 seconds respectively and for ^{131}Xe, 105 and 111 seconds respectively. One of each type of cell was selected for detailed experiments.

Figures 5-6 and 5-7 show the results of pump time experiments for cell number 367 (no hydride). At low temperatures, the T_p and T_2 for ^{129}Xe is several hundred seconds while for ^{131}Xe one calculates 130-140 seconds for T_p and ~50 seconds for T_2. Because the Kalman fit employed in data analysis can tend to lock on a particular short value for ^{131}Xe T_2 when the ^{129}Xe T_2 is long, the error margins for the ^{131}Xe data could be large at low temperatures. In spite of this, the trends in these data are unmistakable. The pump times and the transverse relaxation times for ^{129}Xe are the same within experimental error while the pump time for ^{131}Xe is larger than the transverse relaxation time by about a factor of two, and both the transverse and longitudinal relaxation times for the ^{131}Xe are only weakly temperature dependent over the temperature range of interest.

Figure 5-8 shows the results of a fit of the pump time data for ^{129}Xe to the functional form of equation (3) with the resulting parameters indicated in the figure.

A simple linear fit to equation (1) provides

$$\overline{\sigma v}^2 = 3.22 \times 10^{-10} \text{ cm}^4 \text{ sec}^{-2}$$

$$\frac{1}{T_2'} = 1.70 \times 10^{-3} \text{ sec}^{-1}$$

Figure 5-6. ^{129}Xe Longitudinal and Transverse Relaxation Rates versus Temperature for Cell No. 367

1.0

1.1

1.25 1.4 1.6

2.8 2.5
3.2 2.2
3.6
4.0 2.0

1.8

MICROCOPY RESOLUTION TEST CHART
NATIONAL BUREAU OF STANDARDS 1963-A

Figure 5-7. ^{131}Xe Longitudinal and Transverse Relaxation Rates versus Temperature for Cell No. 367

$\sigma \bar{v}^2$ = 3.52 x 10^{-10} CM^4 SEC^{-2}

X = 3.90 x 10^{-6} SEC^{-1} DEG$^{-\frac{1}{2}}$

E = 0.044 eV

DEGREES C

$\frac{1}{\tau_p}$ IN SEC^{-1}

Figure 5-8. Fit to ^{129}Xe Pump Time Data for Cell No. 367

and permits comparison with earlier data although equation (3)
is considered now to be a better model. Note that, compared
with the spin exchange term, the temperature dependence due to
the wall interaction is quite small. This has been discussed
in connection with the double oven experiment.

As with cell number 367, a study of the hydride containing cell
number 370, showed a $T_p \cong T_2$ for ^{129}Xe and a somewhat larger T_p
than T_2 for the ^{131}Xe. Data were taken over a very limited
temperature range. Nevertheless, the trend was clear. The
temperature dependence of the ^{129}Xe follows the familiar curve
and a plot of relaxation rate versus $N_{Rb}/\bar{v}$ provides a nearly
straight line of slope 4.23×10^{-10} cm^4 sec^{-2} and intercept
5.51×10^{-3} sec^{-1}. The ^{131}Xe data shows hardly any temperature
dependence with, for this sample, T_p in the range 140-160 sec-
onds and T_2 at 102-113 seconds. As compared with the non-
hydride coated cell, the hydride coated cell showed the same
trend as cells 359, 360, and 361. The non-coated cell exhibited
much longer T_2 for ^{129}Xe at low temperature than the treated
cell.

Finally, these initial studies of Corning 1720 glass as compared
with Pyrex glass point to some general conclusions. For all
samples studied, the ^{129}Xe isotope showed the same value of longi-
tudinal and trasverse relaxation times for a given cell at a given
temperature over the temperature range examined. This is consis-
tent with the discussion presented in Section III for field gradient
relaxation in the normal experiment in the case where gradients
perpendicular to the optical axis are not large. The measured
longitudinal relaxation time for ^{131}Xe was always found to be
larger than the transverse relaxation. Both kinds of cells
exhibit the same general trends in relaxation parameters as a
function of temperature. Both kinds of cells can exhibit the

previously unexpected relaxation effects in the frequency shift experiment. However, certain interesting differences have been found and those are discussed in the next and final section. Most notably, ^{129}Xe relaxation time at 80°C appears much shorter for untreated pyrex than for untreated 1720 glass or hydride treated cells. One can conclude also from these studies that hydride coating leads to improved ^{131}Xe relaxation rates for 1720 glass as it does for pyrex cells.

5.4 CONSIDERATIONS FOR FUTURE WORK

Results of studies of relaxation in Corning 1720 glass cells are very encouraging. Although both 1720 glass and Pyrex glass hydride treated cells seem to have similar characteristics, the relaxation times of the Xenon 129 isotope in 1720 teardrop uncoated cells have been found to be longer than for comparable Pyrex cells. As 1720 glass is known to be superior to Pyrex from the point of view of alkali attack, further studies of 1720 glass cells should be pursued. Geometry should be investigated to determine whether, as suspected, the difference between T_p and T_2 for the ^{131}Xe, known to be due to quadrupolar interaction[3], arises from the non-spherical shape of the cells studied thus far. More coatings (e.g., mixed alkali hydrides) should be studied.

5.5 BIBLIOGRAPHY

1. R.M. Herman, Phys. Rev. 137, A1062 (1965).

2. C.H. Volk, T.M. Kwon, and J.G. Mark, Phys. Rev. A 21, 1549 (1980).

3. T.M. Kwon, J.G. Mark, and C.H. Volk, Phys. Rev. A 24, 1894 (1981).

SECTION VI

ALKALI HYDRIDE CHEMISTRY

6.1 INTRODUCTION

The promise of alkali hydride cell coatings for promoting desirable characteristics in ^{131}Xe NMR relaxation has been noted in a previous AFOSR report[1], and as part of the research program for 1981-82, an investigation of factors involved in producing desirable hydride coatings was undertaken. It was postulated that a more nearly uniform coating of the cell wall surface might lead to control and prediction of magic angle behavior in ^{131}Xe relaxation. To test this, cells prepared from Corning 1720 glass have been compared with Pyrex cells of similar fill. The 1720 glass cells have the advantage that they can be heat treated at a higher temperature than the Pyrex, thereby removing more waters and hydroxyls which may be present on the glass surface. It was postulated that such "clean glass" surfaces might be more conducive to uniform alkali hydride deposition. This section reviews some thermodynamic and physical properties of alkali hydrides and presents some simple calculations based on the thermodynamic data while taking into consideration the nature of the glass surfaces and cell constituents. Some experimental results for magic angle behavior of the 1720 glass and Pyrex cells are presented and discussed.

6.2 REVIEW OF ALKALI METAL CHEMISTRY

Experimental results presented in this report are for rubidium containing systems only. However, our interests extend to cesium and, possibly, potassium containing cells, some of which will be investigated in the future. Furthermore, there appears to be available in the recent literature much more information

on alkali hydrides other than rubidium hydride[2-8]. Therefore, in order to estimate rubidium compound properties where limited data are available it is necessary to make comparisons with available results for compounds of other alkalis.

To understand what compounds must be considered and what reactions may take place, it is necessary to consider the various constituents available for reaction with the alkali metal. A typical cell fill includes helium and nitrogen as buffer gases, a certain amount of hydrogen gas, and excess rubidium metal. The cell surface is composed of constituents present in the glass along with some paramagnetic impurities. The latter are of low enough concentration to be insignificant as far as chemistry is concerned but can contribute to relaxation effects, especially for ^{129}Xe. The Corning 1720 glass is an alkali resistant, calcium containing aluminosilicate glass formed largely from CaO, B_2O_3, Al_2O_3 and SiO_2. Pyrex is a borosilicate glass which also contains small amounts of Na_2O, K_2O, and Al_2O_3. The main consideration here is that aluminosilicate glasses are largely Al_2O_3, CaO, and SiO_2 while Pyrex is mostly SiO_2 and B_2O_3. Both kinds of glass will have waters and hydroxyls on the surface unless a method is employed to remove them. These surface groups are expected to be among the most reactive species the alkali metal will encounter.

The alkali metals considered here are sodium, potassium, rubidium and cesium. Lithium, the first alkali metal has, in general, somewhat different properties from the next four and francium is out of the range of interest. For sodium through cesium one sees fairly consistent trends in physical properties, some of which are presented in table 6-I. It is useful to note similarities and differences for these four elements. The first ionization energies are similar and electropositivity increases

TABLE 6-I. SOME PHYSICAL PROPERTIES AND THERMODYNAMIC
DATA FOR THE ALKALI METALS

	Na	K	Rb	Cs
Atomic number	11	19	37	55
Electronic Configuration	2-8-1	2-8-8-1	2-8-18-18-1	2-8-18-18-8-1
Formula Weight	22.9898	39.1020	85.4678	132.9054
Density, g/ml	0.97	0.86	1.52	1.87
Crystal Structure	BCC	BCC	BCC	BCC
Metallic radius, $\overset{\circ}{A}$	1.572	2.025	2.16	2.35
Covalent radius $\overset{\circ}{A}$	1.54	1.96	2.11	2.25
Ionic radius $\overset{\circ}{A}$	0.95	1.33	1.48	1.69
Electronegativity (SR)	0.70	0.56	0.53	0.49
1st ionization energy in kcal/mole	119	100	96	90
2nd ionization energy in kcal/mole	1086	732	632	540
Melting point ^oC	97.8	63.2	39.0	28.6
Heat of fusion, kcal/mole	0.62	0.55	0.52	0.50
Boiling Point ^oC	890	766	701	685
ΔH^o for M (g) at 298.15K, kcal/mole	25.65	21.33	19.33	18.180
ΔG^o forM (g) at 298.15K, kcal/mole	18.354	14.49	12.690	11.748
S^o at 298.15K M (s)	12.24	15.34	18.35	20.37
cal/deg mole M(g)	36.712	38.295	40.626	41.942
C_p at 298.15K M (s)	6.75	7.07	7.424	7.69
cal/deg mole M (g)	4.968	4.968	4.968	4.968
Data from references 8 and 9				

down the series indicative of increasing reactivity. A slight
trend to larger radius down the series, whether metallic,
covalent, or ionic, may account for greater activity of sodium
in attacking glass in diffusion controlled processes. The
greater volatility of the heavier alkalis is clear from the
Gibbs energy of formation for the gas at 298.15K. Noting the

similarities and trends will help to establish confidence for
qualitative predictions for properties of compounds of rubidium
or cesium where only data for sodium and/or potassium exist.

The alkali metals are very reactive and combine readily with
molecular oxygen. The properties of some oxides, M_2O, peroxides,
M_2O_2, and superoxides, MO_2 are presented in table 6-II. Proper-
ties of hydroxides are presented also. The oxides react readily
with acids or water to form the hydroxides, the strongest bases
available. The values of the Gibbs energies tabulated show the
chemical stability, although, of course, they give no indication
of the rate of chemical reaction; however, the formation of all
the compounds listed in table 6-II is known to take place readily.
It is because of the ease of formation of oxides and hydroxides
that it is desirable to remove as many surface waters and
hydroxyl groups as possible prior to filling a sample cell. Also
the extreme stability of alkali compounds with the glass con-
stituents should not be overlooked. For example, sodium metasil-
icate, Na_2SiO_3, has a Gibbs energy of formation of 298.51K of
-349.19 kcal/mole and certain Na-Al-Si-O compounds and certain
Na-B-O compounds have Gibbs energies of formation in the range
-800 to -1000 kcal/mole[8]. Thus the alkalis could be expected to
form extremely stable compounds with the constituents found in
glass. The actual attack of the glasses by rubidium, however,
appears to take place over months or longer and is probably a
diffusion controlled process not kinetically favored at the
temperatures of interest. Of course, in order to attack the
glass, the alkali probably needs to break already established
bonds. Thermodynamic quantities such as ΔH^o_f and ΔG^o_f at 298K
for SiO_2, Al_2O_3, and CaO are comparable to those for the oxides
of the alkalis. Thus, for the purposes of this discussion, the
interaction of the alkali metal with the glass will be ignored,

TABLE 6-II. SOME PHYSICAL PROPERTIES AND THERMOCHEMICAL DATA FOR OXIDES AND HYDROXIDES OF THE ALKALI METALS

Oxide	Color	Mp (°C)	H_f^o at 298.15K kcal/mole	G_f^o at 298.15K kcal/mole
Na_2O (c)	White	920	-99.00	-86.74
K_2O (c)	Yellowish – white	>490	-86.4	-
Rb_2O (c)	Yellow	>567	-81	-
Cs_2O (c)	Orange	490	-82.64	-73.65
Na_2O_2 (c)	Pale yellow	-	-112.10	-107.00
K_2O_2 (c)	Orange	-	-118.1	-101.6
Rb_2O_2 (c)	Dark brown	-	-112.8	-
Cs_2O_2 (c)	Yellow	-	-59	-
NaO_2 (c)	-	-	-62.2	-52.2
KO_2 (c)	Orange-yellow	380	-68.10	-57.23
RbO_2 (c)	Dark orange or brown	412	-66.6	-
CsO_2 (c)	Orange	432	-68.4	-
Hydroxide				
NaOH (c)	-	-	-101.723	-90.709
NaOH (amorp)	-	-	-112.360	-100.187
KOH (c)	-	-	-101.521	-90.61
KOH (amorp)	-	-	-115.29	-105.29
RbOH (c)	-	-	-99.95	-
RbOH (amorp)	-	-	-115.00	-105.46
CsOH (c)	-	-	-99.72	-
CsOH (amorp)	-	-	-116.70	-107.38

Data taken from Ref. 8 and 9

and emphasis will be placed on the more immediate question of alkali hydride chemistry.

A system consisting of a glass cell of 2 ml volume, typical of the cells reported on in this section, will be assumed. An excess of alkali metal, M, is introduced into the cell. In practice, rubidium metal is distilled into the appropriately heat treated cell on a vacuum line. Thus, the cell wall is initially covered with metal. It is assumed the rubidium metal will begin to react with any surface water and/or hydroxyl groups present. After the introduction of buffer gases and hydrogen, the cell is sealed off. At this time the cell body is thermally isolated from the tip-off region. After sealing, the cell body is heated in a flame while the tip is cooled. This drives the metal into the tip-off region and probably accelerates any reaction with the surface waters and hydroxyls. The cell is then placed in a curing oven at around 80°C for two weeks or longer. During this time a white film of metal hydride develops on the surface of the cell in those cells containing hydrogen gas. Cells without hydrogen remain clear.

Consider the approach to equilibrium of the reaction

$$M \text{ (s)} + 1/2 \text{ } H_2 \rightleftharpoons MH \text{ (s)} \text{ .} \qquad (1)$$
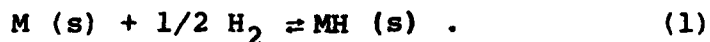
Available data for this reaction are presented in table 6-III. As only data for NaH is available, explicit calculations are made for that case. A detailed calculation at 298.15K for NaH starts with the general expression for the equilibrium constant at constant pressure for the reaction (1).

TABLE 6-III. SOME PHYSICAL AND THERMOCHEMICAL
PROPERTIES OF ALKALI METAL HYDRIDES

Formula	NaH	KH	RbH	CsH
Formula Weight	23.9978	40.1100	86.4758	133.9134
Structure	NaCl	NaCl	NaCl	NaCl
Color	White	White	White	White
Melting Point °C	(700-800 decomp)	d	d >200	d
Density g/ml	1.40	1.43	2.59	3.42
M-H distance (crystal) Å	2.44	2.85	3.02	3.19
M-H distance (gas) Å	1.89	2.22	2.37	2.49
ΔH^O_f at 298.15K kcal/mole MH (s)	-13.450	-13.80	-12.5	-12.950
ΔG^O_f at 298.15K kcal/mole MH (s)	-8.00	-	-	-
S^O 298.15K cal/deg mole MH (s)	9.564	-	-	-
C_p 298.15 cal/deg mole MH (s)	8.700	-	-	-
ΔH^O_f at 298.15K kcal/mole MH (g)	31.13	31.4	-	27.7
ΔG^O_f at 298.15K MH (g)	26.02	26.9	-	23.1
S^O 298.15K cal/deg mole MH (g)	44.997	45.96	-	51.40
C_p 298.15K cal/deg mole MH (g)	7.24	7.421	-	7.54

Data from references 8 and 9

$$k = e^{-G^O_f/RT} = e \frac{+ 8 \times 10^3 \text{ cal/mole}}{1.987 \frac{\text{cal}}{\text{deg mole}} (298.15 \text{ deg})}$$

$$= 7.32 \times 10^5 \qquad\qquad (2)$$

404720

Most generally

$$k = \frac{a_{NaH(s)}}{a_{Na(s)} \; a_{H_2(g)}^{\frac{1}{2}}} \qquad (3)$$

for reaction (1). The activity, a, of a solid in the pure
state at one atmosphere pressure is set equal to one and the
activity $a_{H_2(g)}$ is assumed approximately equal to the pressure
in atmospheres. One then calculates a pressure of 1.87×10^{-12}
atm or 1.42×10^{-9} torr of H_2 at equilibrium from equations (2)
and (3). This can be compared with a value 1.24×10^{-7} torr for
H_2 over a fully equilibrated mixture of $C_s(s)$ and $C_sH(s)$ at
298.15K calculated from the expression given in Reference 5. The
trends exhibited in tables 6-I, 6-II, and 6-III for properties
of alkali metals and their compounds lead to the conclusion
that the equilibrium pressure of hydrogen at 298K over a salt-
metal mixture for potassium and rubidium is probably in a range
comparable to 10^{-9} to 10^{-7} torr. This is considerably below the
pressure of 4-10 torr typically introduced into the cell volume
and suggests that initially the large amount of available
hydrogen will tend to drive the reaction to completion. As we
have yet no data on the rate or reaction other than our qualita-
tive observation that a white film forms on the cell wall in
rubidium containing cells after a few days at $80^{O}C$, we cannot
say when the reaction arrives at equilibrium. Also, it is
necessary to discuss more thoroughly the limitations of the
calculation just presented.

The calculation was carried out for 295.15K while in fact the
reaction takes place at a slightly elevated temperature of about
380K. (For rubidium, that is above the melting point.) The
expression for the variation of the equilibrium constant with
temperature,

$$\left[\frac{\partial \ln K_P}{\partial T} \right]_P = \frac{\Delta H^O}{RT^2} \qquad (4)$$

predicts that, for exothermic reactions (negative ΔH^O), the equilibrium will shift somewhat to the left. This means less NaH(s) is formed at elevated temperature. However, the thermodynamic data do not reveal the nature of the kinetics of the reaction and, for the cells discussed here, it has been observed that the elevated temperature favors the formation of the rubidium hydride coating. One can calculate $K_P(T)$ from ΔH^O and C_P data if the temperature dependence of C_P is available. Over such a limited temperature range, both could be taken as constant in a first approximation. Also, it should not be overlooked that as the system is a sealed cell, the appropriate thermochemical quantities to consider would be the Helmholz energy, A, rather than the Gibbs energy and, of course, the heat capacity at constant volume C_V rather than C_P. G differs from A (and H from E) by the PV work which, while insignificant for solids and liquids, must be taken into account for gas phase reactions. Estimates of PV work over the temperature range of interest, based on the perfect gas law and even taking the changing number of moles of Rb(g) (very small) into consideration, suggest that the calculation at 298.15K are valid: The equilibrium is strongly in the direction of MH(s) in the temperature range of interest and, when equilibrium has been attained, one can assume the reaction has gone to completion. Of course, at much higher temperatures, the hydride will decompose (cf. table 6-III) and this has been observed by treating RbH coated cells with a flame and has also been observed for CsH(s) but, for the temperature range of interest, both thermochemical data and our observations dictate the formation of RbH(s).

A simple calculation based on ideal gas behavior places 1.08×10^{-7} moles/torr as the amount of H_2 introduced into a cell. Thus, 10 torr of hydrogen can react to produce $\sim 2 \times 10^{-6}$ moles of RbH. That is, about 200 μgm of rubidium will be consumed in a complete reaction. At present, methods for estimating the amount of rubidium are imprecise so, based on past experience, an attempt is always made to introduce an excess of rubidium into the cells.

6.3 EXPERIMENTAL RESULTS: COMPARISON OF PYREX AND CORNING 1720 CELLS FOR HYDRIDE COATING AND MAGIC ANGLE BEHAVIOR

Two sets of four cells each of teardrop shaped cells suitable for use in the double oven experiment were prepared. One set was prepared using Pyrex glass and the other using Corning 1720 glass. Both sets were filled with excess ^{87}Rb, 0.2 torr ^{129}Xe, 0.8 torr ^{131}Xe, 100 torr He, and 40 torr N_2. In addition, 10 torr of H_2 was added to two cells of each set. Prior to filling, the 1720 glass was baked out on the vacuum line at a somewhat higher temperature than the Pyrex set. After filling and sealing, the cells were placed in the curing oven. After about one week, one of the 1720 glass cells was removed from the oven for a series of experiments including some of the pump time experiments reported on in Section V. After 7-8 weeks of aging, the remaining 1720 glass cells were removed from the oven and after 11 weeks of aging the Pyrex cells were removed from the curing oven. By this time, both the 1720 glass and the Pyrex cells containing hydrogen had developed a thin, somewhat opaque coating. To the naked eye, the coating of the 1720 glass cells appeared less transparent in spite of the shorter time spent in the curing oven. The more transparent Pyrex cells, however, exhibited a brownish cast to the coating when compared with the 1720 cells. This may indicate the formation of some oxides of rubidium on the surface (cf. table 6-II). The 1720 cells,

GUIDANCE & CONTROL SYSTEMS
Litton 5500 Canoga Avenue, Woodland Hills, California 91365   FSCM 06481

prepared in a way to minimize surface waters and hydroxyls,
appeared milky white. Some experiments on cells from each batch
have been reported in Sections II and V. In this section, magic
angle orientation data are reported for comparison of the merits
of each kind of glass in presenting a surface leading to control
of the magic angle and relaxation time behavior.

Magic angle behavior is studied by assigning a coordinate system
to the cell for the purpose of reorienting the cell in the
precession field in order to search for an exponential ^{131}Xe free
induction decay. It has been shown both experimentally and
theoretically[10] that, as far as ^{131}Xe relaxation is concerned,
many NMR cells exhibit an approximately axially symmetric nature
and, when the axis of symmetry is at the magic angle with
respect to the precession field, the free induction decay ap-
pears as a simple exponential without beats. The magic angle
is that for which $(1-3 \cos^2 \theta)$ equals zero; θ being the angle
between the field and the cell symmetry axis.

Figures 6-1 and 6-2 show representative magic angle data for
four different cells. Figure 6-1 presents data for a hydride
cell and a non-hydride cell of Pyrex glass. Figure 6-2 presents
similar data for 1720 glass cells. The time scale of the sweep
in figure 6-1 is 150 sec, and in figure 6-2 it is 250 sec.
There are obvious differences in relaxation times but inspection
of these data and other available to us would suggest to us that
the use of 1720 glass offers no special advantage in control-
line magic angle behavior. Both kinds of cells seem to present
a range of acceptable orientation as large as $\pm 20^{\circ}$.

More insight into what is going on as far as relaxation is con-
cerned can be seen by comparing hydride treated cells with non-
hydride treated cells. First note, in figures 6-1 and 6-2,

GUIDANCE & CONTROL SYSTEMS
5500 Canoga Avenue, Woodland Hills, California 91365

FSCM 06481

PYREX CELL NO. 366
78.4°C HYDRIDE COATED

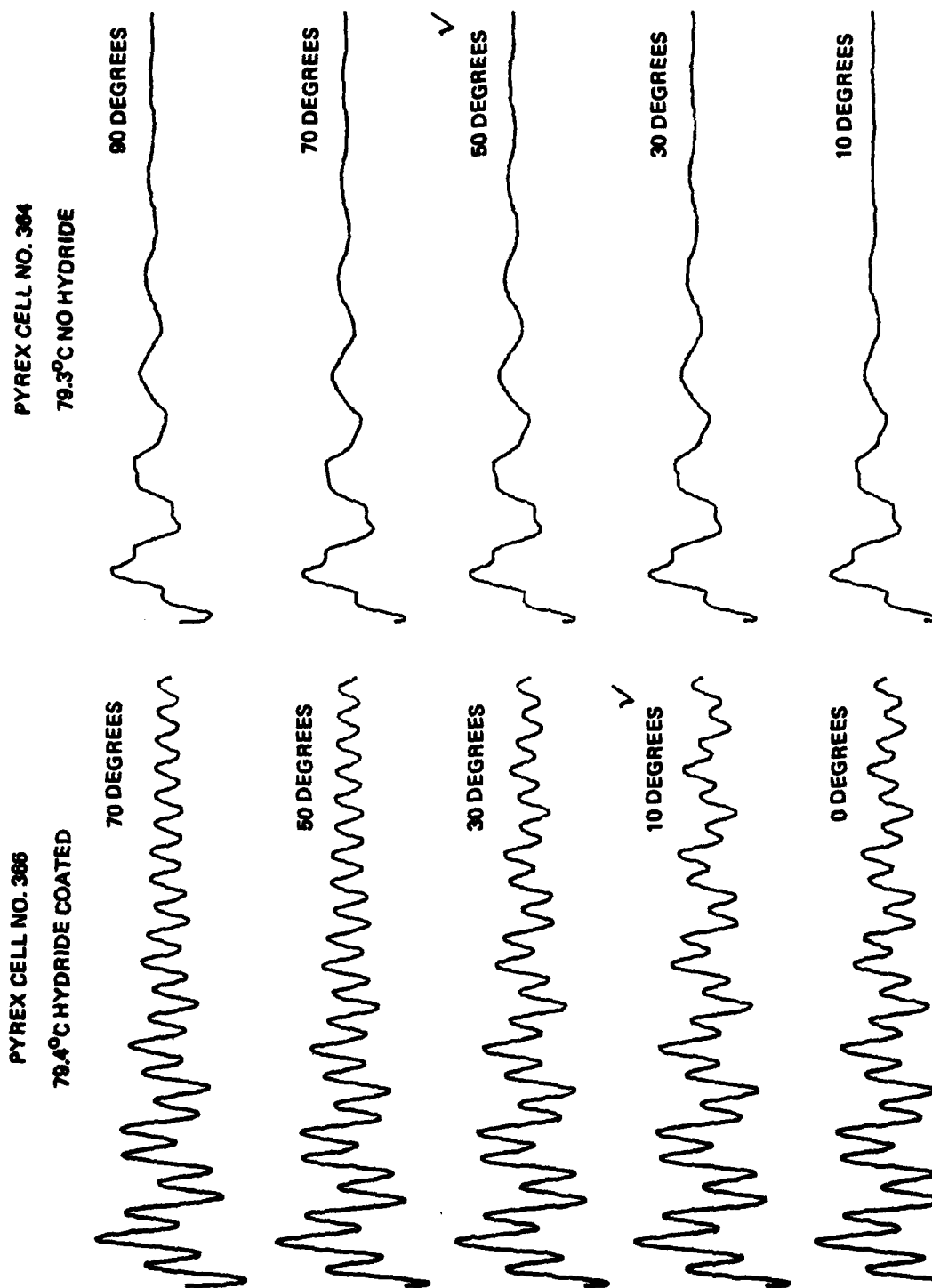PYREX CELL NO. 364
79.3°C NO HYDRIDE

Figure 6-1. Magic Angle Orientation of Pyrex Cells in Ten to Twenty Degree Steps. Preferred orientation is checked. Angles are measured between a selected cell axis and the field.

GUIDANCE & CONTROL SYSTEMS
5500 Canoga Avenue, Woodland Hills, California 91365

FSCM 06481

1720 GLASS CELL NO. 368

78.3°C NO HYDRIDE

90 DEGREES

70 DEGREES

50 DEGREES

1720 GLASS CELL NO. 370

78.2°C HYDRIDE COATED

90 DEGREES

80 DEGREES

60 DEGREES

40 DEGREES

20 DEGREES

Figure 6-2. Magic Angle Orientation of Corning 1720 Glass Cells in Ten to Twenty Degree Steps. Preferred orientation is checked. Angles are measured between a selected cell axis and the field.
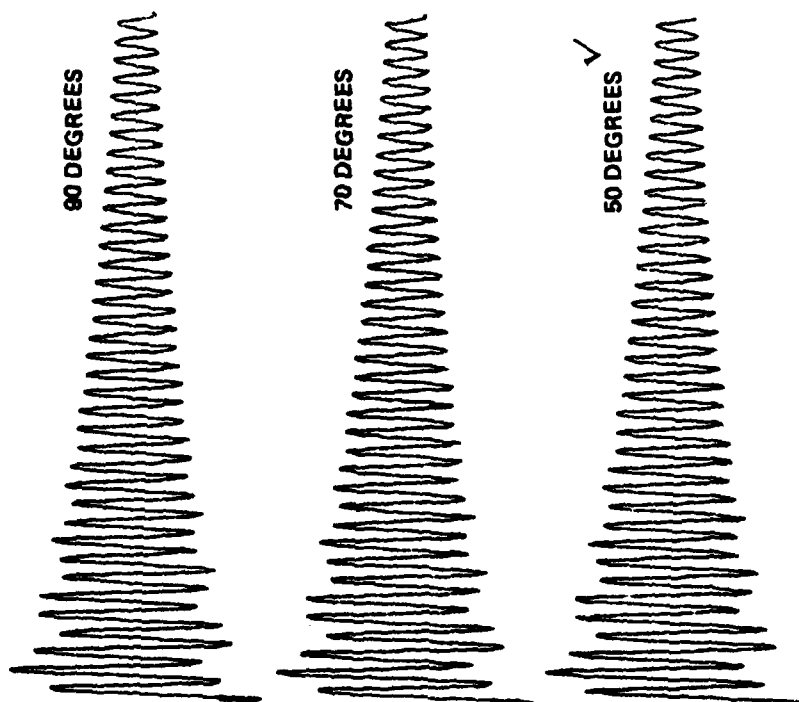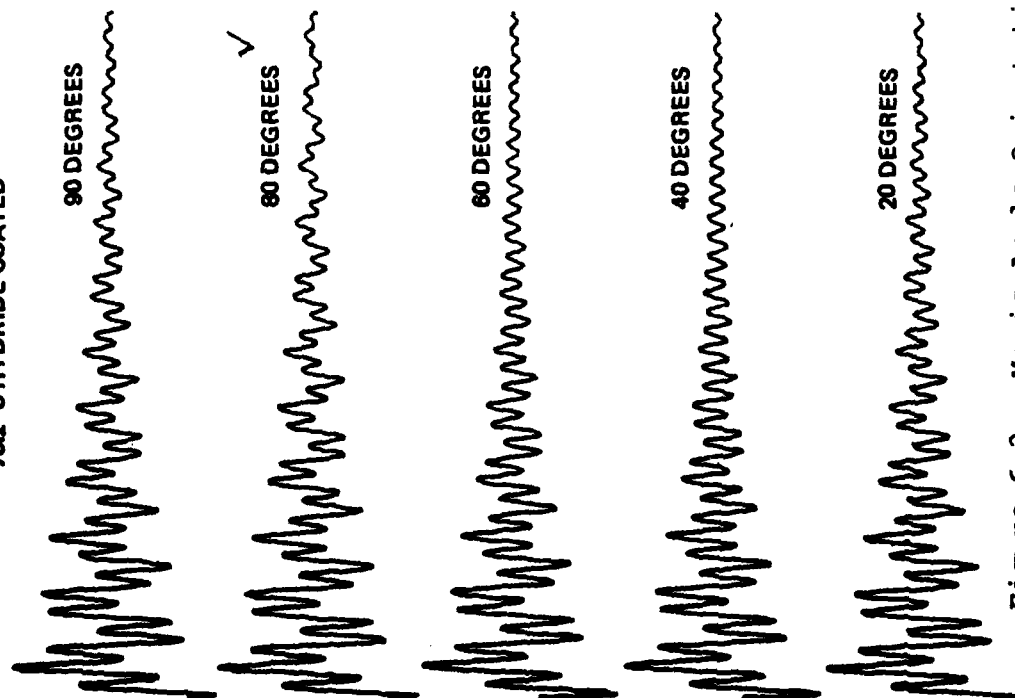
GUIDANCE & CONTROL SYSTEMS
Litton 5500 Canoga Avenue, Woodland Hills, California 91365

that hydride treated cells produce very similar free induction
decay traces. Table 6-IV summarizes available transverse
relaxation time data close to 80°C for a series of both hydride
treated and non-hydride treated cells, some Pyrex and some 1720
glass. Looking at the column of ^{129}Xe results, one can see
that hydride treatment seems to result in over all uniformity
of relaxation times. Without hydride treatment, the relaxation
time in the Pyrex cells is very short, about 20-30 sec., and
for the 1720 glass cells unexpectedly long, about 140-160 sec.
Although Corning 1720 glass has the reputation for having a
large amount of paramagnetic impurities relative to Pyrex, these
data would seem to suggest less paramagnetics in the 1720 glass
than in the Pyrex and also some degree of reproducibility from
batch to batch. Presumably, the hydride formation presents a
surface nearly uniformly the same regardless of substrate, with
the local field due to the protons in RbH intermediate between
that of the bare Pyrex or 1720 glass surfaces. A way to check
this would be to prepare RbD surfaces.

The limited ^{131}Xe data show the opposite trend. As the ^{131}Xe
relaxation is expected to be due to quadrupolar rather than dir-
ect dipolar interaction, the results suggest a stronger surface
interaction for the 1720 glass cells even after the hydride
coating is applied.

The apparent reproducibility of parameters from batch to batch
is interesting also, although similarities are expected at this
somewhat elevated temperature. Nevertheless, this trend is
worthy of notice and is probably due to recently developed
careful control of technique of cell production.

Data are still being taken on the cells listed in table 6-IV
with the goal of refining techniques of measuring wall parameters
and establishing a more nearly complete set of comparative data.

TABLE 6-IV. RELAXATION TIMES OF XENON ISOTOPES IN PYREX
AND CORNING 1720 GLASS CELLS AT CLOSE TO 80°C

	T (°C)	T_2 ^{131}Xe	T_2 ^{129}Xe
Pyrex Cells			
No. 363 No Hydride	79.3	61.7	33.4
364 No Hydride	79.3	56.4	29.8
365 Hydride	79.5	132	90.3
366 Hydride	79.4	121	102
1720 Cells			
No. 367 No Hydride	77.1	47.5	155
368 No Hydride	78.3	45.8	162
369 Hydride	78.2	105	98.4
370 Hydride	78.2	111	97.3
1720 Cells with no ^{131}Xe			
No. 341 No Hydride	79.3	-	140
344 No Hydride	79.4	-	138
359 No Hydride	80.4	-	139
360 No Hydride	79.0	-	138
361 Hydride	78.5	-	84.7
Pyrex Cells with no ^{131}Xe			
No. 336 No Hydride	79.6	-	21.8
337 No Hydride	79.3	-	22.2
334 Hydride	79.4	-	106
335 Hydride	78.7	-	104

6.4 CONSIDERATIONS FOR FUTURE WORK

It has been proposed to study quartz cells. Such cells can be heated to even higher temperatures than 1720 glass and a hydride coating of quartz may lead to desired ^{131}Xe relaxation characteristics. Further efforts should be made to standardize cell preparation techniques (e.g., preparation of a standard buffer gas mix). Furthermore, as hydride treatment has been seen to shorten somewhat the ^{129}Xe relaxation time in 1720 cells, a study of RbD coating might be undertaken. This would determine whether the changing ^{129}Xe relaxation is due to direct dipolar relaxation during wall encounters. In connection with these additional studies, cell history should be monitored.

6.5 BIBLIOGRAPHY

1. T.M. Kwon, AFOSR, Annual Technical Report, Contract No. F49620-77-C-0047 (1981).

2. B. Sayer, M. Ferray, J. Lozingot, and J. Berlande, J. Chem. Phys. 75, 3894 (1981).

3. S.C. Yang, Y.K. Hsieh, A.C. Tam, W.T. Zemke, K.K. Verma, and W.C. Stwalley, J. Chem. Phys. 75, 3679 (1981).

4. K.V.L.N. Sastry, E. Herbst, and F.C. DeLucia, J. Chem. Phys. 75, 4753 (1981).

5. N.D. Bhaskar, J. Camparo, M. Ligare, and W. Happer, Phys. Rev. Lett. 46, 1387 (1981).

6. A.C. Tam and W. Happer, J. Chem. Phys. 64, 2456 (1976).

7. A. Tam, G. Moe, and W. Happer, Phys. Rev. Lett. 35, 1630 (1975).

8. D.D. Wagman, H.W. Evans, V.B. Parker, R.H. Schumm, and R.L. Nuttall, Selected Values of Chemical Thermodynamic Properties, NBS Technical Note 270-8, 1981.

9. R.T. Sanderson, Chemical Periodicity (Reinhold, New York, 1960).

10. T.M. Kwon, T.G. Mark, and C.H. Volk, Phys. Rev. A 24, 1894 (1981).

DATE
ILME